# SEA ICE PHYSICAL PROCESSES AND BIOLOGICAL LINKAGES WITHIN THE NORTH WATER POLYNYA DURING 1998

BY

C.J. MUNDY

A Thesis
Submitted to the Faculty of Graduate Studies
In Partial Fulfillment of the Requirements
For the Degree of

MASTER OF ARTS

Department of Geography
University of Manitoba
Winnipeg, Manitoba

THE UNIVERSITY OF MANITOBA

FACULTY OF GRADUATE STUDIES

*****

COPYRIGHT PERMISSION PAGE

# Sea Ice Physical Processes and Biological Linkages within the North Water Polynya During 1998

BY

C. J. Mundy

A Thesis/Practicum submitted to the Faculty of Graduate Studies of The University of Manitoba in partial fulfillment of the requirements of the degree of Master of Arts

# ABSTRACT

Sea ice is a major component of the Earth's climate system and is believed to be a sensitive indicator of climate change. The North Water (NOW) refers to a region of anomalous sea ice conditions at the northern end of Baffin Bay. The dynamic sea ice cover is due to the presence of the NOW polynya. An explanation for the polynya's occurrence has yet to be confirmed. In this thesis I studied the spatial and temporal patterns of sea ice cover within the North Water (NOW) in the context of polynya formation and maintenance mechanisms. Further, biological implications of the NOW's sea ice cover patterns were examined. To accomplish this I developed a sea ice classification scheme for RADARSAT-1 ScanSAR imagery obtained throughout 1998. I extracted sea ice type and concentration and constructed a Geographic Information System (GIS) database for analysis of spatial and temporal trends in sea ice cover over this annual cycle.

Spatially, the results identified a clear and consistent pattern of sea ice cover throughout 1998. Areas of increased ice deformation (evidenced by the presence of compressive deformed ice types) along the east coast of Canada with a lesser degree of deformation towards Greenland and the Canadian Archipelago were inferred. Temporally, the polynya opened southward along the Canadian coast and eastward towards the Greenland coast. Subsequently, the polynya appeared

to be largely controlled by the latent heat mechanism with the exception of the west Greenland coast. There were some areas of lower ice deformation along the coast of Greenland that could also be explained, at least in part, through sensible heat inputs (i.e., both oceanic and atmospheric). These areas of lesser ice deformation also corresponded to the occurrence of shallow mixed layer depths earlier than surrounding areas. Consequently, these areas have the potential to accommodate an earlier primary production bloom.

This thesis represents an advancement in the development of our understanding of ocean-sea ice-atmosphere processes that occur within the North Water and its polynya. Links between the polynya's sea ice cover, physical mechanisms, biological production and climate variability and change were made. Further analysis within the NOW Study research network will examine these links in more detail.

# ACKNOWLEDGEMENTS

Reaching the end of a thesis is quite an accomplishment, but it could not be done alone. There are so many people that I would like to thank. In no particular order... I would like to extend my appreciation to Dr. David G. Barber. Your supervision helped steer me through tough decisions and your "down to earth" nature and friendship always made you easy to talk to and approach when difficulties arose. You have placed me in incredible positions and situations that will continually assist me in my future endeavors and I am very thankful for that. I look forward to spending at least another year with you as a Research Associate.

Thank you to all the residents of rooms 203, 205, 229, 225 and 114 of the Isbister Building who I know have all leant their ears for my many questions. More specifically, thank you Johnnies (Yackel, Iacozza and Hanesiak) for many helpful ideas which contributed to this thesis as well as putting up with being called Johnny. Thank you Ron Hempel, for without you the grid and therefore this thesis may not have yet been a realization. Thank you roomy (Steve Quiring) for your much needed assistance during that summer and your never-ending assistance ever since. Thanks David Mosscrop for all the assistance both inside and outside the lab. Dr. Tim "the name" Papakyriakou, thanks for helping explain the many faces of energy to me and for boosting my ego at times.

Thank you Dr. Alan J.W. Catchpole and Dr. Gordon G.C. Robinson for your patience and many suggestions when I first proposed my thesis, for critically reviewing the near final product and for not stumping me too much during my defense.

I extend my thanks to the Department of Geography, the Centre for Earth Observation Science (CEOS) and the University of Manitoba who have leant me the support, facilities, space and time required to complete my thesis. Thank you Trudy Baureiss, Mary Anna, Aggie Roberecki, Suzanne Beaudet, Dr. J. Brierley and Dr. G. Smith for all of the much-needed assistance.

I would like to thank Katherine Wilson who provided me with great conversations on our theses topics as well as always being there for me when I had troubles with the dataset. Thanks Ken Asmus for your unequaled field preparedness and your bottomless toolbox. While I am in the ballpark, I would also like to thank the Canadian Ice Service (CIS) for all their support.

Thank you Dr. Yves Gratton for providing me with the mixed layer depth data used in this thesis. I would also like to thank Dr. Peter Minnett for access to the ship-based meteorological data also used in this thesis.

I extend my appreciation to everyone involved in the International North Water Polynya Study (NOW) 1998 campaign, including the crew and officers of the CCGS *Pierre-Raddison*. I would like to thank the University of Manitoba for their support through a Graduate Fellowship. Thanks to the Northern Scientific Training Program (NSTP) for their field assistance grants. As well, thank you

Polar Continental Shelf Project (PCSP) for your technical and logistical support in the field.

As many people do, I would like to use a cliché to end this section... Last, but certainly not least, I thank my family for their support throughout my Masters degree, the band for helping me chase other goals in my life, Kate for always being there for me and all my friends.

# TABLE OF CONTENTS

# LIST OF FIGURES

# LIST OF TABLES

# CHAPTER 1: INTRODUCTION

The Earth's climate – a complex interaction between incoming solar radiation, emitted Earth radiation and the characteristics of the planet's surface and atmosphere – has been ever-changing throughout its history. However, increased atmospheric $CO_2$ levels and a climate warming over the past century have raised public concern. A question of whether this change has an anthropogenic origin or is simply the natural variability of the Earth's climate has been posed (World Climate Research Program (WCRP) objective – in McBean 1992). In order to answer this question we must first be able to detect and understand change in relation to the physical interactions causing the change. Throughout the last couple of decades climate change research has largely focused on polar regions where it is thought the change will occur earlier and will likely be amplified relative to temperate and tropical regions of the planet (e.g., Barry et al. 1993).

Due to the many difficulties associated with research in polar regions (i.e., low temperatures, inaccessibility, 24 hr winter darkness and high logistical expenses), polar marine systems have remained poorly understood relative to other regions of the planet. However, their sensitivity to climate variability, importance to many biological species and profound influence on ocean circulation and global climate are well recognized. One of the most unique and

vital components of these regions is a temporally and spatially dynamic sea ice cover.

Sea ice: (i) influences global ocean thermohaline circulation by supplying cold, dense brine through accretion (freeze-up) and fresh surface water through ablation (melt) (Aagaard and Carmack 1989); (ii) provides a platform for deposition of snow, which in combination control the ocean-sea ice-atmosphere (OSA) exchange of mass, heat and momentum (Maykut 1978; 1982) and affect the surface radiation balance through changes in albedo (Barry et al. 1993); and (iii) has both direct and indirect consequences on biological production (e.g., Welch et al. 1992). Furthermore, sea ice has been hypothesized as a sensitive indicator of climate change through possible feedback mechanisms operating across the OSA interface (Barry et al. 1993). Mounting evidence of climate change includes temporal trends of decreasing Arctic pack-ice extent (e.g., Parkinson et al. 1999) and thickness (e.g., Rothrock et al. 1999).

Sea ice is both spatially and temporally variable. Over an annual cycle, the ocean's ice cover profoundly modifies up to 15% of the Earth's surface. Advance and retreat of sea ice cause most of this change. Parkinson et al. (1999) found the Arctic average seasonal coverage (1978-1996) of sea ice extents to range from a minimum of $7.0 \times 10^6$ km$^2$ in September to a maximum of $15.4 \times 10^6$ km$^2$ in March. Interannual variations among these averages are quite substantial with regional oscillations demonstrating an approximate ten-year cycle (Mysak and Venegas 1998).

Throughout the winter months, the extensive Arctic sea ice cover is dotted with anomalous openings referred to as polynyas and leads. Modeled and observed results have demonstrated new ice (<30 cm) and open water to only cover 1% (Thorndike et al. 1975) to 2.6% (Mclaren 1988) of the total Arctic Ocean during this time. However, heat exchange through open water and new ice surfaces can be two orders of magnitude greater than surrounding snow covered sea ice (Maykut 1978). Consequently, polynyas and leads dominate regional heat budgets (Maykut 1978) and significantly influence salt flux to the oceans (Carmack 1990) and heat flux to the atmosphere in winter (Maykut 1982).

Polynyas and leads have been distinguished through definitions set forth by the World Meteorological Organization's official glossary (WMO 1970). A lead is a linear feature, which occurs due to ice divergence along weak points in the ice. A polynya is defined as any nonlinear-shaped area of open water and/or sea ice cover < 30 cm thick enclosed by a much thicker ice cover (WMO 1970). It can be restricted on one side by a coast, termed shore polynyas, or bounded by fast ice, termed flaw polynyas. Polynyas that occur in the same position every year are called recurring polynyas (WMO 1970). The latter type can also be sub-divided into: those which remain open throughout winter and those which can freeze over during the coldest months, yet open in late winter or early spring. In contrast to leads, which form and freeze over periodically (e.g., < 1 day; Bauer and Martin 1983), polynyas, once formed, generally remain open until the surrounding ice cover breaks-up.

Two generalized mechanisms, termed latent and sensible heat, act to form and maintain polynyas (Smith *et al.* 1990). A latent heat mechanism involves wind and/or current driven divergence of ice (along a coast, ice shelf, grounded ice berg or landfast ice structure) with the latent heat of fusion, released from continual ice accretion, balancing heat loss to the atmosphere and hence maintaining open water. A polynya formed under this type of mechanism is expected to be associated with high ice deformation (i.e., ice deformation caused through surface turbulence). Alternatively, a sensible heat mechanism impedes the formation of ice through a warm oceanic heat input and would therefore be less likely associated with high ice deformation. Due to a polynya's dependence on atmospheric and oceanic processes affecting its sea ice cover, the significance of a polynya is strongly linked to the significance of sea ice. Consequently, polynyas are thought to be sensitive to climatic change (IAPP 1989).

The presence of recurring polynyas in the Arctic makes them important to all biological life (Stirling 1980, 1997; Massom 1988) including indigenous peoples (Schledermann 1980). They provide overwintering areas for many marine mammal species including: polar bears (*Ursus maritimus*), ringed seals (*Phoca hispida*), bearded seals (*Erignathus barbatus*), walruses (*Odobenus rosmarus*), beluga (white) whales (*Delphinapterus leucas*), narwhals (*Monodon monoceros*) and bowhead (Greenland Right) whales (*Balaena mystiscetus*) (e.g., Stirling 1980, 1997; Finley and Renaud 1980). In the spring, they can account for early and enhanced primary production blooms (e.g., Lewis et al. 1996), which provide

food for higher trophic level feeders (Welch et al. 1992). Subsequently, polynyas are important to early spring migrations for all of the mammal species mentioned above and many seabird species. Some of the more prominent seabird species include: dovekies (*Alle alle*), thick-billed murres (*Uria lomvia*), black guillemotts (*Cepphus grille*), black-legged kittiwakes (*Rissa tridactyla*), ivory gulls (*Pagophila eburnean*), glaucous gulls (*Larus hyperboreus*) and northern fulmars (*Fulmaris glacialis*) (Nettleship and Evans 1985).

The North Water (NOW) refers to a region of anomalous sea ice cover in northern Baffin Bay (Fig. 1.1). It encompasses both Canadian and Greenland waters (Fig. 1.1), which makes the region of international interest. Further, it is home to the largest recurring polynya found in the Canadian Archipelago. The NOW polynya has also been acknowledged as perhaps the most biologically significant polynya in the Canadian Arctic due in part to its size and permanence (Stirling 1980; 1997). Consequently, the NOW has drawn attention from a multitude of different academic fields including circumpolar specialists from both the physical and social sciences. Of particular interest to researchers are the physical mechanisms that act to form and maintain the polynya and their relationship to climate change and local biology.

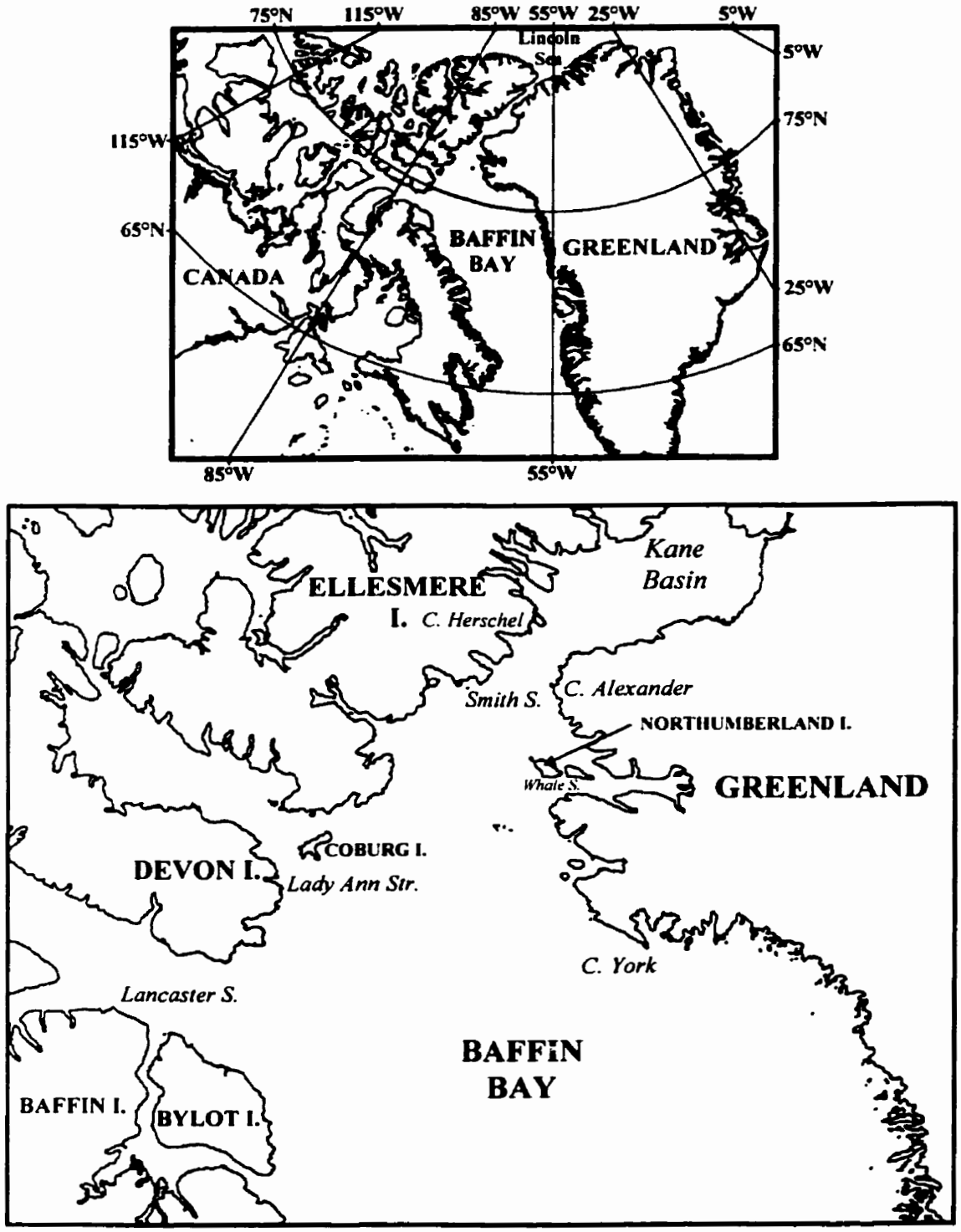


**Figure 1.1.** A map of the North Water of northern Baffin Bay.

As discussed above, the formation, circulation and subsequent contributions of Arctic sea ice to the freshwater flux into the North Atlantic play an important role in the thermohaline circulation of the global ocean (Aagaard and Carmack 1989). Contributions of sea ice through the Canadian Arctic Archipelago were assumed to be negligible as the majority of ice in this region was thought to be stationary (e.g., Aagaard and Carmack 1989). More recently, very thick sea ice has been observed through animations of 85.5 GHz Special Sensor Microwave Imager (SSM/I) imagery and Arctic buoy deployments to periodically drain through the NOW, alternating with the formation of ice bridges along its path towards Baffin Bay (Agnew 1999). Furthermore, the accretion of new ice produced in the open water of the NOW contributes substantially to this exported volume. A rough calculation of the volume of ice exported through this region came out to an order of magnitude less than that through Fram Strait supporting the importance of this contribution (Agnew 1998).

With the advent of the RADARSAT-1 satellite and its onboard synthetic aperture radar (SAR) sensor, we are now able to monitor the surface at spatial and temporal scales representative of regional sea ice processes independent of weather conditions. In this thesis I use RADARSAT-1 ScanSAR wide beam mode images and surface validation data to examine the spatial and temporal patterns of sea ice in the NOW throughout 1998. Interpretation of the results is based on the potential contributing polynya mechanisms (i.e., latent versus sensible heat) in order to test what has been found in other parallel studies and

provide insight where data collection has been lacking. Further, biological implications of the North Water's sea ice cover patterns are examined.

More specifically, the main objectives of this thesis are: (1) to develop a robust ScanSAR sea ice classification scheme; (2) to examine the spatial and temporal patterns of sea ice cover within the North Water (NOW) in relation to the potential physical mechanisms responsible for the NOW polynya's occurrence, and (3) to relate the sea ice spatio-temporal patterns to the potential for biological productivity within the NOW.

This thesis is separated into six chapters. The significance of this research and the problem being investigated are outlined in the first chapter. In the second chapter, I provide a background on theory and terms used in the thesis. Following this, a description of data collection, analysis framework and analytical methods is provided in the third chapter. In chapter four I discuss a purpose-built (i.e., objective 1) sea ice classification scheme for RADARSAT-1 ScanSAR wide beam mode data collected over the North Water. In the fifth chapter I discuss the results relating to objectives 2 and 3 of this thesis. Finally, in chapter six I present conclusions and recommendations for future analysis.

# CHAPTER 2: BACKGROUND

In this chapter I provide an overview of sea ice, the North Water and Synthetic Aperture Radar (SAR), segmented into 3 sections. The first section describes the evolution and subsequent charateristics of sea ice. In section two I examine our current knowledge pertaining to the North Water (NOW). In the final section I describe the basic theory of Synthetic Aperture Radar (SAR) data in relation to remote sensing of sea ice. In particular I introduce the Grey Level Co-occurrence Matrix (GLCM) as a tool in separating various ice types from SAR imagery.

## *2.1 Sea Ice Types: Evolution and Characteristics*

Since the 1970's, sea ice has been extensively studied as it is thought to be a sensitive indicator of climate change (Barry et al. 1993) and plays an active role in the global climate (e.g., Aagaard and Carmack 1989). This section describes the evolution of sea ice types in differing environments and subsequent

characteristics including some key definitions that will be used throughout this thesis[1].

Sea ice is defined as any form of ice found within the ocean that has originated from the freezing of seawater (WMO 1970). Seawater is a combination of pure water and various dissolved solids (salts) and gases with an approximate salinity of 35‰. It should be noted that ocean salinity varies greatly between water masses, particularly at polar latitudes (Carmack 1990). The formation of ice from seawater is a complex process where the salt and gas components are squeezed out and trapped within as the pure water component creates hydrogen bonds forming crystals of ice. The result is a mixture of ice, brine (a concentrated salt-water mixture), solid salts (if temperatures are cold enough) and gas (Weeks and Ackley 1986).

Based on mobility, sea ice is distinguished as either fast ice or pack ice. Fast ice refers to ice that is fastened to land and is therefore immobile. It may form *in-situ* or by freezing of free-floating ice to the shore or fast ice edge. Alternatively, pack ice refers to mobile ice or any form of ice that is not fast ice.

Temporally, sea ice develops through the following chronological stages: (i) new ice, (ii) nilas, (iii) young ice, (iv) first-year ice and (v) old or multiyear ice. New ice refers to very thin ice forms that are a collection of individual crystals not completely frozen together. Nilas and young ice are transition stages based on ice thickness and crystal structure. First-year ice refers to ice developed from

[1] General terminology of sea ice used this thesis is based on mobility, age/thickness and form; however the definitions by no means encapsulate all types of sea ice that have been delineated. For a complete synthesis, please refer to WMO (1970) and/or MANICE (1994).

young ice that is not more than one winter's growth. Old ice has been split up into second-year ice (survived only one summer's melt) and multiyear ice (survived at least two summers' melt) by the WMO (1970). However, most scientific literature uses the term "multiyear" ice in reference to both old ice types (e.g., Weeks and Ackley 1986). I will use the latter reference in that "multiyear" ice will refer to ice that has survived at least one summer's melt. Throughout this temporal development sea ice can demonstrate numerous forms and features depending on environmental conditions. These developed forms and features are the basis for further sea ice distinction.

Ice crystals begin to form when seawater is supercooled (i.e., cooled below its freezing point of approximately –1.8°C; Fig. 2.1). Unlike freshwater, the freezing point of seawater is generally higher than its temperature of maximum density (Fig. 2.1). However, like freshwater, the solid state of seawater is less dense than its liquid. Therefore, surface cooling of seawater induces convective mixing up to several meters thick. When the water is supercooled, ice crystals rapidly form around nuclei in this mixed layer and eventually rise to the surface. These initial particles, termed frazil (sea ice crystals suspended in the water column), are disc shaped, highly saline (due to instantaneous accretion that traps a substantial portion of salts) and form the surface layer of all first-year sea ice (Fig. 2.2). This layer is generally characterized by a random crystal orientation (Weeks and Ackley 1986).

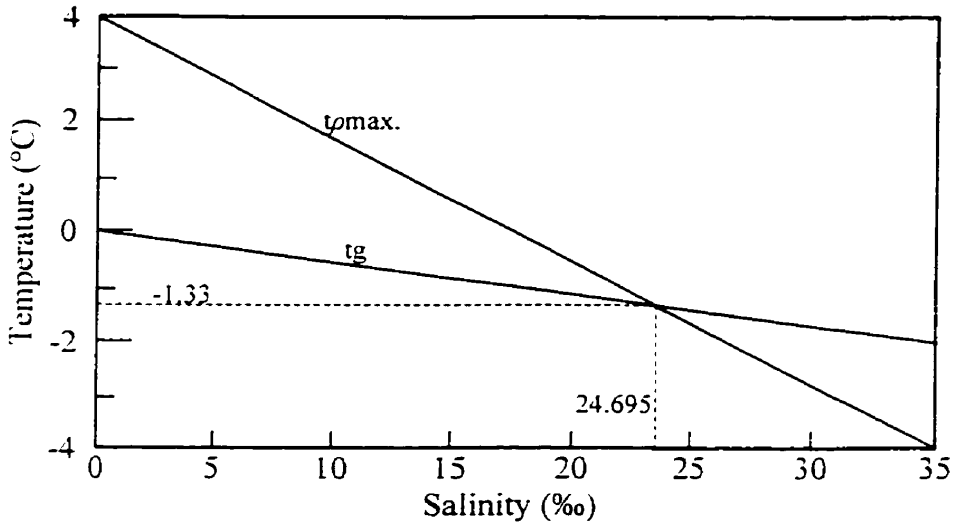


**Figure 2.1.** Temperature of the density maximum (tρmax) and of the freezing point (tg) for seawater of different salinities (After Weeks and Ackley 1986).

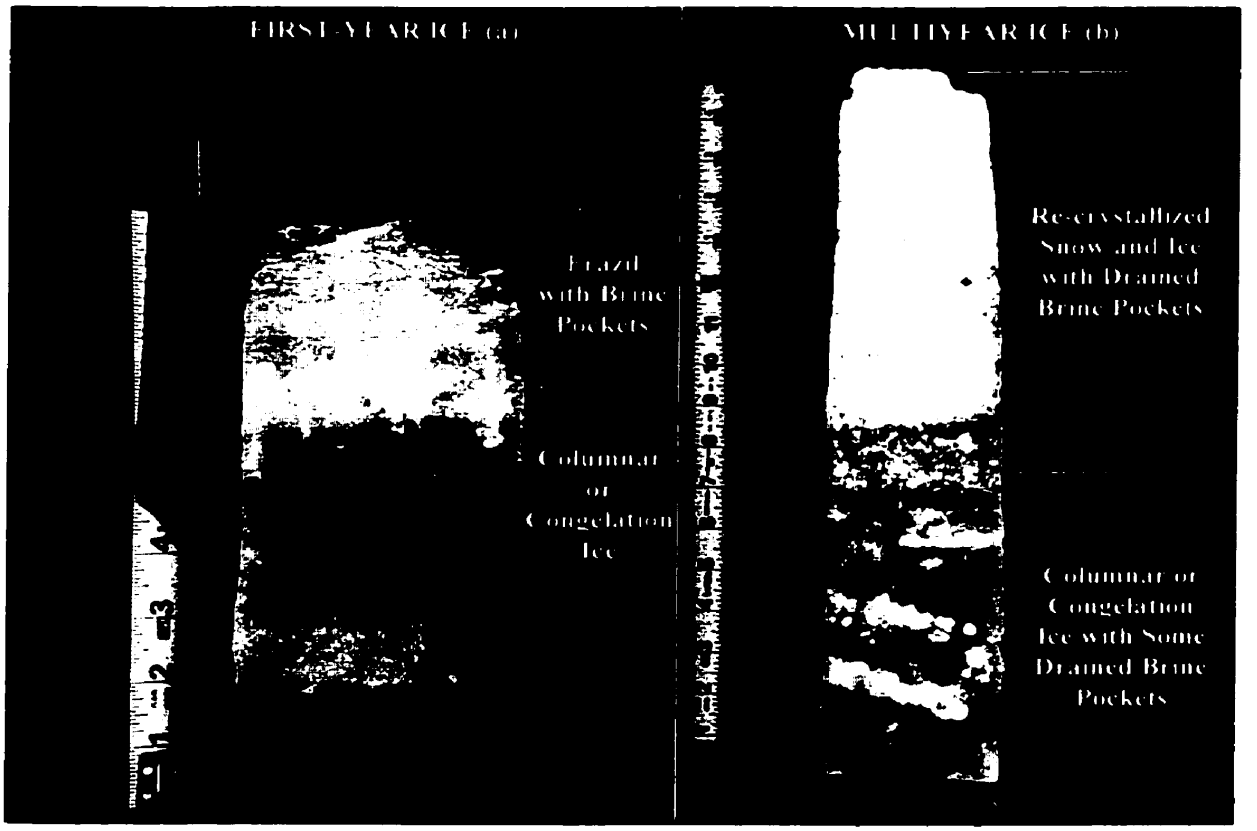


**Figure 2.2.** Ice core half sections of first-year ice (a) and multiyear ice (b), demonstrating basic layers of the ice types.

In calm, cold conditions, frazil accumulates at the surface and quickly congeals. The result is a very thin frazil layer with a uniform, smooth surface and is referred to as sheet ice (Weeks and Ackley 1986). These conditions can occur anywhere in Baffin Bay, but are short lived. They are usually restricted to bays and wind-protected coastlines where ice forms into landfast ice. The initial stage of sheet ice, termed nilas (sheet ice up to 10 cm thick), is very elastic and has a low albedo (Fig. 2.3). The elastic nature of nilas allows the ice to undulate with passing waves and swell and under pressure results in a unique rafting pattern, termed finger rafting (Fig. 2.3).

Under very cold temperatures and high relative humidity frost flowers may form on the surfaces of new ice and nilas. Frost flowers are very saline ice crystal formations (Fig. 2.4). They can reach heights of 15 mm and cover up to 90% of the sea ice surface (Martin et al. 1995). The formation of frost flowers results in the rapid change of sea ice surface albedo and roughness (Martin et al. 1995). Beneath the frost flowers, a high salinity slush layer forms. This layer has been found to affect the signature on many different satellite sensors (Ngheim et al. 1997). Frost flowers are also short lived due to a very fragile structure that can easily break in the wind and/or become covered by snow.

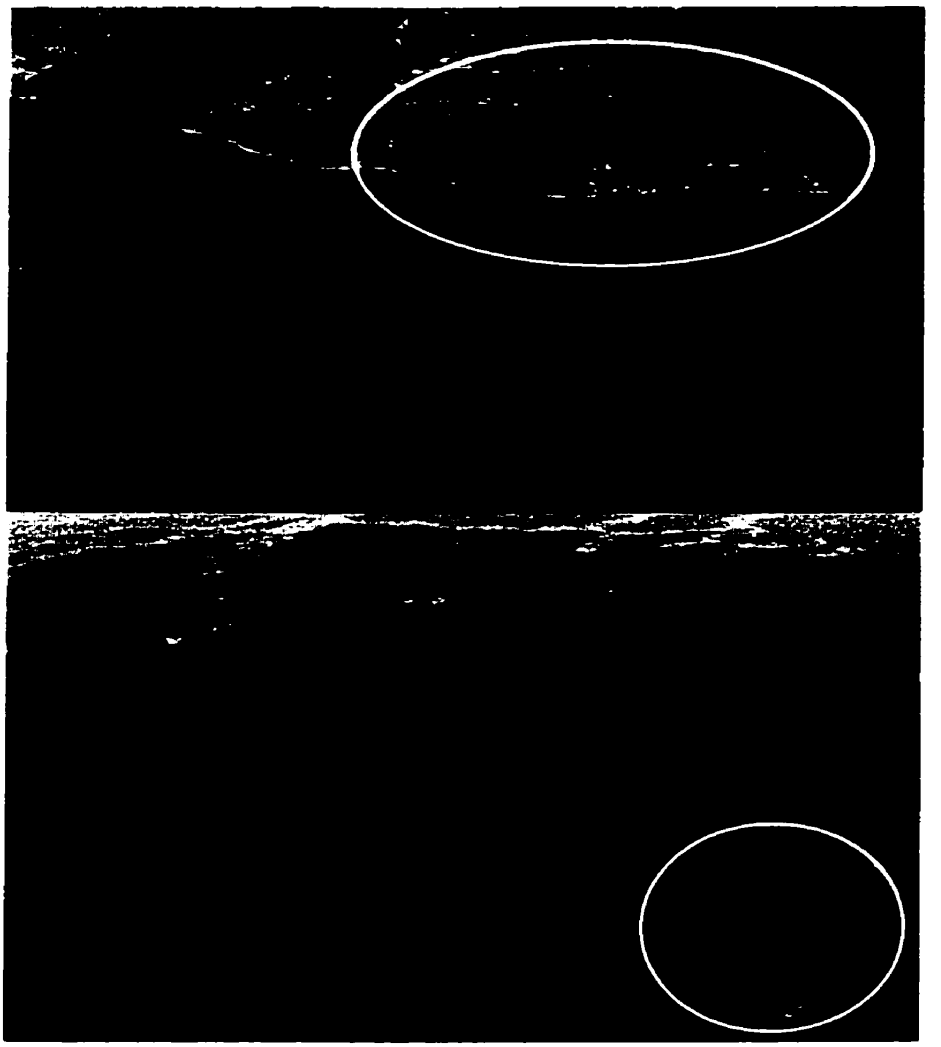

**Figure 2.3.** Nilas formed during a period of wind abatement. Top and bottom pictures are a close-up and horizon view, respectively. Finger rafting is present (examples are circled) and the beginnings of some frost flowers (top picture). Picture was taken in Smith Sound, 1998.

**Figure 2.4.** An icescape of frost flower covered young ice (15 cm thick) formed during a period of cold, calm conditions. Picture was taken in northern Baffin Bay, 1998.

In areas of higher wind and wave turbulence (e.g., conditions of a latent heat polynya mechanism), the frazil layer can be up to a meter thick and much less uniform (Weeks and Ackley 1986). The turbulence favors frazil formation due to mixing of the surface water column which imports more nuclei into the area of supercooled water, provides energy to overcome the frazil's buoyancy and increases abrasive action between crystals (Weeks and Ackley 1986). As frazil accumulates due to wave action at the surface, a "soupy" layer is formed, termed grease ice. Grease ice is a new ice form. It has a very low albedo and dampens local waves creating a distinct oil slick appearance (Fig. 2.5). Closer accumulation of frazil in turbulent open water areas result in the formation of roughly circular pieces of new ice (up to 3 m in diameter and < 10 cm thick) with upturned edges, termed pancake ice (Fig. 2.6). The upturned edges are the

result of wave action, which cause repeated convergence and divergence between neighboring pieces of ice. The repeated contacts create the circular form and push frazil onto the edge of the pancake (Weeks and Ackley 1986).

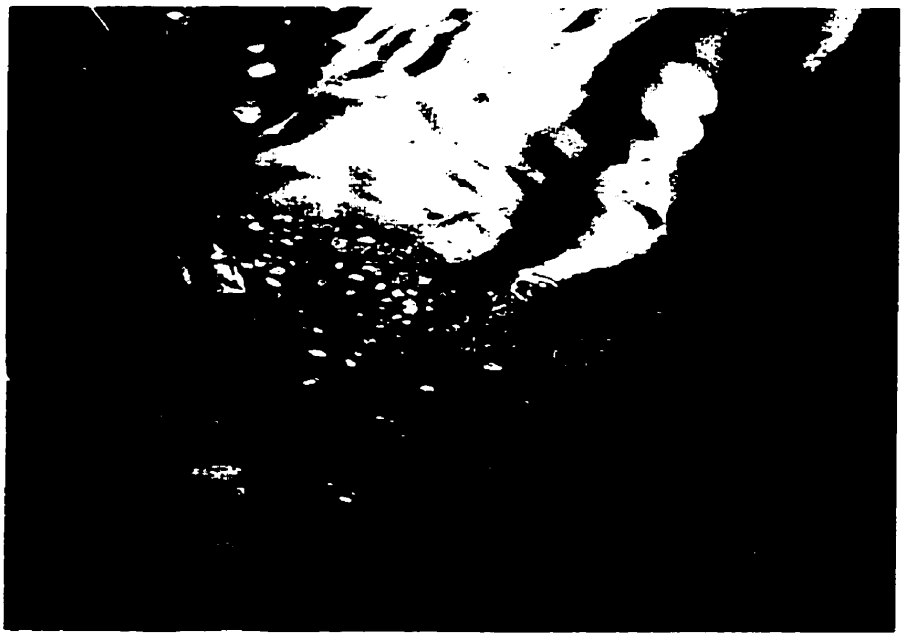

**Figure 2.5.** Grease ice forming on the upper right of the image. Dampening of surface waves has occurred, making the surface appear very smooth. Picture was taken in Smith Sound, 1998.

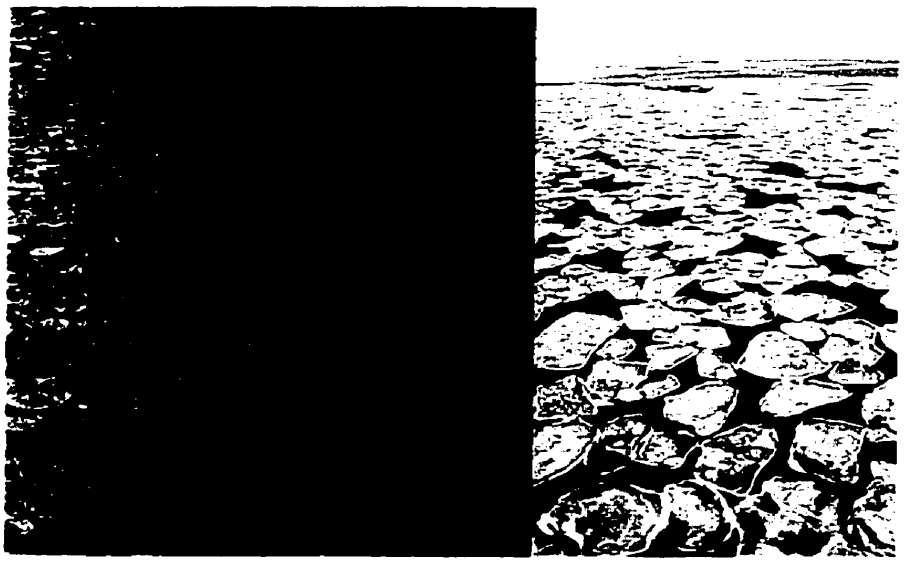

**Figure 2.6.** Pancake ice formed the day before during high wind conditions. Pictures were taken in northern Baffin Bay, 1998 (picture on right courtesy of K. Takahashi and N. Nagao).

The next stage of development is young ice, which has been subdivided into grey ice (10-15 cm thick) and grey-white ice (15-30 cm thick). This stage accounts for the transition from new ice and nilas through to first-year ice. New ice types begin to congeal as they become more compacted and/or a period of calm and cold conditions occurs (Fig. 2.7). This results in floes or sheets of ice of varying diameter. Once an ice surface has been produced, sheet ice will begin to form underneath the congeled grease and/or pancake ice. The ice is now produced as a result of sensible heat being conducted upward along a temperature gradient through the ice volume. Consequently, ice crystals begin to grow on the lower surface of the ice sheet as opposed to frazil formation (Weeks and Ackley 1986). Throughout a thin layer (approximately 5-10 cm), growth selection is made on crystal orientation. Vertical growth predominates creating a characteristic ice structure termed columnar or congelation ice (Fig 2.2; Weeks and Ackley 1986).


**Figure 2.7.** The beginnings of a young ice sheet formed through the congelation of pancake ice. Picture was taken as the ship broke through the ice in northern Baffin Bay, 1998 (picture courtesy of K. Takahashi and N. Nagao).

By the end of the young ice stage, sea ice is much less elastic. Finger rafting no longer occurs, although in areas of high wind and ocean stress rafting of these ice types (i.e., one piece of ice overriding another) can still occur (personal observation 1998). More likely, ice deformation takes the form of rubbling (ridging). For example, pack-ice floes can have upturned edges similar to pancake ice, but are the result of floe collisions and subsequent ice edge deformation. There is also a general trend of lateral ice sheet growth including the congelation of separate floes. This is due to tighter distributions of floes and less wave action as a result of the smaller open water area.

The transition from young ice to first-year ice is simply a thickness delineation. First-year ice has also been subdivided into 3 developmental stages based on its thickness. These stages are termed thin first-year ice (30-70 cm), medium first-year ice (70-120 cm) and thick first-year ice (> 120 cm). All first-year ice types are formed as sheet ice and can be either landfast or pack-ice.

Due to extensive columnar growth, first-year sea ice types have lower salinities by volume and are much less elastic than the younger ice types (Weeks and Ackley 1986). As a consequence, rafting becomes much less common. Under wind and ocean stress, rubbling of first-year ice generally occurs. Rubbling or ridging occurs due to compressive failures within an ice sheet as wind and current action cause converging horizontal pressures (Mellor 1986). This results in the forcing of one portion of the ice sheet upward and the other downward, forming a sail and keel, respectively. Common results of such ridging are the formation of extensive linear features termed pressure ridges (Mellor

1986). As mentioned earlier, rubbling can also occur due to collisions between two separate ice floes. The result is the piling of broken ice above and below each ice sheet. Extensive rubble fields can form as a result of this type of ice deformation and are common in areas of high wind and/or current action (Fig. 2.7). During similar conditions, first-year ice may also break into smaller floes, which take angular forms due to linear failures along hydrogen bonds in the ice (Mellor 1986).

**Figure 2.8.** Rubble field formed along the southern extent of the North Water polynya of northern Baffin Bay, 1998.

When first-year sea ice remains intact after one melt season, the ice is then termed old or multiyear ice. The vast majority of the Arctic Basin is covered by multiyear ice. This ice type is much less saline than first year ice due to preferential melt of brine pockets and subsequent brine drainage that occurs during ablation (melt). As a result of brine drainage and melting snow, pockets of air are formed during freeze-up within the surface layers of multiyear ice. This re-crystallized layer has been termed the active layer (Weeks and Ackley 1986). The surface of Arctic multiyear ice also demonstrates a characteristic rolling, or

hummocky topography (Fig. 2.9), the result of differential melt and freeze-up due to snow distribution (Weeks and Ackley 1986). A final feature of multiyear ice is its floe shape. Floes are generally rounded due to weathering and collisions between other floes. Further, floe size can be up to kilometers in diameter.

**Figure 2.9.** Multiyear ice that had most likely formed in the Arctic Basin. Ice thickness was >7 m on top of the hummock. Picture was taken in Wellington Channel, 1997.

Thickness of a multiyear ice sheet increases through successive winters. For example, the hummocks of very old ice can be well over 5 m (e.g., Fig. 2.9). This is due to annual growth layer additions to the bottom of the sheet, which can be used (in a similar fashion to tree rings) to tell the minimum age of an ice sheet (Weeks and Ackley 1986). Similar to first-year ice, multiyear ice can form

pressure ridges and rubble ice due to wind and current stresses. This deformation can also act to increase the average thickness of an ice sheet.

## *2.2 The North Water (NOW)*

In this section I provide a background on the North Water including: an evolving knowledge on the NOW polynya mechanisms; records of biological abundance and the reasons for their high numbers; and the use of remote sensing in monitoring and investigating the NOW sea ice cover.

### 2.2.1 The NOW Region

The anomalous region of open water found in northern Baffin Bay has been documented since the early part of the 17$^{th}$ century. Used by whalers, this region provided a means to start an early whaling season as a corridor for navigation into Lancaster Sound (Dunbar 1969; Nutt 1969). The open water was also well known to peoples of the Thüle culture and later the Danes who founded a trading settlement in northern Greenland (Dunbar 1969).

Coined as the 'North Water' by the frequenting whalers, the region encompasses Smith Sound and northern Baffin Bay (Fig. 1.1). The waters are equally shared between Greenland and Canada. Three recurring polynyas are recognized within the NOW region: the Smith Sound, Lady Ann Strait and Barrow

Strait – Lancaster Sound polynyas (Steffen 1985). Eventually, the three separate polynyas become contiguous in the early spring forming the NOW polynya.

### 2.2.2 Recent History of Knowledge on the NOW Polynya Formation and Maintenance

The formation and maintenance of the North Water polynya has been of interest since its documented discovery by William Baffin in 1616 (Dunbar and Dunbar 1972). Many famous explorers frequented the area in an attempt to decipher how and why the open water occurred. A debate on the physical mechanisms acting to form and maintain the polynya developed over the following centuries. Summaries of the history of knowledge on the formation and maintenance of the North Water are available in papers by Nutt (1969) and Dunbar and Dunbar (1972).

The Smith Sound polynya has drawn most recent attention due to its size, biological importance and the likelihood of a combined latent and sensible heat mechanism contributing to its formation and maintenance (e.g., IAPP, 1989; Smith et al., 1990; Mysak and Huang, 1992; Lewis et al., 1996). Muench (1971) had concluded that the main factor behind the polynya's occurrence was the blockage of ice entering the area due to an ice bridge and the southward removal of ice due to persistent winds and currents (i.e., a latent heat mechanism). The scientific community generally accepted this conclusion until Steffen (1985)

documented the occurrence of warm water cells off the coast of Greenland and other locations within the North Water.

Steffen (1985) concluded through calculations that sensible heat was an important factor behind the polynya's occurrence throughout winter and early spring. The possibility of a sensible heat mechanism had long been suspected (e.g., Nutt 1969; Dunbar and Dunbar 1972). The suspected source was a well-documented warm water layer at depth moving northward along the west coast of Greenland called the West Greenland current. Steffen (1985) was the first to provide convincing evidence of the current reaching the surface within the NOW. He suggested the warm water cells' existence could be explained by the coastal upwelling of relatively warm (> 0°C) Baffin Bay Atlantic water from the West Greenland current. The upwelling being induced through offshore surface water movement caused in part by the Coriolis force deflecting southward surface water movement to the right. However, Melling et al. (2000) noted that Steffen's (1985) radiation instruments only measured the ocean's skin temperature, creating an ambiguous oceanic interpretation of the data.

Bourke and Paquette (1991) were the next to investigate the contribution of sensible heat in the polynya's formation. Their study focused on the bottom and deep water of Baffin Bay. They noted the highest temperature between the surface and a 300 m depth in the vicinity of Smith Sound was –0.6°C. Bourke and Paquette (1991) concluded that upwelling of this water would not be a significant factor behind the NOW polynyas occurrence. This would later contrast with observations by Lewis et al. (1996).

Modeling efforts followed the work done by Bourke and Paquette (1991). Mysak and Huang (1992) coupled a latent heat polynya model developed by Pease (1987) for the NOW polynya with a reduced-gravity, coastal upwelling model. They concluded that the latent heat mechanism was dominant. However, Mysak and Huang (1994) did conclude that upwelling, which occurred on a slower time scale than the latent heat mechanism, played a role in determining the polynya width toward the Greenland coast.

Darby et al. (1994) used a nonlinear steady state model with an improved coastline as a follow up to Mysak and Huang's (1992) efforts. The steady-state nature of the model limited its application to after the polynya reached an equilibrium length, or after the polynya had opened. Similar to Mysak and Huang (1992), Darby et al. (1994) concluded that the latent heat mechanism was dominant, with the exception of late spring. During late spring, when heat loss to the atmosphere was reduced, they found the eastern ice edge to be largely influenced through a sensible heat mechanism.

Lewis et al. (1996) took a new approach to examining the possibility of a contributing sensible heat mechanism. They examined the primary productivity of the NOW. Collecting biological and oceanographic profiles over a 48 hr period in mid May, they found temperatures in the West Greenland current to be up to 2.4° above its freezing temperature (1.4° warmer than that observed by Bourke and Paquette (1991)) and phytoplankton biomass to be greatest along the west coast of Greenland with a westward decreasing trend. They concluded that sensible heat can play an important role and substantiated this with observations of higher

primary productivity that occurred along the coast of Greenland relative to the coast of Canada.

A factor that has not been examined in models or observations of the North Water is oceanic haline convection caused through brine rejection from freezing sea ice. Mysak and Huang (1992) noted the possibility, but did not include it in their model. However, with the high rates of ice production associated with a latent heat mechanism, one could expect the sensible heat contribution from haline convection to be substantial.

The debate on the importance of sensible heat contributing to the NOW polynya has yet to be finalized. Recent manuscripts (2000) by Barber et al., Melling et al. and Mundy and Barber continue the debate. These papers are discussed in Chapters 5 and 6.

### 2.2.3 Polynyas and Local Biology

The biological importance of recurring polynyas has been noted (Stirling 1980, 1997; Massom 1988). Close correlations have been demonstrated between recurring polynyas and historic Thüle settlements, whose culture largely depends on marine mammals for food (Schledermann 1980). Historically, whaler observations have demonstrated an early spring abundance of mammals and seabirds within and near anomalous open water areas in the Arctic pack-ice (e.g., Nutt 1969). Such observations were indicative of increased biological productivity (Stirling 1980; 1997). Stirling (1997) noted the early presence of

whales near polynyas and the observations of whales later in the season indicated both an early and extended period of food availability. Brown and Nettleship (1981) have made similar observations with seabirds demonstrating that most major colonies of cliff nesting birds in the Canadian Arctic were located in the vicinity of recurring polynyas. Based on these observations Dunbar (1981) hypothesized that phytoplankton productivity was high in polynyas. This hypothesis was later supported (e.g., Hirche et al. 1991; Lewis et al. 1996).

The primary explanation for increased primary production in polynyas, at least in early spring, is related to light limitation. Solar insolation is the main limiting factor during the initiation of primary production in sea ice covered waters (e.g., Gosselin and Legendre 1990; Welch and Bergmann 1989). The attenuation of photosynthetically active radiation (PAR) through sea ice is substantial (Maykut and Grenfell 1975). Furthermore, a snow cover can significantly increase the surface albedo and PAR attenuation (Barry et al. 1993). With ice concentrations of 90% or less, the effects of snow and ice on PAR attenuation become negligible due to transmission and reflection of solar radiation through small leads and cracks. This results in an adequate supply of diffuse light for primary production to occur (Smith 1995). In a polynya, these conditions are available long before adjacent ice covered areas.

Ice algae, a variety of marine microalgae associated with sea ice (also called sympagic or epontic algae), provide an initial source of primary production as they are well adapted to the low light levels available beneath the snow and ice cover. Estimates for ice algal contributions to total primary production range from

10 to 30% over an annual cycle (Alexander 1974; Welch et al. 1992). Within a polynya and along its outer edge, the effects of ice and snow on limiting ice algal production would be negligible.

Phytoplankton, primary producers suspended in the water column, account for the majority of Arctic primary production in an annual cycle (Welch et al. 1992). Both ice and snow cover and water column stability govern light limitation within the water column. As the water column becomes stratified or the mixed layer depth (MLD) shallows, phytoplankton can be entrained in an area favourable to growth relative to light availability (e.g., Maynard and Clark 1987). However, once stabilized the water is depleted of nutrients through consumption and no replenishment. This cycle and 'avoidance' of this cycle has been studied extensively within the marginal ice zone (MIZ) and along ice edges where a phenomenon known as an ice edge bloom occurs (e.g., Alexander and Niebauer 1981; Smith and Nelson 1986; Maynard and Clark 1987; Sullivan et al. 1988; Niebauer and Smith 1989).

Ice edges are very similar to polynyas in that they represent areas of enhanced biological production with elevated levels of mammals and seabirds relative to the surrounding ice-covered and ice-free sea. Although the formation and maintenance of polynyas are much more dynamic than circumstances at a receding ice edge, the mechanisms acting to enhance biological production are comparable (Massom 1988). It is also noted that a polynya actually contains an interior ice edge. Additionally, a polynya's ice edge begins to recede in early spring, earlier than surrounding ice-covered areas (e.g., Ito 1985).

Maynard and Clark (1987) compiled a list of possible components used to explain ice edge blooms previously proposed in literature. These components included: water column stratification through input of low-salinity melt water; nutrient replenishment through wind and tidal driven upwelling at the ice edge; an inoculum from released ice algal populations; and nutrient replenishment and distribution control through mesoscale eddies formed along the MIZ. Each mechanism does not necessarily occur along every ice edge and no single mechanism is needed for a bloom to occur (Comiso et al. 1993).

Although higher primary productivity has been noted as the most important factor in explaining elevated mammal and bird abundances within and adjacent to polynyas (Stirling 1980; 1997; Massom 1988), there are additional explanations for their high numbers. Stirling (1997) nicely summarized these as:

> "calmer water, which makes resting on the surface and diving for food easier than in open sea; access to a substrate to rest upon after periods in the open water; a temporary barrier to migration; a navigational aid to migrating species; a place where marine mammals can breathe and seabirds can feed in heavily ice-covered waters; habitat upon which, or into which, to escape from predators..."

Clearly, explaining the abundance of biology within and adjacent to polynyas is a complex problem. Further, the explanations used for any particular polynya will vary due to different oceanographic and atmospheric conditions. It is clear though, that the abundance is strongly related to sea ice.

### 2.2.4 Life within and adjacent to the NOW

In accordance with the previous subsection, the North Water is one of the most well known biological 'hot spots' in the Arctic. The Thüle culture has had settlements in the area for up to 3000 years, before which it was hypothesized that the polynya was not present (Schledermann 1980). Whalers used the region as a means to start an early whaling season (Dunbar 1969; Nutt 1969). Inuit hunters of Pond Inlet and Arctic Bay of northern Baffin Island also use the area to hunt narwhals and beluga as they follow leads and cracks away from open water in early spring (Stirling 1980). These statements alone indicate a consistent highly productive region with a large marine mammal population to sustain the human needs.

The NOW is also very important to seabirds. Seabirds forage solely in the marine environment and therefore need ice free water to gain access to their prey. Some of the highest seabird concentrations in the world are found within and adjacent to the region. Every year millions (*ca.*14 to 30 million pairs) of birds migrate to the North Water to feed and to breed along both the eastern Canada and western Greenland coasts, where there are widespread cliffs favourable for nesting (Nettleship and Evans 1985; Salmonsen 1981; Boertman and Mosbech 1998). During shipboard surveys conducted in the North Water, Dovekies (*Alle alle*) were the most numerous bird sighted with densities at times of over 1000 birds per square kilometer of water (personal communication N. Karnovsky). The polynya provides the seabirds with an extended period of time in which they can

conduct their breeding activities, which include: post migration feeding, courtship, egg laying and incubation, chick rearing, molting and pre-migration feeding activities. In order to support these numbers of birds, a high level and extended period of primary production would be needed.

Much less information has been collected on the biomass/abundance of mammals, fishes, plankton and ice algae in the region (IAPP 1989). The NOW encompasses a vast area and consequently it is hard to estimate numbers from very few observations. Finley and Renaud (1980) found very few marine mammals during aerial surveys made in mid March and mid May of 1978. They concluded that the North Water was not a major overwintering area for marine mammals. This work was re-visited during the International North Water Study (see section 3.1) by I. Stirling and M. Holst. They found the NOW to be an overwintering area for Bbowhead whales (Holst and Stirling 1999) as well as narwhals and walruses in accordance with Finley and Renaud (personal communication M. Holst).

Lewis et al. (1996) observed that chlorophyll *a* (Chl*a*) concentrations, an estimate of phytoplankton biomass, was comparable with that of an ice edge bloom. The highest Chl*a* concentrations occurred along the western Greenland coast near Northumberland Island with a decreasing trend toward the eastern Canada coast (Fig. 2.10). Chl*a* was also negatively correlated with water column nutrient concentrations, implying that the bloom had initiated along the Greenland coast and was progressively moving westward. Phytoplankton was found to occur in areas where evidence demonstrated the possibility of surface waters

mixing with the West Greenland Current at depth. It was concluded that there was a connection between the sensible heat processes occurring in the vicinity of Northumberland Island and the observed phytoplankton bloom (Lewis et al. 1996).

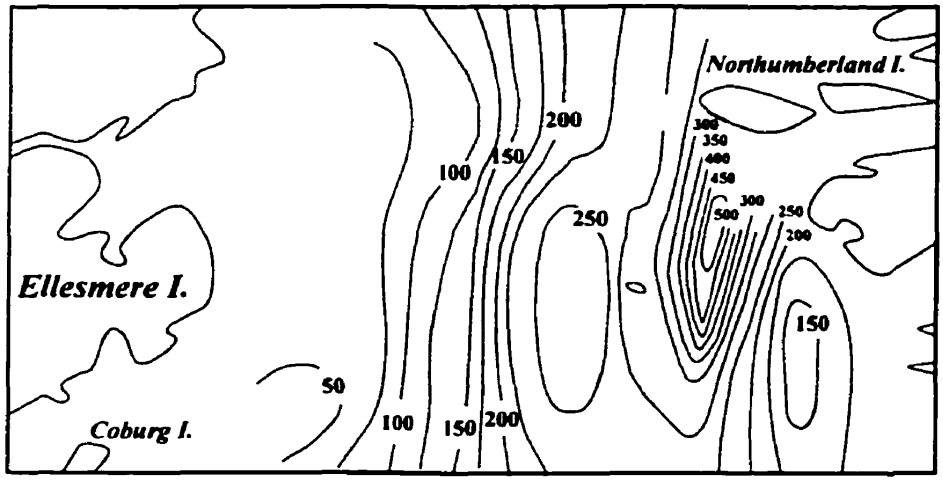


**Figure 2.10.** Areal concentrations of Chl*a* (mg $m^{-2}$) in the upper 30 m (After Lewis et al. 1996).

The International North Water Polynya study (see section 3.1) later based their hypotheses on Lewis et al.'s (1996) conclusion. Two underlying hypotheses were proposed: (1) a sensible heat mechanism would be associated with enhanced primary production due to early stratification, a subsequent warm surface mixed layer and replenishment of nutrients through upwelling; and (2) a latent heat polynya will be associated with a later primary production bloom due to late stratification (NOW proposal 1997). It is noted that initiation of primary production under a latent heat mechanism would still be earlier than adjacent ice covered areas.

### 2.2.5 Sea ice in the NOW

The size of the North Water has made it difficult for past explorers to delineate the extent of open water. Estimates made prior to aircraft and satellite observations were faulty. For example, the North Water was previously thought to be open year round (Nutt 1969). Dunbar (1969) was the first to note through visual aircraft observations that this was not the case. She compiled aircraft observations made by the U.S. Naval Oceanographic Office and the Canadian Meteorological Service between the years of 1954 to 1968. The data were averaged showing the first well defined extent of the polynya for the months of March through June (Fig. 2.11). She concluded that the ice edges along the coasts of Greenland and Canada and within Kane Basin were very consistent between years. Further, she found the southern ice extent was highly variable and dependent on climate and season.

In 1971-72, Dunbar (1972) flew ice reconnaissance flights using radar-scope photography and visual observations. The results were the first conclusive proof that the North Water consisted of very little open water during the winter months. It was found that most open water was restricted to the northern most area near Smith Sound. She also demonstrated that small open water patches occurred throughout the area, creating continual areas of ice formation and many different types of ice (Dunbar 1972).

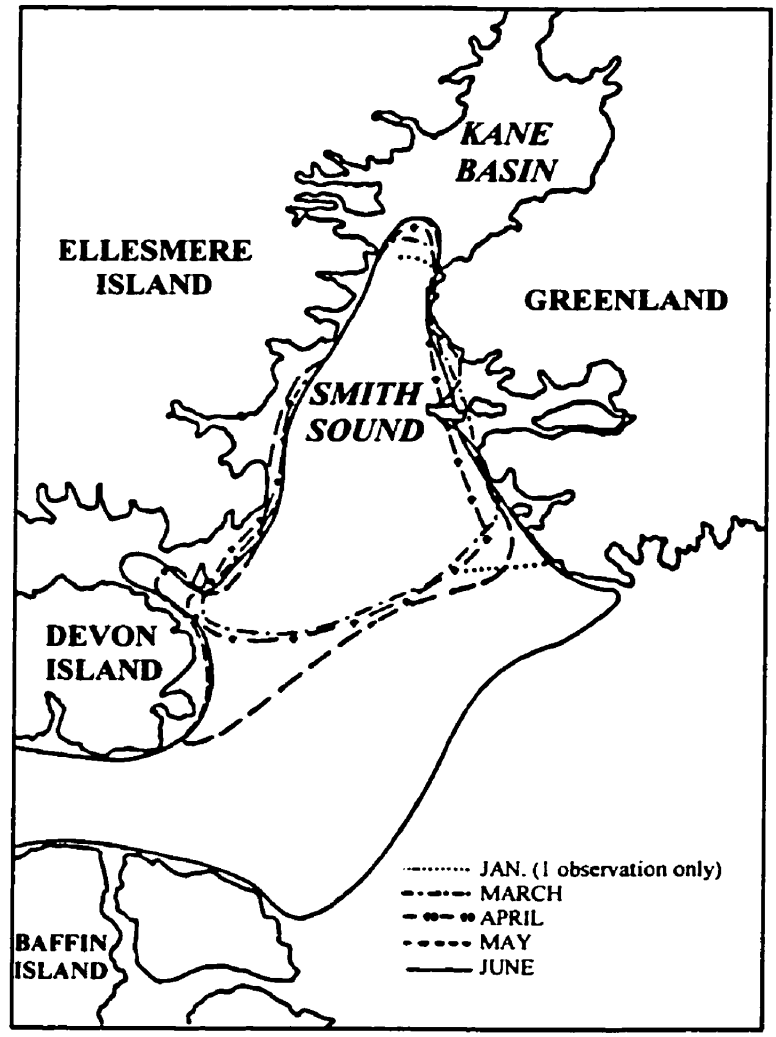


**Figure 2.11.** Mean monthly extent of the North Water (After Dunbar 1969).

Using a collection of thermal infrared data from the NOAA (National Oceanic and Atmospheric Administration) satellite-based AVHRR (Advanced Very High Resolution Radiometer) sensor, Smith and Rigby (1981) came upon the same conclusions as Dunbar (1969). They found the southern extent of the polynya to largely vary within and between years and stated this was due to weather conditions.

Ito and Müller (1982) furthered Smith and Rigby's (1981) statements, concluding ice motion through Smith Sound was strongly influenced by wind. They (Ito and Müller) used data from the near infrared channels of the Landsat satellites (1, 2 and 3). By delineating distinct ice features, such as a re-frozen lead and the edge of an ice floe, and tracking them between images they determined ice motion. A resultant mean velocity of 4.3 km $d^{-1}$ and speeds up to 34.9 km $d^{-1}$ were observed for ice flowing through Smith Sound (Ito and Müller 1982). These measurements were compared to land-based wind observations, which demonstrated a strong connection between ice velocity and wind speed. These were the first large scale measurements of sea ice motion within the NOW. However, there were large errors associated with their estimations and satellite data were temporally sparse due to cloud cover.

Sea ice type in the North Water was first examined by Ito (1985). He visually classified ice types by grey-tone from the same data set as Ito and Müller (1982). Subsequently, he was able to distinguish open water, new ice, nilas, grey ice and 'older ice' (grey-white ice and thicker) as well as landfast versus pack-ice. His observations were made during spring and early summer, as daylight was needed. Sea ice types and the decay were compared between 2 sub-regions, one over Smith Sound and one to the south. He found significant variation between these regions, with higher open water, nilas and grey ice concentrations within Smith Sound. It was concluded that the North Water consisted of a thin ice cover in winter and thus ablated earlier than surrounding areas in the spring (Ito

1985). However, no suggestions were made to explain why the North Water contained thinner ice in early spring.

Steffen (1986) provided the first substantial winter view of the North Water sea ice conditions. Through the use of a thermal infrared sensor on board an aircraft, Steffen (1986) was able to classify six surface classes: open water, dark nilas, light nilas, grey ice, grey-white ice and white ice (i.e., > 30 cm). During November, December and January, he found young ice, nilas and open water covered more than 50% of the Smith Sound polynya. However, the rest of the region, with the exception of small areas in Lady Ann Strait and Lancaster Sound, was near 100% white ice cover. Subsequently, Steffen (1986) noted the polynya in winter was much smaller than previously believed (he quoted Stirling and Cleator 1981). As well, he noted the open water and young ice were almost exclusively limited to the coast of Greenland off of Cape Alexander where he had previously found warm water cells with the same data set (1985).

During February and March Steffen (1986) found concentrations of white ice rose to over 50%. It was suggested in passing that extended periods of wind abatement were responsible for the increasing ice cover. It is noted here and revisited in Chapter 6 that Steffen's (1986) results tie into Ito's (1985) results, explaining why thinner ice would occur in the spring.

Agnew (1998) accomplished the next significant study on sea ice within or around the NOW. Although multiyear ice was known to occur within the NOW in substantial concentrations (e.g., Ito and Müller 1982; de Bastiani 1990), Agnew (1998) was the first to demonstrate a consistent drainage of multiyear ice from

the Arctic Basin and into the NOW. He did so using animations of 85.5 GHz SSM/I imagery. The drainage was found to periodically stop as ice bridges formed with Nares Strait and Smith Sound. He also noted the Lincoln Sea, found at the northern tip of Canada and Greenland (Fig. 1.1), is known to contain some of the thickest multiyear ice within the Arctic Basin due to deformation as it is compressed against the northwest coasts of Ellesmere Island and Greenland. Consequently, the drainage of multiyear ice into the NOW represents a significant contribution to the freshwater budget that was previously assumed to be negligible (Aagaard and Carmack 1989).

The application of both aircraft- and satellite-based remote sensing to the study of sea ice cover in the North Water has been demonstrated. This 'tool' allows for a much larger spatial and temporal coverage than previously attained through field measurements. Subsequently, many insights as to how and why the NOW polynya is formed and maintained were provided. However, there are still many questions left unanswered. New satellites and sensors, such as RADARSAT-1 and its onboard Synthetic Aperture Radar (SAR) sensor, are now better equipped to help answer these questions. Furthermore, there is a trend of increasing spatial and temporal coverage capabilities of these satellite systems, which will provide an ever-increasing amount of information.

## *2.3 Synthetic Aperture Radar*

In this section I describe why and how Synthetic Aperture Radar (SAR) is used extensively as a remote sensing device to detect sea ice types. I further this discussion with an examination of Grey Level Co-occurrence Matrices (GLCMs) and their use in aiding sea ice classifications of SAR imagery.

### 2.3.1 SAR Interactions with Sea Ice

A Synthetic Aperture Radar (SAR) instrument makes use of microwave energy that is virtually unaffected by all weather conditions and can be used day and night. These facts alone make the use of SAR in polar regions a very powerful tool. An additional advantage of using SAR over polar oceans is a unique sensitivity to sea ice. This sensitivity has provided the possibility to distinguish many important surface parameters. Some examples include: open water, wind velocity, sea ice type, age, concentration and snow cover (e.g., Ulaby et al. 1982; Kwok et al. 1992; Bel'chanskiy et al. 1996; Barber and Ngheim 1998).

SAR is an active microwave system. A SAR instrument transmits microwave signals or pulses of microwave energy and then records the portion of transmitted energy that is backscattered from the observed feature. In a SAR image, the amount of backscatter is represented with a relative grey-level scale. For example, the greater the backscatter is, the brighter the image. The amount

of backscatter is dependent on surface roughness, penetration depth of the transmitted energy and the presence of inhomogeneities within the observed material (e.g., gas pockets or salinity changes in sea ice) (Ulaby et al. 1982). These interactions are all controlled by the dielectric properties of the observed material relative to the other materials the signal passes through (e.g., the atmosphere). Dielectric properties define the electrical conductivity of the material relative to the wavelength, polarization and incidence angle of the transmitted energy.

Microwave scattering models separate the scattering process into surface and volume scattering. The relative complex dielectric constant is computed at each interface and as an average for each volume. The relative complex dielectric constant ($\varepsilon*$) given in equation 2.1 is used to express the permittivity ($\varepsilon'$) and loss ($\varepsilon''$) of the material. That is, $\varepsilon'$ is the ability of electromagnetic energy to pass into or through a particular interface or volume and $\varepsilon''$ is a measure of the transfer of energy to the material. The dielectric constant is expressed as the complex sum of a real and imaginary part where j is the square root of negative one.

$$\varepsilon* = \varepsilon' + j\,\varepsilon'' \qquad (2.1)$$

The extent to which an interface will act as a surface is proportional to the relative complex dielectric constant (Ulaby et al. 1982).

Discussed earlier, sea ice is a mixture of ice, brine, solid salts (if cold enough) and gas. Each component possesses a unique dielectric property at microwave frequencies and can exist in different characteristic sizes, shapes, volumes and distributions. Dielectric constants for air, ice and brine are approximately 1, 3 and 80, respectively. The proportion of each component determines the dielectric properties of sea ice. Although small in proportion, the high dielectric constant of brine significantly influences the dielectric properties of sea ice.

In a situation where an interface will predominately cause surface scattering (i.e., high relative complex dielectric constant), such as the interface between air and seawater or saline first-year ice, surface roughness and geometry will primarily determine the amount of backscatter. Calm open water, grease ice, nilas and smooth first-year sea ice all reflect most of the transmitted radiation away from the SAR sensor at the same angie as the incidence angle. This type of reflection is called specular reflection. In a SAR image, these surface types appear as dark signatures due to small backscatter values. Rougher surfaces, such as rough open water, rubbled ice and pancake ice, cause a higher probability of backscatter and therefore appear brighter in a SAR scene. Surface orientation relative to the sensor can also play a crucial role in the amount of energy return to the sensor. The degree of surface roughness is actually a continuum from specular reflection to diffuse reflection where roughness or surface variation ($h$) can be defined by the Rayleigh criterion given in Equation 2.2.

$$h < \frac{\lambda}{8 \cos \theta} \qquad (2.2)$$

where $\lambda$ and $\theta$ are the SAR wavelength and incidence angle, respectively (i.e., if $h$ is true, then the surface is considered smooth).

Like rough surface types, multiyear ice also appears bright in a SAR image. However, surface scattering is not the dominant scattering type for multiyear sea ice. In multiyear sea ice most of the brine has drained through preferential melt of the brine pockets (see section 2.1). The lower salinity results in a lower dielectric mismatch at the air-ice interface. This allows a greater penetration of the radar signal into the ice volume, which then interacts with internal inhomogeneites of the ice. The result is volume scattering.

Volume scattering is dependent on the density, size and geometric shape of scatterers. Scatterers have to be large enough to be resolved or 'seen' by a particular frequency in order to affect the signal. That is, the radar will interact with these ice inclusions only if their characteristic dimensions are at least one tenth that of the radar wavelength (Ulaby et al. 1982). Further, as the size of the particles approaches the wavelength of the signal, scattering increases. The re-crystallized active layer in multiyear ice primarily determines the amount of backscatter. The air pockets within this layer (Fig. 2.2) can cause, if large enough, significant scattering making the ice type appear bright in a SAR image.

As described above, SAR scattering over sea ice is largely dependent on the ice type. Backscatter over first-year sea ice with a saline surface is primarily dependent on surface roughness with very little volume scattering. Alternatively, the low salinity of a multiyear ice active layer and the presence of substantial volume scatters result in a greater importance of volume scattering to the SAR return. These unique interactions cause varying returns between different sea ice types, allowing for the possibility of their discrimination within a SAR scene. However, the distinction between various ice types is not perfect based purely on backscatter. Additional methods such as using spatial information (e.g., texture and contextual information) have to be employed to further distinguish ice types.

### 2.3.2 The Grey level Co-occurrence Matrix

Many investigations attempting to classify Synthetic Aperture Radar (SAR) data have explored the use of spatial information in an attempt to automate or assist in delineating different sea ice types (e.g., Homes et al. 1984; Barber and LeDrew 1991; Nystuen and Garcia 1992; Barber et al. 1993; Smith et al. 1995; Soh and Tsatsoulis 1999). The majority of these approaches examined second-order texture statistics derived from Grey Level Co-occurrence Matrices (GLCM).

Haralick et al. (1973) first defined the use of a GLCM in classifying imagery. The GLCM represents one of many second-order statistical approaches to texture analysis. For clarification, a first-order approach uses image tone (i.e., the grey level values representing relative backscatter in a radar image). Examples

of first-order statistics in radar imagery include the mean, standard deviation and range of a window of pixels (e.g., Nystuen and Garcia 1992). Second-order statistics also make use of grey level. The fundamental difference is that a second-order approach provides a measure of the spatial information between a pixel (image resolution cell) and its neighbors (Barber et al. 1993). The use of second-order approaches such as a GLCM derived statistic also adds robustness to the discrimination of SAR sea ice classes. Further, Shokr (1991) found evidence that second-order texture measures provide unique values for ice types, independent of absolute image calibration, a common problem with SAR imagery.

The GLCM provides the conditional joint probabilities of all pixel pairwise combinations within a given computational window size. Many different algorithms are available to extract specific information from the GLCM. Each provides a separate measure of localized texture. Therefore, some statistics outperform others in delineating sea ice types.

Holmes et al. (1984) accomplished one of the earlier studies on the use of texture analysis on SAR imagery. They confirmed the usefulness of applying a GLCM approach to delineate ice floe boundaries and discriminate multiyear from first-year ice types. Studies by Barber and LeDrew (1991) and Shokr (1991) demonstrated the power of different texture statististics individually and in combinations. However, not all classification studies have shown the same success in the use of GLCM statistics. For example, Nystuen and Garcia (1992) demonstrated only a marginally improved classification through the use of GLCM

statistics and recommended that first-order statistics should be used in order to minimize computational effort. Smith et al. (1995) supported these results though it was apparent that calibration of the SAR images had to be accomplished prior to the use of grey level and first-order texture statistics.

There appears to be a trade-off between the absolute calibration of images and the use of second-order texture statistics. Noted above, second-order textures can provide unique values for ice types independent of absolute calibrations (Shokr 1991). Barber et al. (1993) also noted that a second-order approach would be more dependent on the relative spatial variation. Therefore, second-order texture measures can provide unique information on the spatial variation of grey tones.

In this chapter I have reviewed all major aspects pertaining to my thesis. In the first section I described the evolution of sea ice types in differing environments and subsequent characteristics including some key definitions that will be used throughout this thesis. In the second section I described the North Water and provided a recent history of knowledge on the NOW polynya mechanisms, documents of biological abundance and the potential reasons for their high numbers and the use of remote sensing in monitoring and investigating the NOW sea ice cover. A description of SAR interaction with sea ice was included in the final section. This also included a brief description of the use of GLCMs in SAR sea ice classifications. In the next chapter I describe the methods

used in this thesis. This includes descriptions of the data collection, Geographic Information System (GIS) framework and data analysis.

# CHAPTER 3: METHODS

In this chapter I describe the data used in this thesis and how it was analyzed to meet my stated objectives. The chapter is presented in four interrelated sections: (1) the International NOW Polynya Study, the project from which data were collected for this thesis; (2) the data sets used here, including both satellite and field data and the methods employed to collect and validate the data; (3) the Geographic Information System (GIS) framework that was designed and implemented for the purpose of this thesis; and (4) the spatial and temporal analytical methods used to meet my thesis objectives.

## *3.1: The International North Water Polynya Study*

In 1990, the Arctic Ocean Science Board launched the International Arctic Polynya Programme (IAPP) initiative with the following mission statement: "To intensively study the physical/meteorological processes leading to the formation of polynyas and of the biological and biogeochemical processes taking place within their boundaries" (IAPP 1989).

The North Water polynya is considered to be one of the most productive areas above the Arctic Circle and is located at a latitude thought to be impacted

early and significantly by the present trend in climate change (NOW Proposal 1997). As a result, many leading Arctic specialists from Canada and abroad (Denmark, Poland, United States, Japan, Mexico, Belgium and the United Kingdom) proposed the highly integrative and multidisciplinary International North Water Polynya Study. This was the second polynya study (the first was the Northeast Water Polynya Study in the Greenland Sea during 1992 and 1993) to be initiated under the umbrella of the IAPP. The NOW project was built around a central hypothesis linking biological productivity of the North Water to local climatic and oceanographic forcing (see Chapter 2) while exploring the response of the ecosystem to the climate change scenario through modeling (NOW Proposal 1997). During the summer of 1997 (onboard the *CCGS Louis ST. Laurent*) and the spring and summer of 1998 (onboard the *CCGS Pierre Radisson*) field data of various oceanographic, meteorological, biological and biogeochemical variables were successfully collected within the NOW polynya. Data used in this thesis were collected during the 1998 expedition.

### *3.2 Data*

Critical for understanding the mechanisms behind polynya formation and maintenance is our ability to monitor them. During The International North Water Polynya Study (NOW study) 1998 expedition both satellite and field data were collected. In this section I describe these data, including the methods used to collect and validate them.

### 3.2.1 RADARSAT-1 Data

Launched in 1995, RADARSAT-1 is the newest satellite-borne SAR sensor providing unequalled spatial and temporal coverage of the polar seas. A total of 153 ScanSAR Wide A and B beam mode images were obtained from RADARSAT-1 over the period January 21 through December 7, 1998 (Canadian Ice Service (CIS)). RADARSAT-1 has an operating frequency of 5.3 GHz with HH polarization. ScanSAR images were acquired over the NOW with the following characteristics: swath width of 460 km; 100 m pixel spacing; 8 bit pixels; and swath lengths variable from 1000 to 2000 km. Incidence angles ranged between 20° and 49° across a single scene. Temporal gaps between images ranged from 12 hours to 1 week. The data were also uncalibrated with characteristics such as inter-beam seams and unbalanced radiometric levels across an image causing image intensity to be brighter in the near range.

Images were attained as blocks or segments in a ScanSAR file format, which were processed at the Central Data Processing Facility (CDPF) in Gatineau, Quebec. Each segment was 5000 lines long, with the exception of the final block that was variable in length. Typical scenes were 2 to 4 segments long (i.e., 1000 to 2000 km). Image blocks were concatenated into one scene before use.

### 3.2.2 Field Data

Field data were obtained from April through June 1998 using the Canadian Coast Guard Ship (CCGS) *Pierre-Raddison* (Fig. 3.1). Both ship and helicopter provided access to 68 sampling sites. At each sampling site an initial survey of the sampling area provided an estimate of homogeneous floe size (if applicable), ice concentration, ice type and surface roughness (Fig. 3.2). A site photograph followed this survey then ice thickness and freeboard were measured through a 2-inch diameter auger hole. Ice cores up to approximately 70 cm were collected using a 10 cm diameter core auger. These cores were used to measure density and salinity of the upper most layers of the ice. Additional cores were used for an instantaneous temperature profile measurement and for pictures to determine the ice structure (e.g., Fig. 2.2). Positional information from a hand held Global Positioning System (GPS) was also obtained.

**Figure 3.1.** Helicopter view of the CCGS *Pierre-Raddison*. Picture was taken in northern Baffin Bay, 1998.

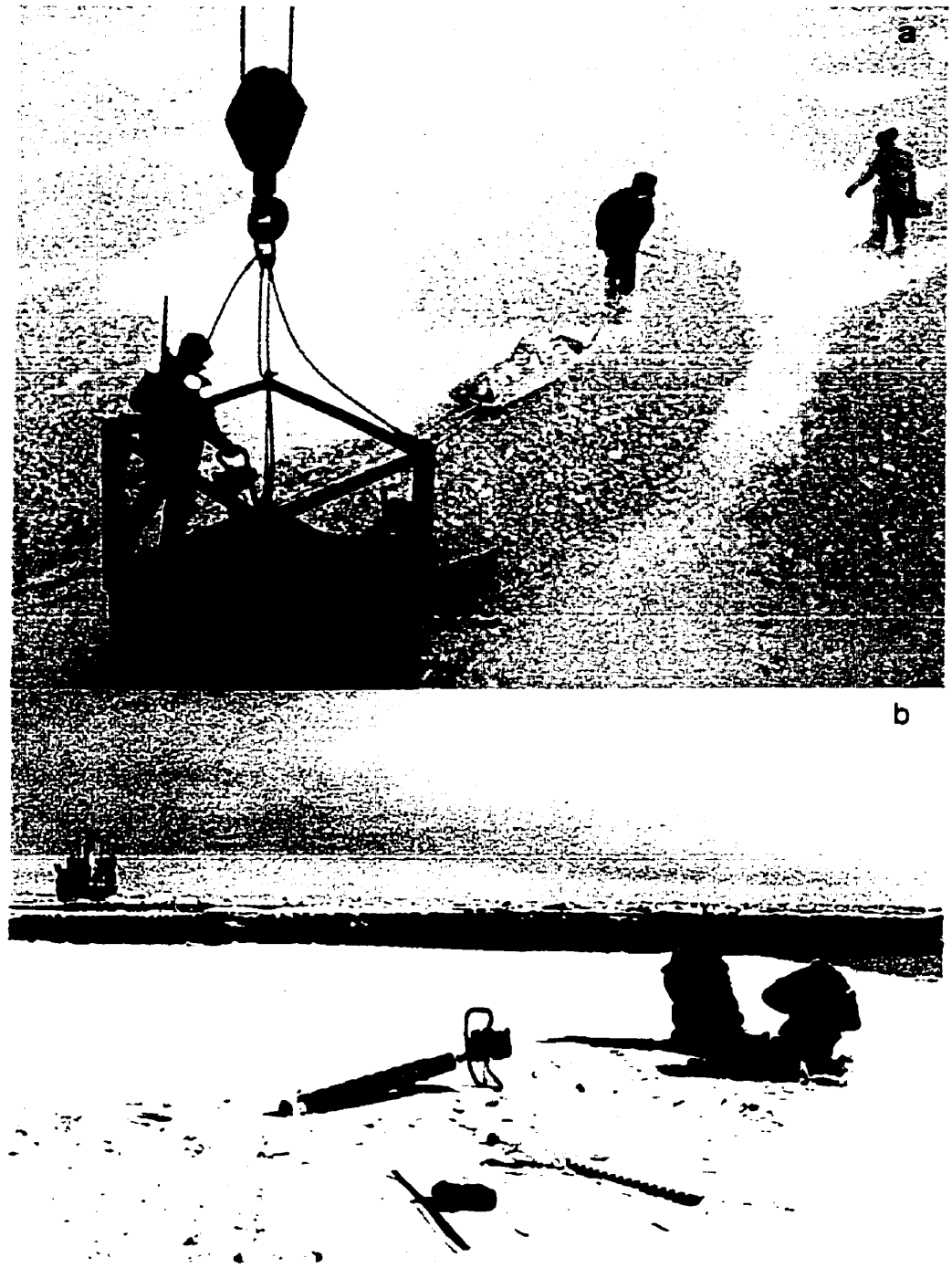


**Figure 3.2.** Pictures of starting a sample site after being craned to the sea ice sample site via a metal 'basket' (a) and sampling an ice floe approximately 50 m in diameter (b). The CCGS *Pierre-Raddison* is visible in the background of the picture b. Pictures were taken in northern Baffin Bay, 1998 (Pictures courtesy of K. Takahashi, N. Nagao and E. Key).

For inaccessible sites (e.g., thin ice or small floe size) a Hi8 video camera was used to document ice type, concentration and floe size. Near continuous video was obtained from a camera mounted on the bridge of the CCGS *Pierre-Radisson* with periodic visual observations of sea ice conditions input to a database. Input to the database included a time stamp and a geographic position obtained from a GPS mounted on the roof of the bridge. Daily check-ups were used to confirm the computer clock was at the same time as the camera clock.

A camera was also mounted on a helicopter and systematic grid surveys were flown in the vicinity of the ship. Flight times were planned near satellite overpass times. They were flown at an opportunistic basis dependent on weather, location and helicopter allocation time. Flight plans followed a 25 km x 25 km square grid pattern that was separated into 5 transects, each 25 km long with a north-south orientation. Before a flight, both the camera and computer clocks were synced with the helicopter's GPS clock. As the camera was mounted on the rear of the helicopter (Fig. 3.3), the camera was turned on prior to the flight. During a flight the computer was plugged directly into the helicopter's GPS and logged the helicopter's position in real time. The passenger in the front of the helicopter also manually logged the flight. This included recordings of: the start and stop time of each transect; the helicopter's altitude and speed at the beginning and end of each transect; identified ice types and the time of the observations; and percent cloud cover.

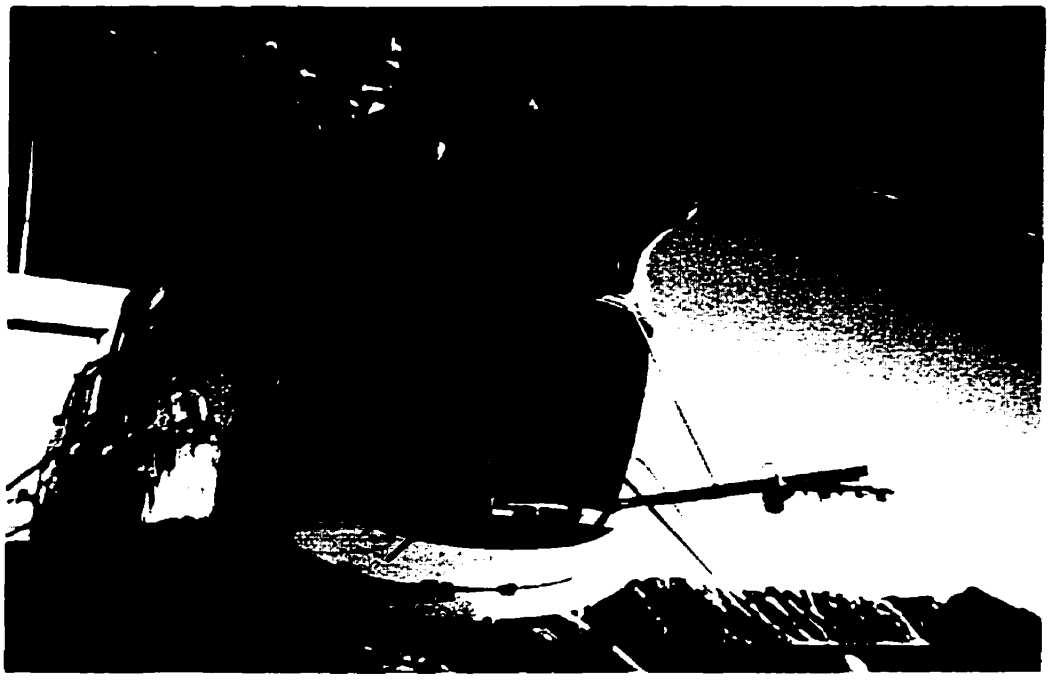

**Figure 3.3.** Photograph of camera and other sensors mounted on the rear of the CCG helicopter during a grid survey.

### 3.2.3 Data Validation

The field data were sorted and identified as to delineate ice types, concentrations and floe sizes within a ScanSAR image. Subsequently, all observations used in this thesis were made near the time of satellite overpass (all scenes were acquired between 2115 and 2245 (ascending pass) and 1150 and 1250 (descending pass) UTC). The process of identifying a field observed ice type with a signature on a ScanSAR image was accomplished within ArcView, version 3.2.

The ScanSAR scene associated with a particular field observation was geo-rectified to a Lambert Equal-Area Azimuthal projection. This projection was

chosen as to minimize the amount of image distortion from the geo-rectification process (also termed image warping and/or geo-coding). In order to geo-rectify a ScanSAR image, Ground Control Points (GCPs) were used. GCPs were associated with each image line within a processed ScanSAR file. The latitude and longitude of the first, middle and last column of each image line were extracted from the file using a program called ScanSAR Viewer (developed by CIS). A Macro was written in Excel to extract 100 equally spaced sets of first, middle and last column positions into a new spreadsheet. This spreadsheet of 300 positions was used to geo-rectify an image.

The GCPs were plotted over both the ScanSAR image and projection using the ArcView extension "Image Warp". A third order polynomial was chosen for the warping formulae. This resulted in a Root Mean Squared (RMS) error between 1 and 2 pixel units for each image. RMS error is an estimation of how well the GCPs fit from the image onto the projection as a result of the warping formulae. Consequently, the RMS error implied that each GCP for an image was warped within 100 to 200 m of the projected GCP. Although this error was larger than the pixel size, it was accepted for the purpose of locating validation signatures of ice types.

The field data were first sorted as being collected close to the time of an acquired ScanSAR scene. The latitudes and longitudes associated with the field data were plotted onto the same Equal-Area projection and matched to signatures on each ScanSAR scene. Validating the field observation location was

the ship's position. The ship was usually visible as a couple of very bright pixels in the ScanSAR imagery (e.g., Fig. 3.4).


**Figure 3.4.** A ScanSAR image sample showing the CCGS Pierre Raddison (arrow pointing to cluster of bright pixels) in an icescape of nilas ice underneath the Kane Basin ice bridge. Date and time of the RADARSAT-1 overpass was April 11, 1998 and 21:18 UTC, respectively.

For the purpose of selecting training and test data for the classification, validated sea ice signatures had to cover at least 30 pixels. After locating a sea ice type signature on the geo-rectified image, it was located on the original image by identifying the ship pixel (if possible) and by finding distinct patterns surrounding the signature. Field validation of 14 separate surface classes concurring with more than 1 acquired ScanSAR image was accomplished (Table 3.1). Different classes were selected based on both WMO (1970) surface ice classes and visual delineation of the SAR signature (Fig. 3.5 and Table 3.2).

**Table 3.1.** Validated surface types for RADARSAT-1 ScanSAR wide beam mode imagery.

| Surface Type | Abbreviation | Ice Thickness (cm) |
|---|---|---|
| Calm Open Water | COW | 0 |
| Rough Open Water | ROW | 0 |
| New Ice /Nilas | NI | < 10 |
| Grey Ice | GI | 10 - 15 |
| Pancake Ice | PI | < 15 |
| Frost Flower Covered Ice | FFI | < 15 |
| Grey-White Angular Floes | GWF | 15 - 30 |
| Medium First Year Ice | MFYI | 30 - 120 |
| Brash Ice | BRI | variable |
| Thick First Year Ice | TFYI | 120 - 210 |
| Rough/Rubble First Year Ice | RRI | > 200 |
| Multiyear Ice | MYI | > 200 |
| Rubble Ice | RI | > 200 |
| Icebergs | IB | variable |

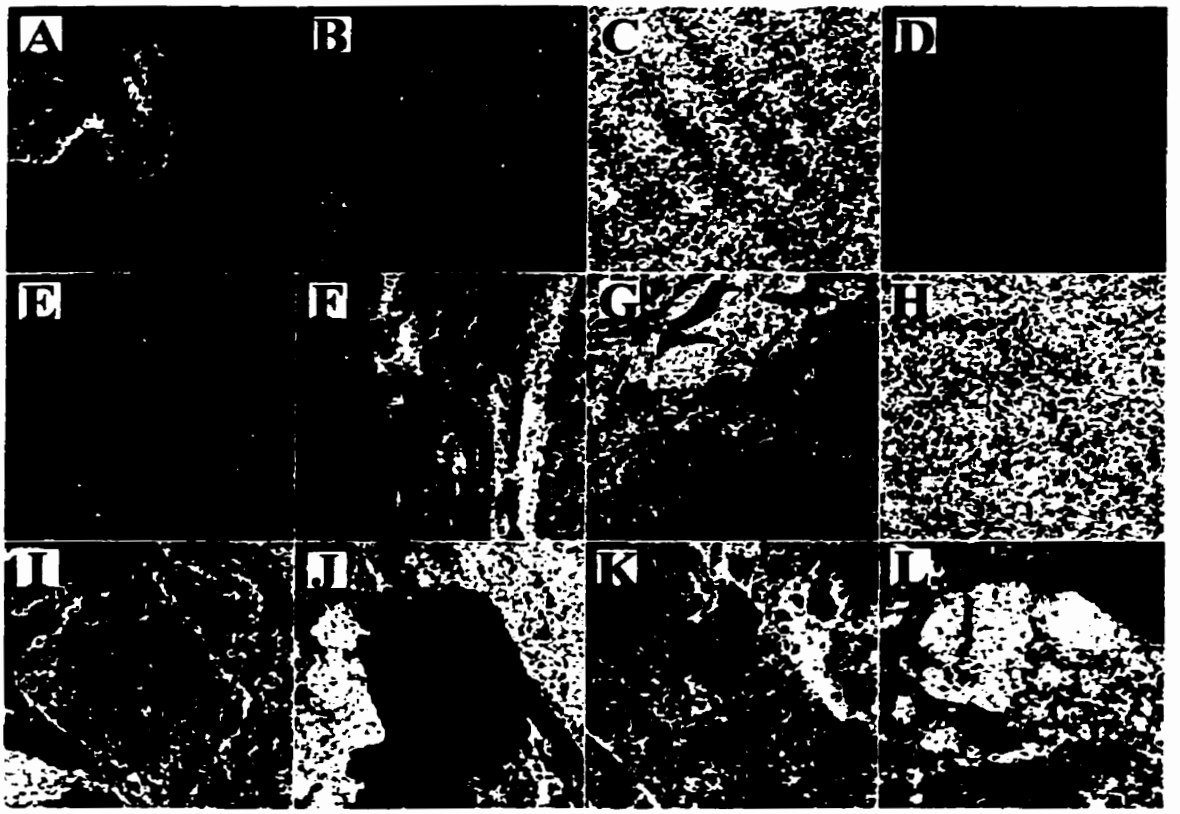


**Figure 3.5.** Surface validated winter ScanSAR imagery (128 x 128 pixels) demonstrating different surface class signatures. Detailed descriptions of windows are provided in Table 3.2.

**Table 3.2.** Window descriptions for Fig. 2.

| | |
|---|---|
| A | The bright signature reaching towards the centre of the window represents brash ice (BRI), which consists of very small ice floes broken up through wave and wind disturbances. The BRI is surrounded by a dark homogeneous signature of calm open water (COW) |
| B | This window represents an area of relatively high iceberg (IB) concentrations. IBs are apparent as distinct white dots and are surrounded by slightly roughened open water. |
| C | This window represents rough open water (ROW) showing a very low frequency wave pattern (approximately a 2 km wavelength) across the diagonal. |
| D | The wavy texture signature covering the majority of the window represents new ice and nilas (NI) with tear fractures and extensive finger rafting. Toward the lower edge of the window, the signature becomes a more constant grey tone, which represents a transition from nilas to grey ice (GI). |
| E | GI with minimal rafting (brighter signature) is present throughout this window |
| F | The bright linear signatures are strips of small pancake ice (PI), less than 0.5 m in diameter, created during a wind event. The darker signature represents open water and frazil and grease ice formation which smoothes the surface |
| G | The bright signature represents newly formed frost flowers on top of a nilas/grey ice cover (FFI). Darker signatures are small leads with a NI cover |
| H | Broken up through wind events, this window is covered with small (< 25 m in length) angular grey-white floes (GWF) with deformed edges where floes converge with each other. |
| I | A large medium thick first year ice (MFYI) floe nearly covers the whole window. A well-defined ridge circles the floe where it has converged with other floes. The floe is actually a conglomerate of smaller angular floes such as those in window H. Consequently, ridging within the large floe was also present. |
| J | The middle of the window is covered with smooth thick first year ice (TFYI) represented by a very dark homogeneous signature. The surrounding brighter signature represents rough surfaced/rubbled first year ice (RRI). |
| K | Two parallel rubble ice (RI) shear zones amongst landfast first year ice are present in this window, represented by very bright linear features oriented at diagonals across the window. Very thick ridging had occurred along these zones. |
| L | The brighter signature represents a multiyear ice (MYI) floe. Dark breaks can be observed within and around the bright signature. These breaks represent leads in and around the MYI floe where new ice types were being formed. |

Training and test data were selected from the original (i.e., not geo-rectified) validated ScanSAR imagery. A total of 30 training windows (consisting of 30 pixels each) and a separate set of test windows (variable in size) were selected for each class. Figure 3.6 depicts the distribution of training and test class selections. These data were used to develop a classification scheme for the ScanSAR data that is described in chapter 4.

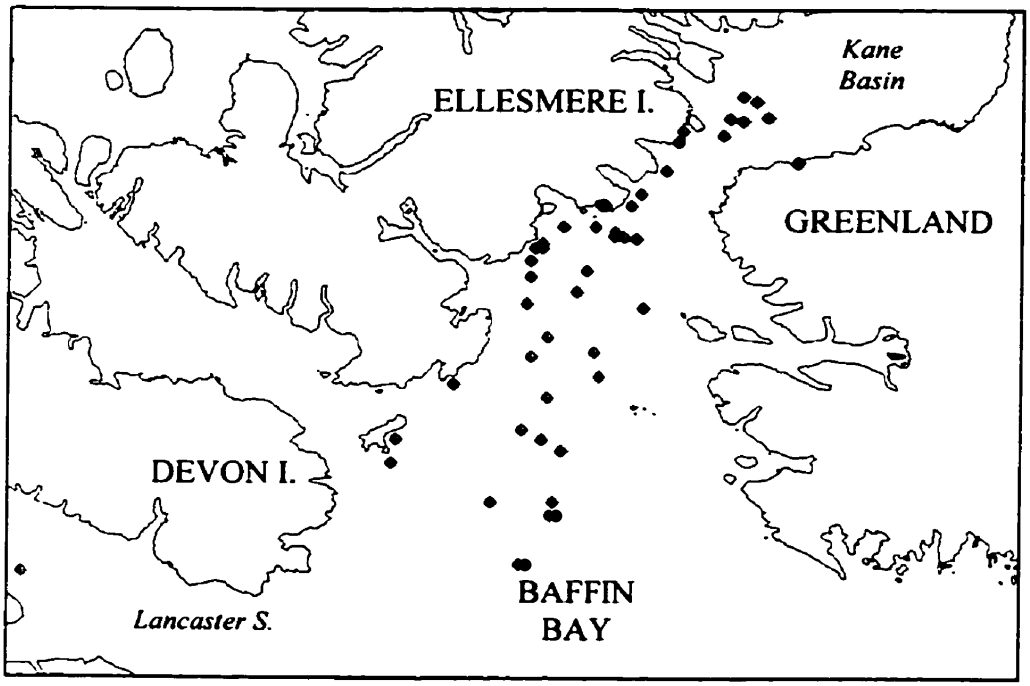


**Figure 3.6.** A map of surface validated training and test class sites.

### *3.3 GIS Framework*

A GIS provides a powerful computer based tool to analyze, manipulate, store and access geographic data. These computer systems (GIS) are specifically

designed to discard redundant data and to organize data, making it easily accessible to the user. This is accomplished through the organization of data into databases or 'layers' that may be linked spatially or though a unique identifier. Additional information, termed attribute data, may be added to the databases. This section describes the GIS framework used in this thesis.

Satellite-borne remote sensing in the form of Synthetic Aperture Radar (SAR) provided the core data set for this study. Inherent with such a data set is a large data volume. For example, one satellite data scene was approximately 60 megabytes of digital data. Consequently, both satellite coverage and data volume issues helped to delineate the study region (Fig. 3.7).

Version 3.2 of Arcview, a Geographic Information System (GIS) software package, was employed in the analysis. The GIS was used to discard redundant data and organize data into a framework for analysis (Fig. 3.7). The base of the GIS framework consisted of a 2 x 2 km vector based grid system. The grid consisted of 90,868 cells centered over the NOW in a Lambert Equal-Area Azmuthal projection with a central meridian of 55°W and reference latitude of 90°N (Fig. 3.7). Each cell was assigned a unique identifier, which provided links between databases (Fig. 3.7). Data used to populate the GIS databases were percent cover of each surface type extracted following classification of the ScanSAR imagery (see chapter 4).

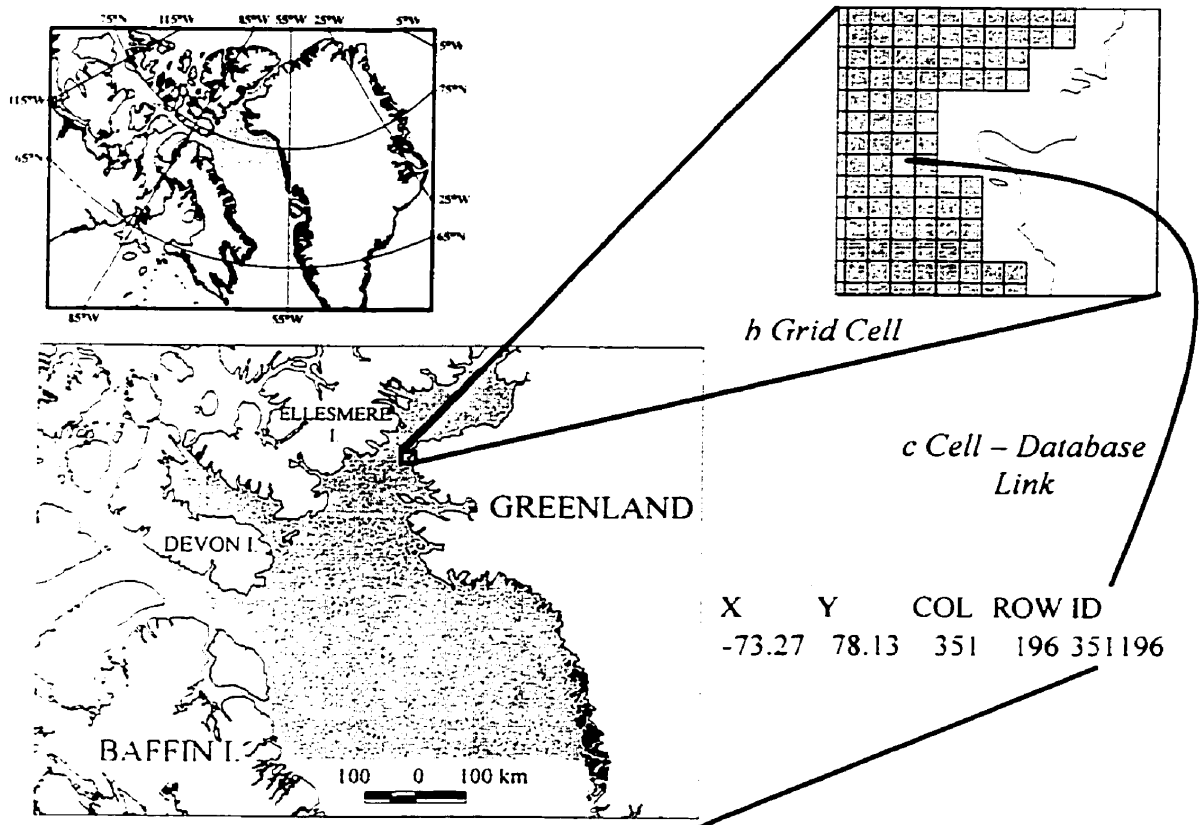


**Figure 3.7.** A diagrammatic representation of the GIS framework demonstrating: the 2 km grid extent (shaded area) (a), the geo-registered 2km grid cell (b), a cell to database link (c) and a database to database link (d).

### *3.4 Analytical Design*

To meet the second and third objectives of this thesis, the analysis first examined the sea ice spatio-temporal patterns. The objectives followed that by observing these patterns I would highlight the nature of the physical processes that create and maintain the polynya. The polynya mechanisms would also be related to biological production as explained previously. In this section I describe the analyses used to meet the second and third objectives of this thesis.

The analysis to meet the second objective was split into a spatial and temporal approach. The first approach defined the database temporally and examined the spatial structure of ice cover, whereas the second approach defined the database spatially and examined the temporal evolution of ice cover.

The first approach focused on three temporal periods: (1) prior to the Kane Basin ice bridge formation, (2) after the Kane Basin ice bridge formation and before melt onset and (3) after fall freeze-up, hereafter referred to as winter, spring and fall, respectively. The spring and fall periods were delineated as before melt onset and after freezing conditions, respectively, with no defined summer period due to the absence of an ice type classification throughout this time. A buffer of at least five days between commencement and completion of periods was used. Consequently, the periods included data from January 21 through February 28 (10 scenes), March 17 through May 26 (40 scenes) and

October 15 through December 7 (32 scenes) for winter, spring and fall, respectively.

The grid data were averaged into the three periods and statistical analysis was used to examine the spatial patterns of sea ice type/concentration for each period separately. The structure of ice cover was examined through a *k*-means convergence cluster analysis on all surface types for each period. This was accomplished within the statistical software package SPSS, version 8.0. The *k*-means procedure takes a nonhierarchical approach, providing an economical method for cluster analysis on large data sets. This method is accomplished by assigning each data unit (grid cell) to the nearest initial *k* cluster centroid (based on an Euclidean metric) (Anderberg 1973). New centroids for each gaining cluster are recomputed and data units reassigned to the nearest centroid. The final result is obtained through an iterative process, repeated until a user defined convergence between the previous and resultant centroids is reached. A 1 percent convergence was used for this analysis. For each period, 2 through 6 clusters were examined iteratively based on the cluster centroid values for each surface type. Selection of the optimal *k* clusters was defined as that point where no new information was obtained when examining $k + 1$.

Additionally, the mean surface type concentration along a 50 km transect was calculated for comparison with similar observations made by Steffen (1986). The 50 km transect was located just west of Cape Alexander (Fig. 3.8).

The second approach examined the temporal evolution of sea ice cover in defined sub-regions. Interpretation of the first approach results prompted the

separation of the grid into spatially defined sub-regions (see chapter 5). Percent sea ice cover > 30 cm thick was averaged for each sub-region based on ScanSAR acquisition dates. Data coverage of a sub-region for any particular date had to be greater than 90% in order to include its average value in the analysis.

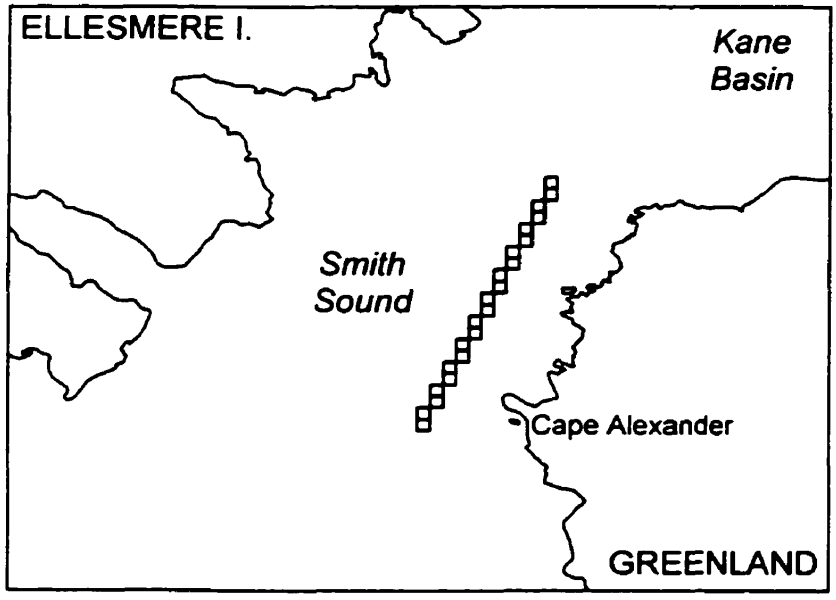


**Figure 3.8.** A 50 km transect of 2 km grid cells used to compare with results obtained in Steffen (1986).

To meet the third objective of this thesis, a qualitative comparison was made between ocean mixed layer depth (MLD) and the results obtained from the spatio-temporal ice cover analysis described above. MLDs were calculated from Conductivity, Temperature, Depth (CTD) casts made during the 1998 International North Water Polynya Study. MLD was defined as a density difference of 0.01 to 0.05 kg $m^{-3}$ from the potential density at the surface ($z > 3.9$ m) and each depth measurement as par Schneider & Müller (1990). Based on

each Leg of the 1998 NOW study expedition, these data were interpolated to a grid using the inverse distance weighted method provided in Arcview, version 3.2. A 10 km radius surrounding each CTD cast point observation was used as a fixed distance for interpolation.

This chapter was written to describe the data used and the methods employed to meet my thesis objectives. In the first section I described the International North Water Polynya Study, from which data for this thesis were collected. Following this was a description of both the RADARSAT-1 ScanSAR wide beam mode imagery and field data collected during the 1998 expedition of the International NOW study. Further, I described the methods used for data collection and data validation. A brief description of the Geographic Information System used to organize data into a framework for analysis was presented. In the final section I described the analytical methods used in the thesis. The next chapter was included out of necessity, as no sea ice classification scheme applicable to this study had been developed for ScanSAR imagery. Subsequently, in chapter 4, I discuss a ScanSAR classification scheme that was developed for the purpose of this thesis.

# CHAPTER 4: SCANSAR SEA ICE CLASSIFICATION OF THE NORTH WATER

The classification of SAR data into sea ice types is a necessity for many polar science projects. For example, a detailed study of ocean-sea ice-atmosphere interactions, such as the International North Water Polynya Study, requires the classification of as many different ice types as possible. Unfortunately, the development of an automated classification scheme or algorithm has not yet been successfully accomplished. The development has been limited by absolute calibration problems of the SAR data and the fact that different ice types may have over-lapping tonal values (e.g., Barber et al. 1991; Kwok et al. 1992; Smith et al. 1995). Classification algorithms have been developed for operational use (Wohl 1995; Ramsay et al. 1997; Shokr et al. 1999). However, none have been fully automated in that they are all dependent on visual interpretations of the imagery from experienced interpreters. Additional methods for improving the classification of SAR include the use of texture (e.g., Barber et al. 1993) and information fusion using data from different satellite sensors (e.g., Haverkamp and Tsatsoulis 1999). These methods have at least begun to reduce some of the ambiguities associated with SAR data.

In this thesis, RADARSAT-1 ScanSAR wide beam mode images were used. There was no available or suitable (for the purpose of this thesis) classification algorithm developed for use with uncalibrated ScanSAR data. Therefore, a new classification scheme was developed and implemented for the purpose of this thesis. The scheme was not fully automated in that it used both tonal and textural information contained within the ScanSAR imagery and visual interpretation of the imagery. Furthermore, the size of the data set created the necessity for an efficient approach that maximized classification precision and minimized image-processing time.

In this chapter I describe the purpose built ScanSAR classification scheme. I split the chapter into 3 sections that describe: (1) the texture statistics that were used as distinguishing variables in the classification scheme; (2) the methods used to develop the classification scheme; and (3) the resultant hierarchical classification scheme used in this thesis.

### *4.1 Texture Statistics*

Studies have demonstrated that when used by itself, image tone in a SAR scene is not able to discriminate between different sea ice types and open water with similar grey levels (e.g., Barber et al. 1991; Kwok et al. 1992; Smith et al. 1995). To alleviate this problem, the implementation of spatial information was introduced to assist in classification of sea ice types in SAR imagery (e.g., Holmes et al. 1984). There is a large number of different approaches available to

obtain spatial information from a SAR scene including both first-order (e.g., Nystuen and Garcia 1992; Smith et al. 1995) and second-order approaches (e.g., Barber and LeDrew 1991). The use of a Grey Level Occurrence Matrix (GLCM) is only one of these approaches. However, studies such as Barber et al. (1993) have demonstrated that texture measures calculated from a GLCM outperform other approaches.

GLCMs provide the conditional joint probabilities of all pixel pairwise combinations within a given computational window size (Barber et al. 1993). That is, a GLCM is specified by the relative frequency of grey level co-occurrences made by grey level *i* with grey level *j*, which are separated by a given displacement vector and confined to a given computational window. The displacement vector is specified by the conditional parameters, interpixel sampling distance ($\delta$) and orientation ($\alpha$). Following Haralick et al. (1973), the computation of a GLCM can be expressed algebraically as Equation 4.1, where $C_{ij}$ is defined in Equation 4.2. For example:

$$\Pr(x) = \{C_{ij} | \delta, \alpha\} \tag{4.1}$$

$$C_{ij} = \frac{P_{ij}}{\sum_{ij=1}^{n} P_{ij}} \tag{4.2}$$

where $P_{ij}$ is the frequency of occurrence of grey levels i and j. As the summation over n is from i and j equal to 1, n is equal to the total number of pixel pairs, which is dependent on the conditional parameters and computation window size.

A texture statistic is calculated from the matrix in order to represent a single measure of image texture for the central pixel of a computation window. As one statistic is only representing a portion of the total information within a GLCM, it is referred to as a point estimate (Barber et al. 1993). Seven commonly used statistics derived from a GLCM (e.g., Haralick et al., 1973; Barber and LeDrew, 1990; Nystuen and Garcia, 1992; Soh and Tsaloulis, 1999) were examined in this thesis and are provided by Equations 4.3 through 4.9. These measures were all calculated using the remote sensing software package PCI, version 6.1.

1. *Homogeneity*

$$\sum_{i=1}^{n}\sum_{j=1}^{n}\frac{C_{ij}}{1+(i-j)^2} \qquad (4.3)$$

This statistic represents a measure of the local homogeneity. It is high when GLCM concentrates along the diagonal.

2. *Contrast*

$$\sum_{i=1}^{n}\sum_{j=1}^{n}C_{ij}(i-j)^2 \qquad (4.4)$$

Contrast represents a measure that works opposite to homogeneity. It is a measure of the amount of local variation in the image. It is highly sensitive to large off diagonal values due to squaring of the difference between i and j.

3. *Dissimilarity*

$$\sum_{i=1}^{n}\sum_{j=1}^{n} C_{ij}|i-j| \tag{4.5}$$

This measure works very similar to contrast. However, the response to off diagonal values is linear and therefore not as sensitive to large values as in contrast.

4. *Entropy*

$$-\sum_{i=1}^{n}\sum_{j=1}^{n} C_{ij}\log_e C_{ij} \tag{4.6}$$

Entropy measures the amount of disorder within a GLCM. This measure is high when the elements of a GLCM have near equal values. As the computation window in the original image approaches a random pattern, the statistic will reach a maximum (Barber et al. 1993). Consequently, small entropy values will represent a homogeneous or uniform texture in the original image.

*5. Energy*

$$\sum_{i=1}^{n}\sum_{j=1}^{n} C_{ij}^{2} \tag{4.7}$$

This statistic, also referred to as angular second moment and uniformity, works opposite to entropy. The measure will be greater when high values appear in the GLCM. Therefore, high energy is a measure of local homogeneity.

*6. Correlation*

$$\sum_{i=1}^{n}\sum_{j=1}^{n} \frac{(i-\mu_x)(j-\mu_y)C_{ij}}{\sigma_x \sigma_y} \tag{4.8}$$

where $\mu x$ and $\mu y$ refer to the mean of row i and j, respectively and $\sigma x$ and $\sigma y$ represent the standard deviation of row i and j, respectively. This is a measure of linear dependency of grey levels relative to the displacement vector creating the GLCM. Therefore, high values will represent a heterogeneous texture of the original computation window.

*7. Mean*

$$\sum_{i=1}^{n}\sum_{j=1}^{n} i \cdot C_{ij} \tag{4.9}$$

This is simply a measure of the mean of row i within a GLCM. It is an additional measure available in the PCI software.

Before the above texture statistics were calculated, the conditional parameters, quantization scheme and computational window size had to be decided upon. Barber and LeDrew (1991) have demonstrated when examining the surface texture of SAR sea ice types, the GLCM conditional parameters, $\delta$ and $\alpha$ gave optimum results when equal to 1 and 0° (parallel to SAR look direction), respectively. Consequently, these parameters were used in this thesis. Furthermore, prior to the formation of a GLCM, data were quantized (in this case from 256 to 16 grey levels) in order to keep the time for matrix computations moderate. Soh and Tsatsoulis (1999) have shown 8 level quantization to be unrepresentative of an original 256 level data set, whereas a 64 level representation provided optimal results. However, time required to process 64 levels was deemed to be excessive in this case due to the extremely large data volume of SAR imagery. A decision was made to quantize to 16 levels and justified based on results of Marceau et al. (1990). A 7 by 7 pixel window was also chosen for GLCM computations. This window was large enough to calculate a meaningful joint-distribution of grey tones, yet small enough to delineate a surface type (Shokr et al. 1995).

### *4.2 Classification Procedure*

Using SPSS, version 8.0, a Multiple Discriminate Analysis (MDA) was performed on the training data. A MDA works in a similar fashion to a Principal Component Analysis (PCA), however it maximizes inter-group variation as

opposed to maximizing variation over the complete data matrix (Manly 1986). Based on N dimensions (i.e., distinguishing variables), a MDA calculates N-1 canonical discriminate functions that maximize the discrimination between *k a-priori* groups in a diminishing order. That is, the first canonical discriminate function maximizes the inter-class variation by minimizing the residuals. The second function also maximizes the inter-class variation, however is limited to being statistically orthogonal to the previous function, and so on (Manly 1986). In this thesis, N was initially represented by 8 variables; grey level and 7 texture statistics, whereas *k* was initially represented by 14 surface classes (Fig. 3.5 and Tables 3.1 and 3.2). A contingency table that demonstrates the training data performance on distinguishing itself using a Mahalanobis minimum distance classifier is outputted by the MDA in SPSS. The resultant contingency table was examined and logical decisions were made to discard or pool classes. A MDA was then performed on the new set of classes. An iterative merge and split classification process was repeated until the criterion of an overall agreement of 90% or greater was obtained amongst the training data.

The *pooled within-groups* absolute correlation between a discriminating variable and standardized canonical discriminate functions was used to determine the best discriminates. These variables were further examined using the Maximum Likelihood Classification (MLC) technique available as part of the Multispectral Package in PCI. A MLC uses the training data means and standard deviations to calculate normally distributed probability density functions that are used to determine if a pixel falls within a class or not. Following the MLC, a 7 by

7 mode filter was used to smooth out erroneously classified outlier pixels. The results were compared with the independent set of test windows. In order to eliminate chance agreement between the classified and test pixels, the Kappa coefficient (K) and standard deviation ($K_s$) were used to represent the overall classification agreement (Bishop et al. 1975).

Once the MLC and filter pass were employed, areas of open water, new pack-ice, old pack-ice and landfast ice were visually identified and a polygon was used to segment these areas. Interpretation of the four surface categories largely followed Volume II of the operational Canadian Ice Service SAR Ice Interpretation Guide (1994). Additional information was obtained through examination of the images in a temporal sequence. For example, landfast ice was defined as ice that had not moved for a period of 3 days.

Three images were randomly selected to examine reproducibility of the manual digitization procedure. An open water polygon was outlined on each. Areas for each polygon were extracted. The polygons were deleted and then re-digitized with the area of each polygon extracted. This procedure was repeated 10 times. Each area calculation was divided by the maximum observed area for each separate polygon, normalizing the observations to 1. The resultant 30 samples were used to calculate a standard deviation as an estimation of error.

Once classified into surface ice type, images were geo-rectified to the grid's projection using the 300 GCP spreadsheet obtained from each ScanSAR file (see section 3.2.3). Percent cover of each surface type was then extracted into

the grid database. Calculations involved input of 400 pixels (20 x 20 100 m pixels) for each 2 km by 2 km grid cell.

### *4.3 Classification Results*

Results from the initial MDA (ice bergs were discarded due to mode filter pass) showed an overall agreement of 69.8% (Table 4.1), which did not satisfy the required 90% criterion. Confusion amongst the classification results generally occurred between: new/nilas ice (NI) and grey ice (GI); pancake ice (PI), frost flower covered ice (FFI), grey-white angular floes (GWF), brash ice (BRI), rough/rubbled first-year ice (RRI), rubble ice (RI) and multiyear ice (MYI); calm open water (COW) and thick first-year ice (TFYI); and rough open water (ROW) and medium first-year ice (MFYI) (Table 4.1).

**Table 4.1.** Contingency table of percent agreement between classified and training data, obtained from the initial Multiple Discriminate Analysis (MDA) results.

| | | Classified Data | | | | | | | | | | | | |
|---|---|---|---|---|---|---|---|---|---|---|---|---|---|---|
| | | NI | GI | PI | FFI | MYI | GWF | RI | BRI | RRI | TFYI | COW | ROW | MFYI |
| Training Data | NI | 73.3 | 16.7 | 0.0 | 0.0 | 0.0 | 0.0 | 0.0 | 0.0 | 0.0 | 0.0 | 0.0 | 0.0 | 10.0 |
| | GI | 10.0 | 86.7 | 0.0 | 0.0 | 0.0 | 0.0 | 0.0 | 0.0 | 0.0 | 3.3 | 0.0 | 0.0 | 0.0 |
| | PI | 0.0 | 6.7 | 13.3 | 26.7 | 6.7 | 13.3 | 6.7 | 16.7 | 10.0 | 0.0 | 0.0 | 0.0 | 0.0 |
| | FFI | 0.0 | 0.0 | 3.3 | 56.7 | 0.0 | 10.0 | 0.0 | 6.7 | 3.3 | 0.0 | 0.0 | 0.0 | 20.0 |
| | MYI | 0.0 | 0.0 | 0.0 | 0.0 | 86.7 | 0.0 | 6.7 | 3.3 | 3.3 | 0.0 | 0.0 | 0.0 | 0.0 |
| | GWF | 0.0 | 0.0 | 0.0 | 6.7 | 3.3 | 66.7 | 0.0 | 3.3 | 20.0 | 0.0 | 0.0 | 0.0 | 0.0 |
| | RI | 0.0 | 0.0 | 0.0 | 0.0 | 6.7 | 0.0 | 70.0 | 13.3 | 0.0 | 0.0 | 0.0 | 6.7 | 3.3 |
| | BRI | 0.0 | 0.0 | 3.3 | 10.0 | 10.0 | 16.7 | 13.3 | 40.0 | 6.7 | 0.0 | 0.0 | 0.0 | 0.0 |
| | RRI | 0.0 | 0.0 | 0.0 | 3.3 | 3.3 | 13.3 | 0.0 | 10.0 | 70.0 | 0.0 | 0.0 | 0.0 | 0.0 |
| | TFYI | 3.3 | 0.0 | 0.0 | 0.0 | 0.0 | 0.0 | 0.0 | 0.0 | 0.0 | 90.0 | 6.7 | 0.0 | 0.0 |
| | COW | 0.0 | 0.0 | 0.0 | 0.0 | 0.0 | 0.0 | 0.0 | 0.0 | 0.0 | 23.3 | 76.7 | 0.0 | 0.0 |
| | ROW | 0.0 | 0.0 | 0.0 | 10.0 | 0.0 | 0.0 | 0.0 | 0.0 | 0.0 | 0.0 | 0.0 | 76.7 | 13.3 |
| | MFYI | 6.7 | 20.0 | 0.0 | 3.3 | 0.0 | 0.0 | 0.0 | 0.0 | 0.0 | 0.0 | 0.0 | 0.0 | 70.0 |

The decisions employed to improve the overall agreement included: (1) the removal of PI, BRI, FFI, ROW and RRI; and (2) pooling of NI and GI, and COW and TFYI. PI, BRI and FFI ice were removed due to low internal agreements of 13.3%, 43.0% and 57.0%, respectively, following the previous decision results. NI and GI were pooled as they were very similar ice classes with low class separation. This resulted in a new combined surface class, new/nilas-grey ice (NGI). COW and TFYI were pooled due to low signature distinction. However, they were later distinguished in the digitization decision rule step (see below). ROW had a relatively low separation and was removed for later distinction using the digitized masks. RRI was discarded because the range of its distinguishing variables substantially overlapped with those of GWF and RI types. This had caused GWF and RI types to have lower internal agreements. The removal and pooling of the various classes mentioned above resulted in an overall agreement that increased to 92.9%.

The final MDA results were used to choose the best discriminating variables. The GLCM mean statistic and grey level showed the highest correlation with the first canonical discriminate function (Table 4.2). Entropy and homogeneity texture statistics demonstrated the highest correlation with the second canonical discriminate function (Table 4.2). Furthermore, the first two orthogonal axes accounted for over 95% of the cumulative variation. Consequently, these 4 variables were found to be the best discriminators and were further compared using the MLC results.

**Table 4.2.** Correlation of discriminating variables with canonical discriminate functions, obtained from final MDA results.

| Discriminating Variables | Canonical Discriminate Function | | | | |
|---|---|---|---|---|---|
| | 1 | 2 | 3 | 4 | 5 |
| Mean* | 0.9106542 | 0.1552256 | -0.2452172 | -0.1581488 | 0.0666754 |
| Grey Level | 0.872853 | -0.1564822 | 0.1990048 | -0.3294128 | 0.1297005 |
| Entropy* | 0.2719501 | 0.7699825 | 0.347271 | 0.1245344 | -0.0112164 |
| Homogeneity* | -0.2663441 | -0.6786722 | -0.252193 | -0.1340387 | 0.3449382 |
| Dissimilarity* | 0.2461895 | 0.5659545 | 0.366691 | 0.4648278 | -0.2040342 |
| Energy* | -0.1685385 | -0.4860088 | -0.1160521 | 0.1407771 | 0.0113202 |
| Correlation* | 0.0480985 | 0.1652966 | 0.3839215 | 0.0105962 | 0.0321643 |
| Contrast* | 0.2024588 | 0.3655016 | 0.4611714 | 0.7063506 | -0.1671786 |

* Grey Level Co-occurrence Matrix derived statistics
Shading represents the highest absolute *pooled within groups* correlation

The best MLC was obtained when combining the entropy texture statistic with either the GLCM mean or grey level (Table 4.3). Both results were statistically indistinguishable at an $\alpha$ of 0.01 (i.e., tested against a Type I error). However, factoring in the time taken to calculate an extra GLCM derived statistic (i.e., mean), grey level and entropy provided the optimum result.

An estimation of error for the polygon segmentation of open water, new pack-ice, old pack-ice and landfast ice resulted in a standard deviation of 0.0024. This result inferred that over 99 out of 100 times, the mask would be within 0.72% of the average area. Specific combinations of the classified and polygon themes resulted in different surface types (Fig. 4.1).

**Table 4.3.** Kappa coefficients (K) and standard deviations ($K_s$) for combinations of discriminating variables based on Table 4.2 results.

| Discriminating Variable | Grey Level | | Mean | |
|---|---|---|---|---|
| | K | Ks | K | Ks |
| Grey Level | 0.725 | 0.004 | 0.704 | 0.004 |
| Mean | 0.704 | 0.004 | 0.752 | 0.004 |
| Entropy | 0.841 | 0.003 | 0.845 | 0.003 |
| Homogeneity | 0.726 | 0.004 | 0.741 | 0.004 |

Since SAR sea ice signatures (backscatter) are seasonally dependent (Livingstone et al. 1987), a final step had to be incorporated in the classification scheme. Signatures are generally stable until water in liquid phase appears in the snow pack. The water dramatically changes the dielectric properties of the sea ice surface and volume, changing backscatter over different sea ice types, including a reversal in the multiyear and first-year sea ice signatures (Barber et al. 1995). The date at which water appears is referred to as melt onset (Livingstone et al. 1987). Yackel et al. (2000) determined melt onset dates (defined from the time series SAR scattering) over landfast ice sites within the North Water (NOW). Melt onset dates along the eastern coast of Ellesmere Island were averaged, which resulted in a date of May 30. After melt onset, ice types were deemed indistinguishable using the classification scheme. Following freeze-up, determined through observations of new ice formation within the SAR imagery, the ice type classification scheme was again implemented. The complete hierarchical ScanSAR classification is depicted with a flow chart (Fig. 4.1). Once classified, the images were inputted into the GIS database as outlined in section 3.3.

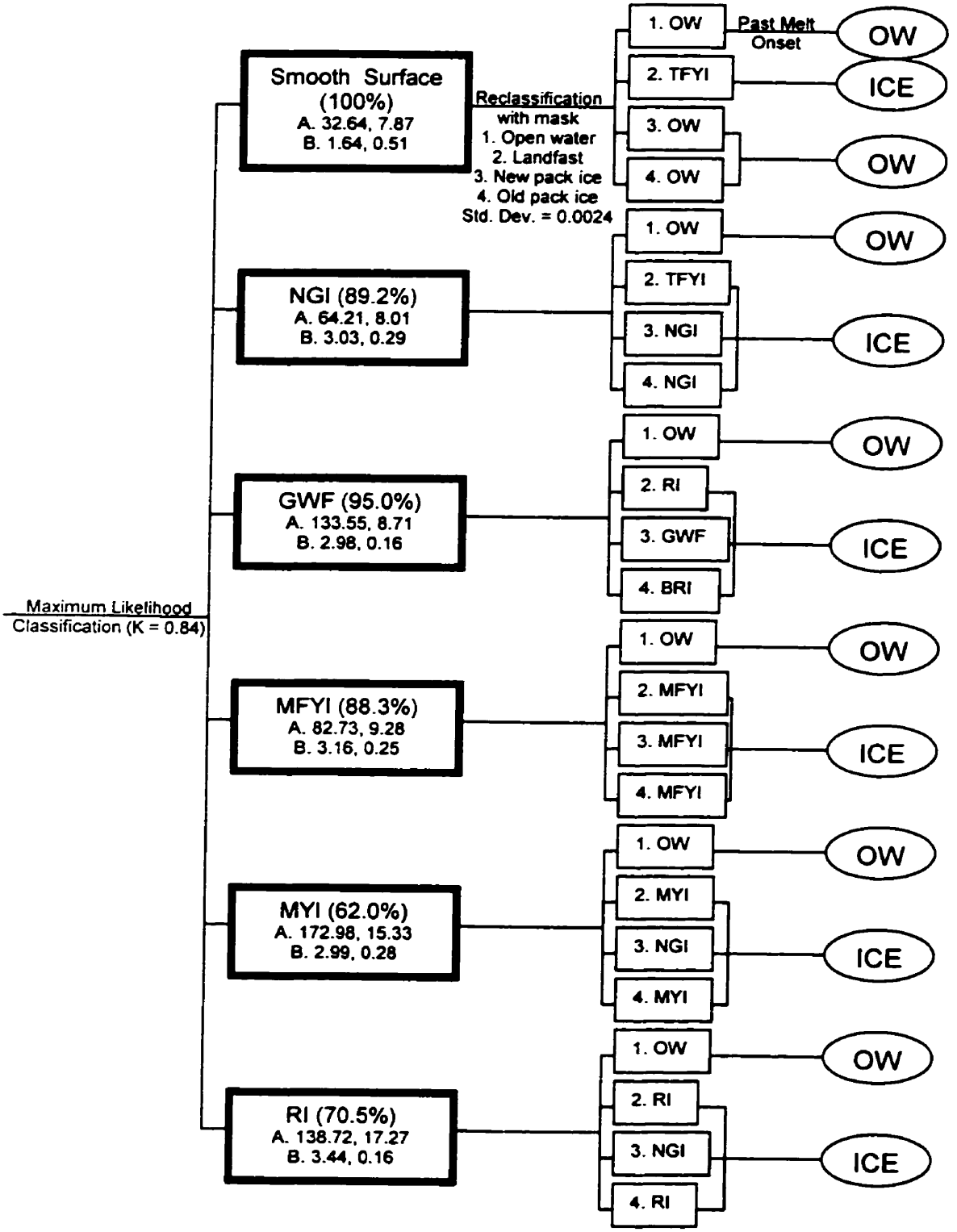


**Figure 4.1.** Flow chart of surface type classification scheme. Signature statistics (Mean, Std. Dev.) for grey level (A) and entropy (B) are provided.

After the images were classified, an additional error source was observed in the data. The classification scheme resulted in the delineation of an extensive area as having near 100% young ice cover off the coast Greenland near Cape York. This result was improbable and attributed to the location of the original training data collection. Training and test data collection occurred toward the northwest side of the NOW (Fig. 3.4). This is an area of constant disturbance, with high current and wind velocities. In an area such as this, the only smooth surfaced pack-ice types are new ice types formed during calm conditions with minimal rafting (e.g., the original NI and GI training data). After such a break in the 'normal' conditions, ocean or atmospheric disturbances would cause the ice to raft and deform, in essence, roughening the surface. This would cause an increase in SAR backscatter. Consequently, as the classification moves further from the location of training data site locations, delineation is more of smooth versus rougher ice types as opposed to newer versus older ice types, respectively. Considering the volume of ice, a relative delineation can be made in that smoother ice is relatively thinner than rougher ice that has been compacted and deformed.

In this chapter I described the development of a purpose built hierarchical classification scheme to classify sea ice types within RADARSAT-1 images. This included: (1) a description of how the distinguishing variables were obtained from the ScanSAR imagery, (2) a description of the methods used to develop the

classification scheme and (3) the classification results and finalized scheme. In the next chapter I present the results and discussion of the analysis used to meet objectives 2 and 3 of this thesis.

# CHAPTER 5: RESULTS AND DISCUSSION

In this chapter I examine the spatial and temporal patterns of the North Water (NOW) sea ice cover using the data and analysis described in the two previous chapters. I relate the observed patterns to the physical polynya mechanisms and biological implications in the NOW polynya by examining three interrelated themes: (1) sea ice spatial patterns; (2) sea ice temporal evolution and (3) relationships between the mixed layer depth and sea ice patterns.

## *5.1 Sea Ice Spatial Patterns*

The *k*–means cluster approach provided a natural grouping of ice type/open water concentration combinations, demonstrating a clear structural pattern within each seasonal period. This statistical distinction provided the basis for inferences from natural ice type combinations to the physical mechanisms that could cause the combinations. The main trends were observed when *k* equaled 3 or 4 clusters, depending on the period being analyzed. As more clusters were specified for a *k*–means analysis, no additional spatial structure was observed.

### 5.1.1 Winter Period

Spatial structure of the region for the winter period (WP) was best represented with 4 clusters (Fig. 5.1). WP cluster 1 consisted mainly of high TFYI concentrations and was located within the landfast ice along all coasts. Thick first-year ice (TFYI) was an extensive stationary surface class restricted to sheltered landfast ice, which explained the grouping of landfast TFYI with itself.

WP cluster 2 represented a combination of medium RI and MFYI concentrations and the highest MYI concentrations relative to other cluster compositions (Fig. 5.1). Throughout Smith Sound and south, grid cells classified as cluster 2 were found toward the west side of the region, following the eastern coast of Canada. Predominate composition of this group consisted of rough surface classes inferring an area of high ocean and/or wind stress. This result is consistent with the well-documented southward currents and predominate northerly winds along this area (e.g., Nutt 1969; Muench and Sadler 1973; Barber et al. 2000).

Cluster 2 also populated nearly 100% of the grid cells just north of Smith Sound (Fig. 5.1). This clumped distribution had classified an area of high MYI and RI concentrations (Fig. 5.2a and b, respectively). This observation can be explained by: (1) Kane Basin at this location narrows considerably, which would cause the congestion of sea ice; (2) the composition of large MYI floes could act to block the northern entrance to Smith Sound; and (3) cold temperatures would cause further congelation of separate ice floes.

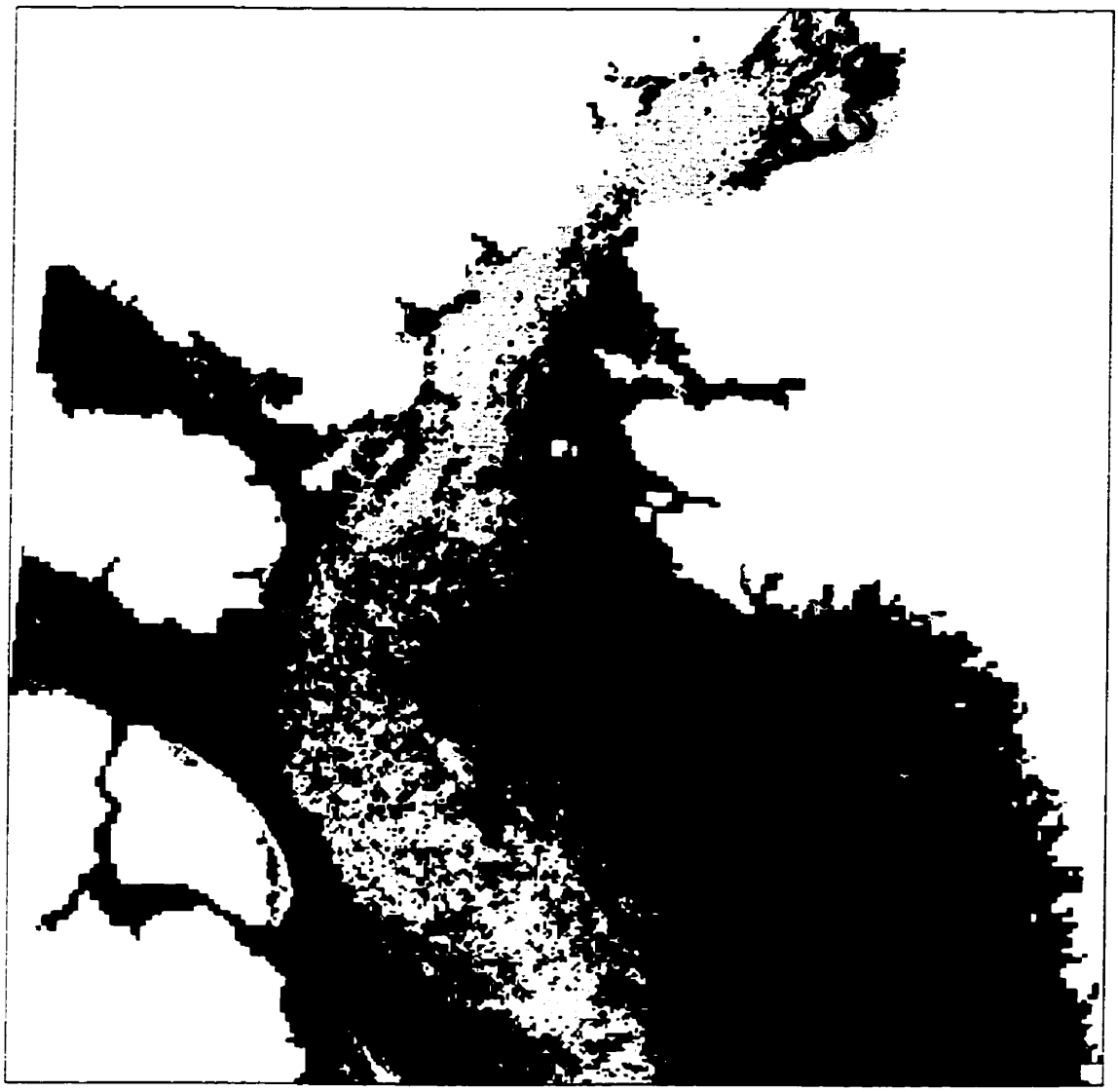

| | Cluster/ Percent Cover (%) | | | |
|---|---|---|---|---|
| Ice Type | 1 | 2 | 3 | 4 |
| OW | 0.25 | 0.77 | 0.76 | 2.05 |
| NGI | 1.04 | 9.33 | 23.80 | 78.54 |
| GWF | 0.01 | 0.70 | 2.11 | 0.13 |
| MFYI | 10.18 | 38.88 | 58.60 | 17.95 |
| TFYI | 86.15 | 1.94 | 2.22 | 0.20 |
| MYI | 0.68 | 13.31 | 2.00 | 0.20 |
| RI | 1.69 | 35.07 | 10.50 | 0.93 |

**Figure 5.1.** 1998 winter period (Jan. 21 through Feb. 28) *k*-means cluster results for the GIS grid. The table provides the mean surface type composition for each blue-shaded cluster.

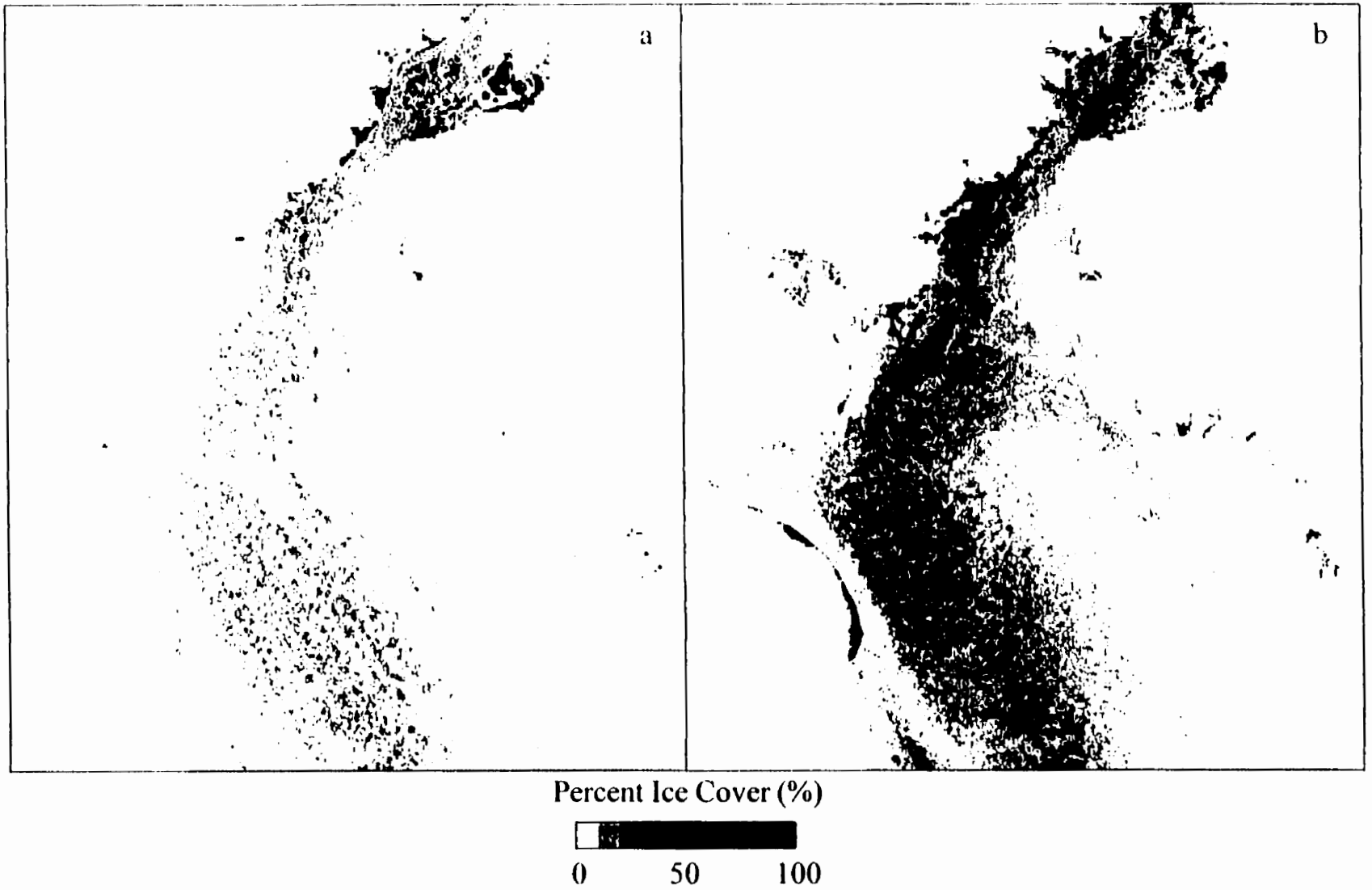


**Figure 5.2.** Averaged 1998 winter period (Jan. 21 through Feb. 28) concentrations of multiyear (a) and rubble (b) sea ice types.

Multiyear ice has been observed through animations of 85.5 GHz SSM/I (Special Sensor Microwave Imager) to periodically drain through Nares Strait alternating with the formation of ice bridges along its path towards Baffin Bay (Agnew 1998). Therefore, the majority of MYI found in this area would have an Arctic Basin origin. Furthermore, the Lincoln Sea, found at the northern tip of Canada and Greenland (Fig. 1.1), is known to contain some of the thickest MYI within the Arctic Basin due to deformation as it is compressed against the northwest coast of Greenland.

With no Kane Basin ice bridge present during the winter period, cluster 2 may also be interpreted as depicting a "thoroughfare" of sea ice. Ito and Müller (1982) had calculated a mean ice velocity of 4.3 $km \cdot d^{-1}$ in a southward direction through Smith Sound with a maximum observation of 34.9 $km \cdot d^{-1}$, which was strongly influenced by wind. Further, Wilson et al. (2000) found monthly averaged ice velocities of up to 8.64 $km \cdot d^{-1}$ (March, 1998) through Smith Sound. These southward sea ice velocities combined with thick MYI composition represent a poorly documented contribution to the freshwater flux out of the Arctic Basin into Baffin Bay.

The tendency of cluster 2 to occur tightly along the western side of the region through and south of Smith Sound may be interrelated with the distribution of cluster 3 (Fig. 5.1). Composition of cluster 3 for the winter period was a combination of NGI and MFYI with relatively high GWF concentrations. Steffen (1985) documented a consistent occurrence of warm water cells off the coast of Greenland near Cape Alexander and Cape York. He explained the cells'

existence as the upwelling of warm (0°C) Atlantic Baffin Bay water compensating a mass movement of water westward throughout Smith Sound. With congestion of sea ice in Kane Basin and the presence of strong and consistent northerly winds, the Coriolis force deflects surface mass flow to the right of the wind, inducing upwelling along the Greenland coast (Steffen 1985). The spatial distributions and compositions of WP clusters 2 and 3 throughout Smith Sound support this explanation. These distributions within Smith Sound can be additionally explained through katabatic (downslope) winds off the coast of Greenland. Bromwich et al. (1996) have modeled strong downslope winds over the Greenland Ice Sheet driven mainly by radiative cooling of the sloping terrain. Their results, substantiated through surface observations, demonstrated strong (> 10 m $s^{-1}$) offshore winds, which deviate to the right (north) due to the Coriolis force. In the vicinity of Smith Sound, these katabatic winds would be opposite in direction to the predominate northerly winds documented for the area. Therefore, these winds could cause divergence of ice off the coast of Greenland. Similar to Steffen's (1985) explanation, offshore mass transport of surface waters could cause upwelling of warm Atlantic waters from depth. There is no way of distinguishing between an oceanic and atmospheric forcing on this ice using the NOW study 1998 data set. Thus this observation is left as a speculation consistent with the same general observations of Steffen (1985).

Cluster 4 grouped the lowest concentrations of RI and MYI. Therefore, the spatial transition from clusters 2 through 3 to 4 infers a trend of decreasing ice deformation towards Greenland and west into Lancaster Sound. This observation

is discussed later in relation to the occurrence of open water along the west Greenland coast, south of Whale Sound and north of Cape York (Fig. 1.1), during the spring and fall periods.

Results from the 50 km transect demonstrated only 38% open water and ice types < 30 cm thick for the winter period (Table 5.1). This contrasted with Steffen's (1986) observation of an average 78.5% (averaged from January 22, February 2 and March 2 observations in Table IV; Steffen 1986). From this discrepancy the Smith Sound polynya was inferred to be temporally sporadic. The amount of ice in this area will depend on the congestion of sea ice in Kane Basin, the timing of ice bridge formation and the strength of northerly winds. Interannual variations in this phenomenon were investigated in Barber et al. (2000).

**Table 5.1.** Surface type composition along a 50 km transect for the winter, spring and fall periods of 1998 (Jan.21 through Feb. 28, Mar. 17 through May 26 and Oct. 15 through Dec. 7, respectively).

| Period | Percent Cover (%) | | | | | | | |
|---|---|---|---|---|---|---|---|---|
| | OW | NGI | GWF | MFYI | BRI | TFYI | MYI | RI |
| Winter | 6.72 | 26.18 | 4.84 | 33.79 | 0.00 | 0.00 | 7.40 | 21.06 |
| Spring | 26.06 | 30.09 | 9.19 | 31.48 | 0.14 | 0.00 | 0.68 | 2.36 |
| Fall | 15.26 | 23.98 | 7.57 | 33.58 | 0.00 | 0.00 | 6.43 | 13.19 |

### 5.1.2 Spring Period

In the spring period (SP), spatial patterns were most informative using 3 clusters. As with the winter period (WP), thick first-year ice accounted for the highest surface concentration of cluster 1 during the spring period (Fig. 5.3). SP cluster 2 was also similar to WP cluster 2 in that the rough surface classes were represented with their highest mean concentrations within this group.

The ratios of each surface cover for cluster 2 differ between the separate periods. This result can be explained by the presence of the Kane Basin ice bridge in the SP. The ice bridge prevents the import of sea ice into the region south of the bridge (Ito and Müller 1977). Resultant declines in multiyear (MYI) and rubble ice (RI) were compensated through increases in MFYI and NGI mean concentrations. However, due to consistent surface turbulence within the area, RI showed relatively high concentrations.

The spatial distribution of cluster 2 for the SP was again prominent along the east coast of Canada (Fig. 5.3). An additional area along the southwest coast of Greenland was classified as cluster 2 (Fig. 5.3), which contained a high concentration of RI (Fig. 5.4a). This area corresponded to a small area classified as cluster 3 in the WP (Fig. 5.1). Northward flow of the West Greenland current along the Greenland coast (e.g., Nutt 1969) combined with predominate southerly winds in this area (Barber et al. 2000) could cause the occurrence of deformed ice. Furthermore, the enhanced circular motion of ice referred to as the

North Baffin Bay gyre (Smith and Rigby 1981; Wilson et al. 2000) may have also contributed to the deformation of sea ice observed in this area.

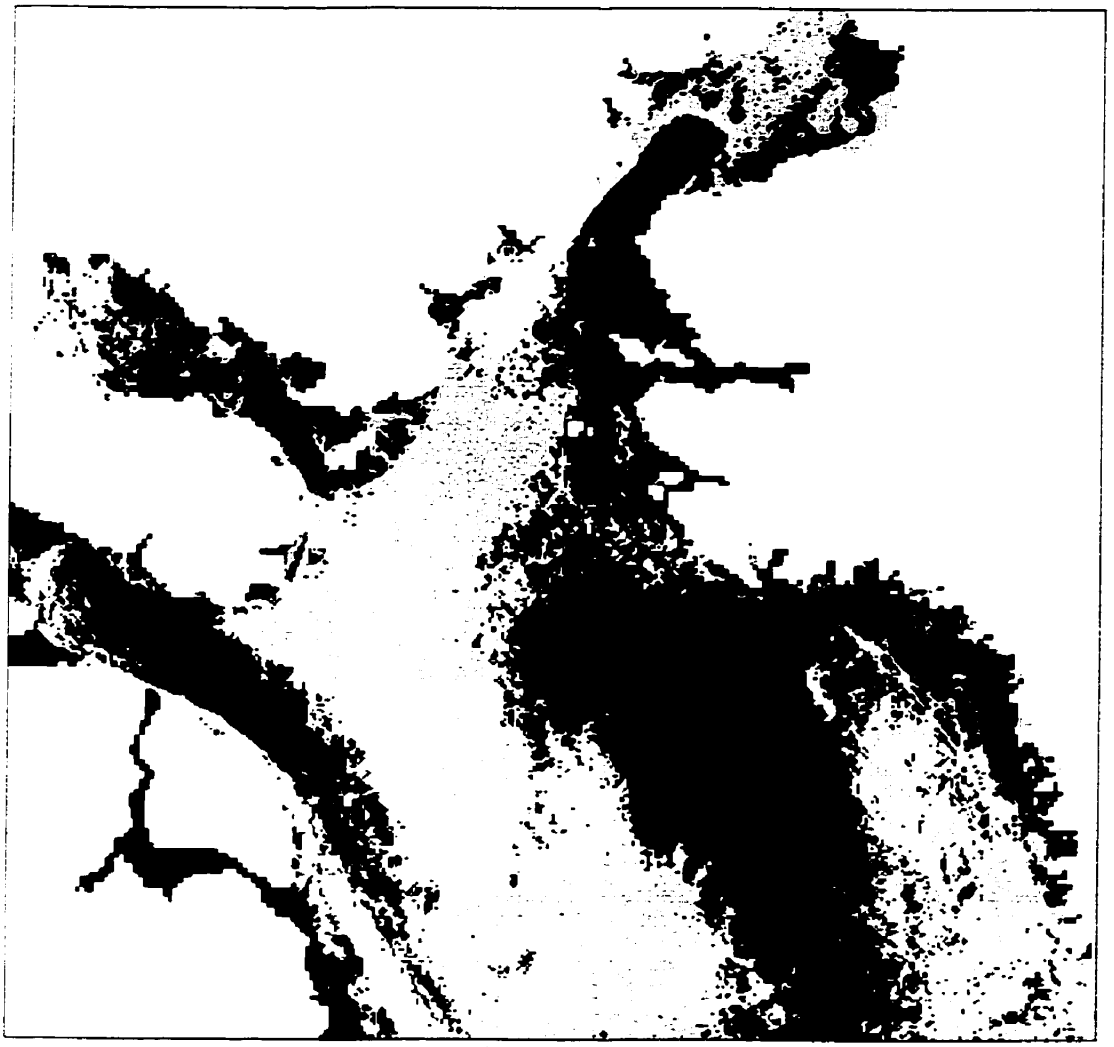

| | Cluster/ Percent Cover (%) | | |
|---|---|---|---|
| Ice Type | 1 | 2 | |
| OW | 0.73 | 2.65 | 6.62 |
| NGI | 0.58 | 17.39 | 44.96 |
| GWF | 0.03 | 1.00 | 1.51 |
| MFYI | 18.69 | 59.34 | 41.36 |
| BRI | 0.03 | 0.23 | 0.14 |
| TFYI | 76.38 | 4.30 | 1.25 |
| MYI | 0.64 | 2.28 | 0.62 |
| RI | 2.93 | 12.82 | 3.54 |

**Figure 5.3.** 1998 spring period (Mar. 17 through May 26) *k*-means cluster results for the GIS grid. The table provides the mean surface type composition for each blue-shaded cluster.

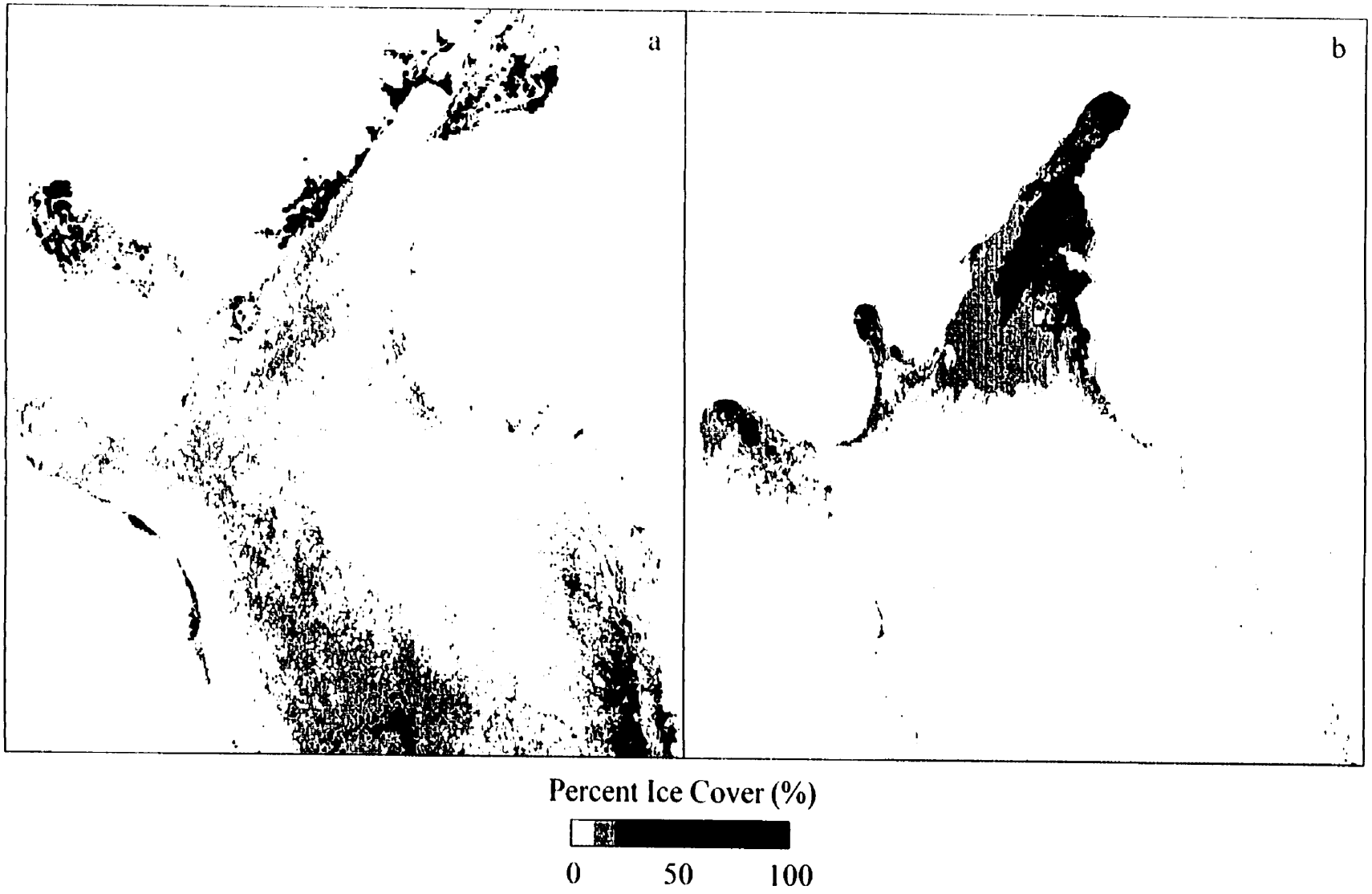


**Figure 5.4.** Averaged 1998 spring period (Mar. 17 through May 26) concentrations of rubble sea ice (a) and open water (b).

SP cluster 3 was composed of low RI and MYI concentrations relative to cluster 2 (Fig. 5.3). The distribution was similar to clusters 3 and 4, substantiating the interpretation of relatively low sea ice deformation towards Greenland and Lancaster Sound. An exception of this similarity was observed within the Smith Sound area. The presence of the Kane Basin ice bridge and the subsequent large divergence of ice essentially masked the ability of a cluster analysis to naturally separate the east and west sides of Smith Sound. However, the previously discussed explanations of westward water mass movement and induced upwelling was supported through the mean concentration distribution of OW during the spring period (Fig. 5.4b). This result was in good agreement with the location of warm water cells mapped by Steffen and Ohmura (1985), further supporting their existence.

An additional area of very high open water concentrations just south of Coburg Island was observed (Fig. 5.4a). Offshore winds and/or southward currents and winds on either side of the island causing divergence of ice can explain the location of the open water. Further, the ice divergence and subsequent water mass movement could induce upwelling along the southern edge of Coburg Island. Although no *in-situ* observations of water temperature were made for this position during the spring period in 1998, Steffen (1985) did find water temperatures to be above -1.8°C during both the 1978/79 and 1980/81 winters.

The 50 km transect demonstrated 65.3% surface cover < 30 cm thick (Table 6). As discussed above, the more extensive area of lower ice concentration was

due to the presence of the Kane Basin ice bridge. I inferred that the Smith Sound polynya, using the strict definition of a polynya (WMO 1970), is not consistently present until the Kane Basin ice bridge becomes a permanent structure.

### 5.1.3 Fall Period

The fall period (FP) was best represented with 3 clusters (Fig. 5.5). Interestingly, the FP demonstrated a similar spatial structure to the other two periods. However, the distribution and proportions of most surface type concentrations were different.

Over 50 % of FP cluster 1 consisted of a RI and MYI mixture (Fig. 5.5). Similar to both the WP and SP cluster 2, the FP cluster 1 distribution concentrated at the north end of Smith Sound and kept toward the eastern coast of Canada north of Cape Alexander. This distribution further supports both explanations discussed above (i.e., deflected eastward water mass movement or offshore katabatic winds). Furthermore, cluster 1 supports observations of multiyear ice transport out of the Arctic Basin.

FP cluster 2 classified a combination of NGI and MFYI with relatively high concentrations of OW and GWF (Fig. 5.5). This cluster illustrated the advancement of newly formed sea ice into the NOW during the fall period (FP), 1998.

FP cluster 3 consisted of a combination of open water (OW) and medium first-year ice (MFYI). It delineated small areas near Cape Alexander and off the

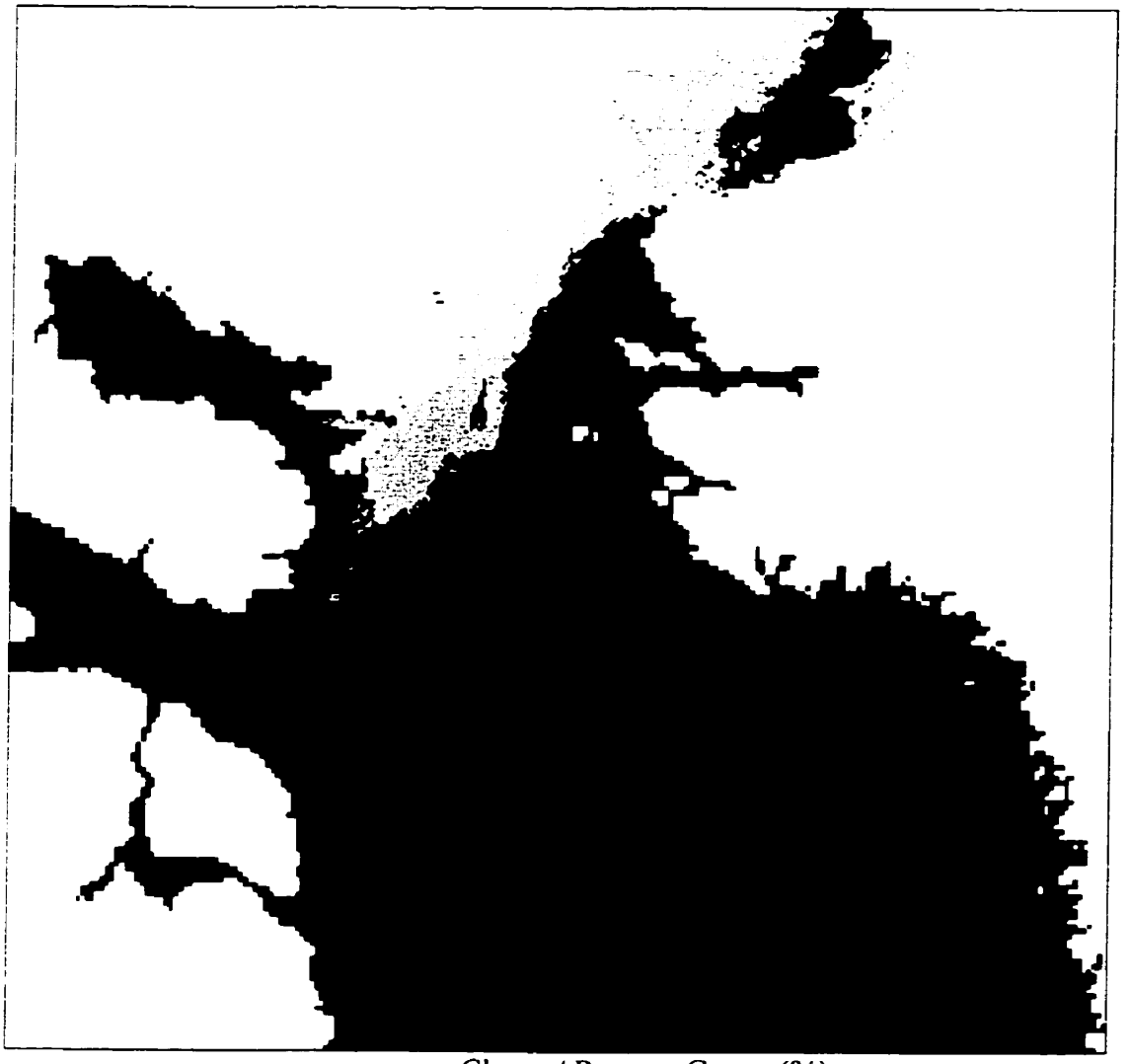

| | Cluster/ Percent Cover (%) | | |
|---|---|---|---|
| Ice Type | 1 | [redacted] | [redacted] |
| OW | 3.22 | 12.37 | 45.03 |
| NGI | 8.34 | 32.18 | 16.71 |
| GWF | 2.12 | 12.63 | 8.41 |
| MFYI | 25.13 | 37.14 | 28.05 |
| TFYI | 8.37 | 1.18 | 0.94 |
| MYI | 11.69 | 0.46 | 0.04 |
| RI | 41.54 | 4.05 | 0.80 |

**Figure 5.5.** 1998 fall period (Oct. 15 through Dec. 7) *k*-means cluster results for the GIS grid. The table provides the mean surface type composition for each blue-shaded cluster.

southern tip of Coburg Island (Fig. 5.5). However, it was mainly distributed towards the south end of the grid with an extension north along the west coast of Greenland and into Whale Sound (Fig. 5.5). The southeastern portion was predominately OW, whereas the southwestern portion of this distribution consisted largely of MFYI (Fig. 5.6a and b, respectively). Prior to freeze-up, the area was covered by 100% OW. Whereas, near the FP end (i.e., December 7, 1998), sea ice nearly covered the whole region, with the exception of the southwest Greenland coast. Barber et al. (2000) demonstrated predominant southerly winds in this vicinity from 1979 to 1996. They also showed a late fall accretion in the same vicinity. It was suggested that these winds could import warmer air from southern Baffin Bay and could contribute to the late fall freeze-up. Accordingly, the same mechanism is used to explain the open water observed in this study. The influx of warmer air and/or warmer surface water from southern Baffin Bay could impede ice formation and cause ice divergence.

Advection of this atmospheric and/or oceanic heat source may have reached even further north. During the winter and spring periods, an area of relatively low ice deformation was inferred along the Greenland coast between Whale Sound and Cape York. Furthermore, high open water concentrations were observed along this location for both the spring and fall periods (Fig. 5.4b and 5.6a, respectively). As a latent heat polynya mechanism is consistent with relatively large surface forcing that causes ice divergence and deformation, the observation of open water along this location implied the occurrence of a

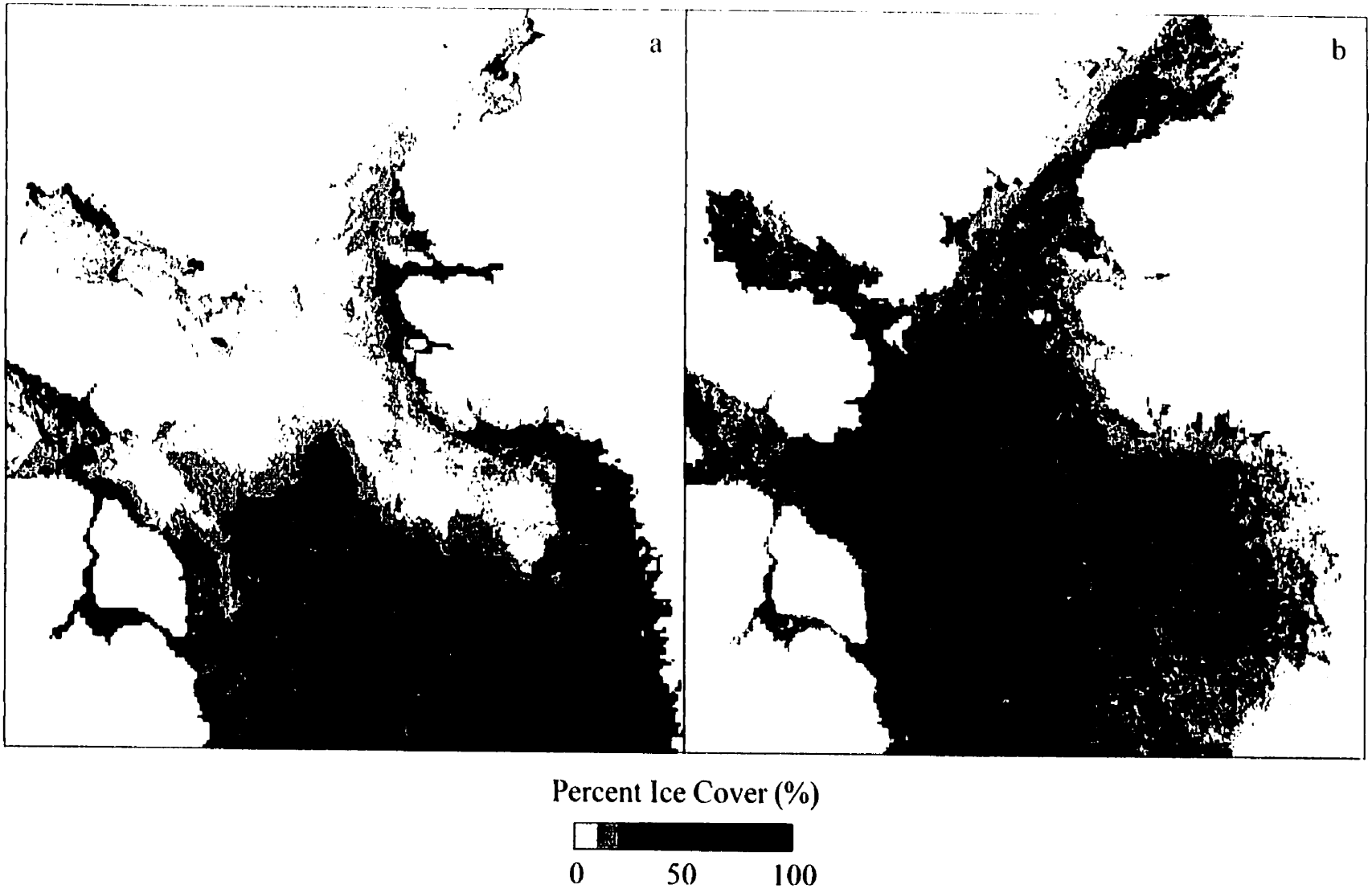


**Figure 5.6.** Averaged 1998 fall period (Oct. 15 through Dec. 7) concentrations of open water (a) and medium first-year sea ice (b).

sensible heat input. The heat input could impede ice formation during freeze-up resulting in a thinner ice cover, which would subsequently ablate earlier in the spring. This mechanism was actually suggested, yet not explained, by Ito (1985).

During the fall period (FP), open water (OW) had higher concentrations within and south of Whale Sound than north near Cape Alexander (Fig. 5.6a). Furthermore, FP cluster 3 was largely absent in the vicinity of Smith Sound (Fig. 5.5). Smith Sound appears to be separated from the west Greenland coast south of Whale Sound and hence the surface heat influx from south Baffin Bay (see above) due to the presence of Northumberland Island and its neighboring islands (Fig. 1.1). Consequently, the occurrence of a mechanism independent to the explained upwelling along Smith Sound was inferred. This inference was corroborated by an observed mode of late fall accretion and early spring ablation (separate from the Smith Sound vicinity) along the Greenland coast from 1979 to 1996 (Barber et al. 2000).

The 50 km transect contained a composition of only 46.8% open water/ice cover < 30 cm thick (Table 5.1). This was considerably less than Steffen's (1986) observations, when averaged resulted in 91.4% open water/ice cover < 30 cm (average obtained from December 2, 20 and 29, 1980 from Table IV; Steffen, 1986). As discussed earlier, the lower concentrations observed during this investigation may have been the result of less sea ice congestion at the northern end of Smith Sound than in Steffen's (1986) study.

### *5.2 Sea Ice Temporal Evolution*

The results discussed in the previous section demonstrated a clear and consistent spatial pattern in each defined seasonal period. Interpretation of the results prompted the separation of the grid into 14 sub-regions for the temporal analysis used in this section (Fig. 5.7). The following provides a detailed account of the temporal evolution of sea ice cover within these defined sub-regions in the North Water throughout 1998.

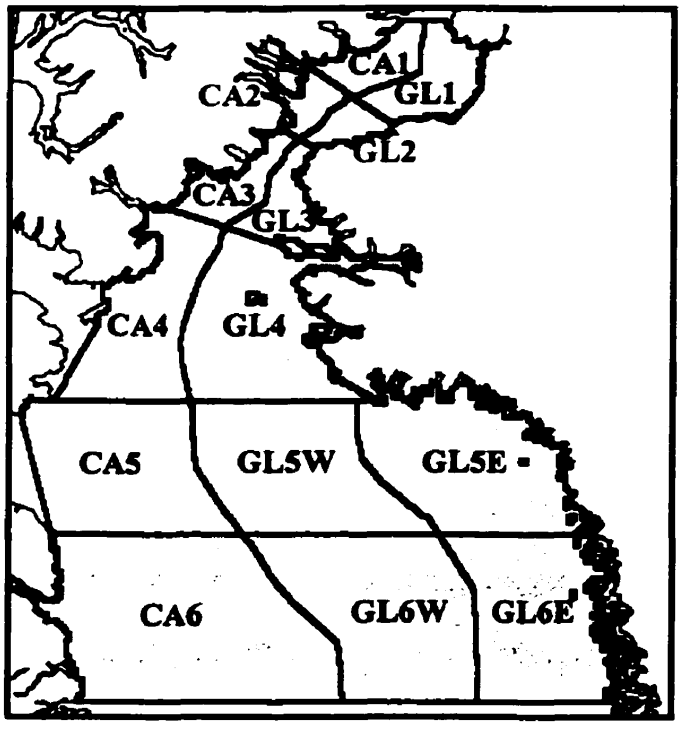


**Figure 5.7.** Map of the North Water sub-regions.

The entire grid was first assigned proximity to either Greenland or Canada (i.e., delineated with pre-fixes GL or CA, respectively). Further separation included sub-regions: north of the 1998 Kane Basin ice bridge formation (1); in the vicinity of the Kane Basin ice bridge (2), in Smith Sound (3), between Whale Sound and Cape York (4) and in northern Baffin Bay (north and south sub-regions correspond to 5 and 6, respectivley). GL5 and GL6 were also separated into east (E) and west (W) sub-regions (Fig. 5.7). Sub-regions within Jones Sound and Lancaster Sound were not included due to low temporal satellite coverage over these areas.

To assist interpretation of the results, four stages were delineated on the time series graphs (Fig. 5.8 and 5.9). The stages included: (i) before the Kane Basin ice bridge formed (before March 3), (ii) during the presence of the ice bridge (March 03 to June 10), (iii) after the ice bridge broke (June 10 to October 5) and (iv) during freeze-up (after October 5).

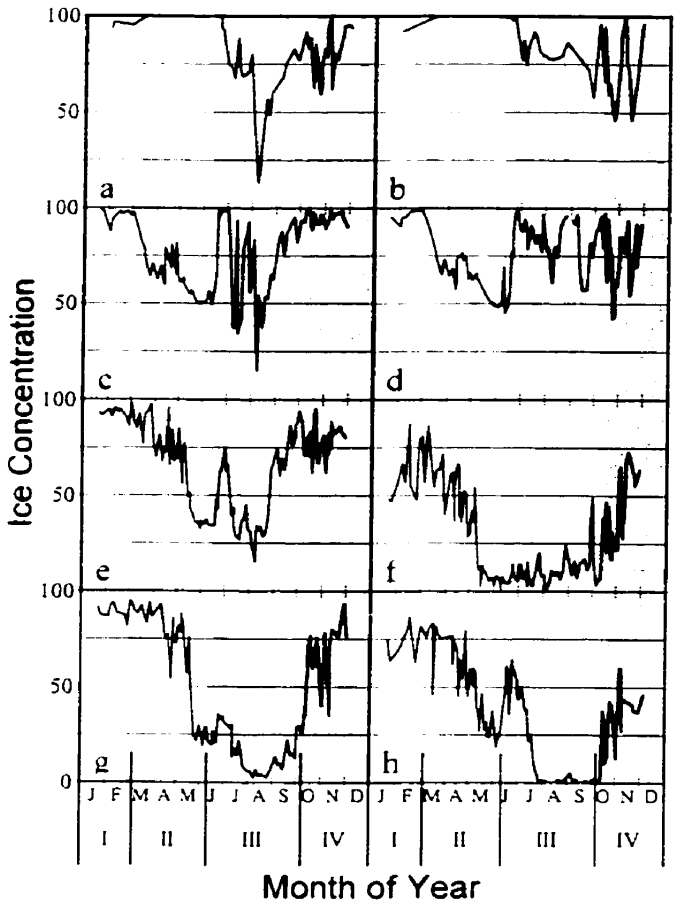


**Figure 5.8.** Sea ice concentration time series during 1998 for CA1 (a), GL1 (b), CA2 (c), GL2 (d), CA3 (e), GL3 (f), CA4 (g) and GL4 (h). I, II, III and IV depict the four temporal stages outlined in the text.

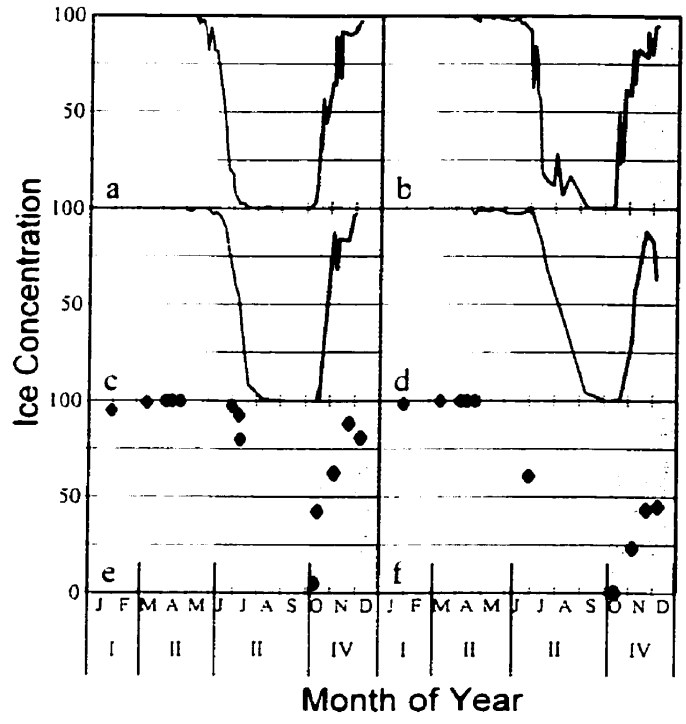


**Figure 5.9.** Sea ice concentration time series during 1998 for CA5 (a), GL5W (b), CA6 (c), GL6W (d), GL5E (e) and GL5E (f). I, II, III and IV depict the four temporal stages outlined in the text.

### 5.2.1 Prior to Ice Bridge

Prior to formation of the Kane Basin ice bridge, the North Water (NOW) sea ice is advected continually from the Lincoln Sea into Baffin Bay. North of Cape York, sea ice concentrations were close to but slightly below 100% concentrations due to the consistent motion of the pack-ice and subsequent crack and lead formation (Fig. 5.8). South of Cape York, the pack within Baffin Bay had a more compact distribution and did not demonstrate the lower ice concentrations (Fig. 5.9).

Greenland sub-regions between Smith Sound and Cape York (i.e., GL3 and GL4) both demonstrated average sea ice concentrations less than 75% prior to the ice bridge formation (Fig. 5.8). As discussed earlier, these results can be explained through either coastal upwelling (Steffen 1985) or by offshore katabatic winds that have been modeled to occur along the coast of these sub-regions (Bromwich et al. 1996). I note again that no observations of ocean surface temperature were made in this vicinity during the expedition.

### 5.2.2 Ice Bridge Present

Once the bridge formed, sea ice cover north of the bridge (i.e., CA1 and GL1) became landfast and demonstrated near 100% concentrations (Fig. 5.8). In the vicinity of the bridge and Smith Sound, the latent heat mechanism was dominant. Ice concentrations dropped slightly then stabilized at a point where air temperatures, winds and/or currents were balanced by newly formed sea ice that accumulated at the southern extent (Fig. 5.8). This process is typical of a latent heat polynya mechanism such as described by Pease (1987).

The polynya opened rapidly in May (Fig. 5.8). From April 29, 1998, the air temperature increased from approximately –11 to –1.1°C by May 2, leveled off at an averaged -5°C until May 8 where it decreased to –12.2°C on May 12, then steadily increased to approximately 0°C by the end of May (Minnett 2000; Fig. 5.10). Further, 3 strong peaks of winds coming from the north (i.e., near 0/360°) occurred throughout May (Minnett 2000; Fig. 5.10). During this period I speculate that a positive feedback loop was created. Warmer temperatures resulted in less

new ice formation and higher winds resulted in more stress on the polynya's southern ice extent. This resulted in more open water, which absorbed greater amounts of solar energy and provided a longer north-south fetch for wave development. The increased absorption and wave stress would cause increased lateral and mechanical sea ice ablation (e.g. Hall and Rothrock 1985). All of these factors would feedback into creating a larger open water area in the NOW.

Within Smith Sound, a substantial difference was observed between average ice concentrations of CA3 and GL3 (Fig. 5.8). Both sub-regions showed a slight decreasing trend after the formation of the ice bridge. Once the polynya began to open in May, ice concentrations in GL3 dropped to less than 15% (Fig. 5.8). The low concentrations were attributed to a small amount of landfast ice along the Greenland coast in this vicinity. The lower landfast concentration in GL3 was due to the offshore movement of water described above. Further, sensible heat inputs from upwelling along the Greenland coast may have also contributed to the lower ice concentrations observed in GL3.

In GL4, the extensive opening of the polynya was not as dramatic as compared with CA4 (Fig. 5.8). This was attributed to the direction of sea ice motion in this area. Wilson et al. (2000) demonstrated that sea ice moves northward in this region as a consequence of the north Baffin Bay gyre. Consequently, ice was advected into this sub-region as opposed to being exported southward.

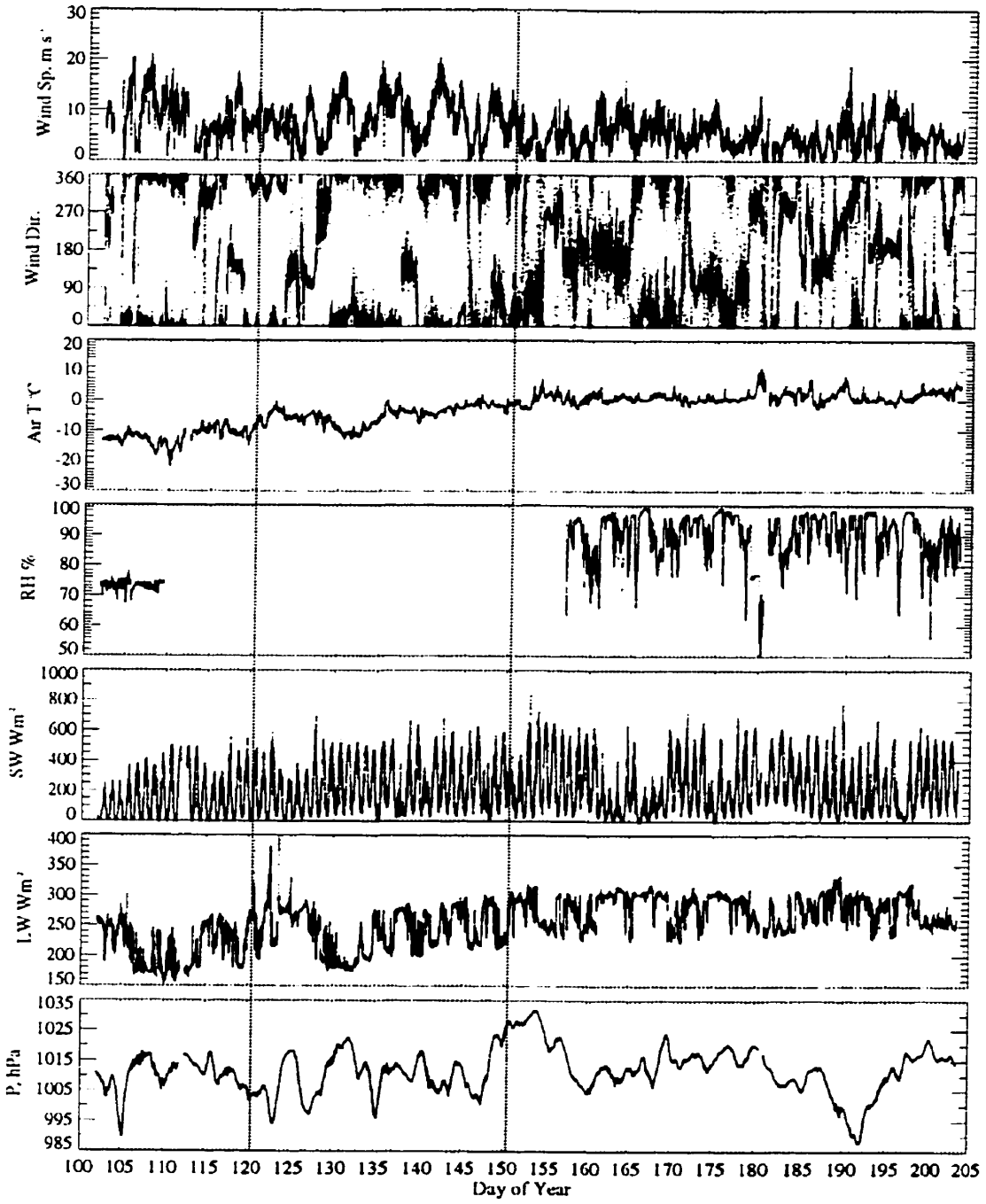


**Figure 5.10.** Meteorological variables including wind speed (Wind Sp.), wind direction (Wind Dir.), air temperature (Air T), relative humidity (RH), incident short wave (SW) and long wave energy (LW) and pressure (P) collected in transit on board the CCGS *Pierre Raddison* during the 1998 North Water Polynya Study Expedition (After Minnett 2000). Vertical dashed lines were added to highlight the month of May (Day of Year 121 to 151).

### 5.2.3 After Ice Bridge

After the ice bridge broke, sea ice emptied through Kane Basin and into the NOW in a strong pulse. This pulse was observed as a decrease in CA1 and GL1 ice concentrations and subsequent increases in sub-regions to the south (Fig. 5.8). The pulse of sea ice was not observed in GL3, as ice did not flow through this sub-region (Fig. 5.8). The sea ice was essentially pushed towards the Canadian side of Smith Sound due to the offshore water mass movement described above. As mentioned above, the increase in sea ice concentrations in GL4 was due to an increased import of sea ice from the south (Wilson et al. 2000).

Within CA4, the sea ice pulse was greatly diminished and south of Cape York the pulse of sea ice was not observed (Fig. 5.8 and 5.9, respectively). Furthermore, throughout July, August and September, sea ice was continually observed to flow though Kane Basin. However, the sea ice appeared to ablate before it reached Cape York. The ablation of sea ice in this region was probably accentuated by lateral melt and mechanical erosion from the open ocean (e.g., Hall and Rothrock 1985).

During August and September, sea ice concentrations increased within Kane Basin and CA3 (Fig. 5.8). The increase was attributed to increased ice flowing into the area from the north. During this time, temperatures had cooled enough to slow the ablation of sea ice.

### 5.2.4 Fall Freeze-up

Fall freeze-up began in mid October (determined from ScanSAR imagery). The accumulation of newly formed sea ice combined with the influx of ice from the north was observed throughout the whole region (Fig. 5.8 and 5.9). Nearly all sub-regions demonstrated ice concentrations increasing to values close to that observed in January, with the exception of GL4 and GL6E.

GL6E can be explained by predominate southerly winds observed in the area along the Greenland coast (Barber et al. 2000). As explained in section 5.1, the southerly winds could import warm atmospheric air masses and/or warm surface water from southern Baffin Bay, impeding ice formation in the local area. Similarly, GL4 can be explained by the same influx of warmer air temperatures and/or surface water, in addition to offshore ice divergence.

## *5.3 Mixed Layer Depth (MLD) and Sea Ice Patterns*

The mixed layer refers to the ocean's surface layer where density is relatively homogeneous throughout. This layer rests on top of a thermocline or halocline through which water density increases dramatically due to a decrease in temperature or an increase in salinity, respectively. A shallow mixed layer depth (MLD) is vital for the entrainment of phytoplankton populations to the surface where they can benefit from non-limiting irradiance. The following compares

mixed layer depths measured during the NOW study 1998 campaign with sea ice cover in the North Water.

Legs1 (March 26 to May 5, 1998) and 2 (May 5 to June 2, 1998) both demonstrated relatively deep MLDs with large ranges (Fig. 5.11a and b, respectively). Their averages (±sd) were 56±34 and 37±22 m, respectively. During Leg 1, deep (up to 157 m) MLDs were observed along the eastern Ellesmere Island coast and shallow (10 to 20 m) MLDs off the coast of Cape Alexander and surrounding the Carey Islands (Fig. 5.11a). During Leg 2, a similar pattern was observed with shallow MLDs along the Greenland coast and deeper MLDs toward the Canadian coast. There was also a general trend of shallower MLDs toward the southeast of the region (Fig. 5.11b).

Throughout April and May (i.e., Legs 1 and 2), northerly winds and temperatures increased resulting in the extensive opening of the NOW polynya. Areas with deep MLDs along the Greenland coast were generally covered by ice, whereas some of the areas with deep MLDs along the Ellesmere Island coast were ice free. A dynamic ice cover was inferred along the Ellesmere Island coast. This was indicative of a latent heat polynya mechanism acting to keep the area ice free. Subsequently, although the area was ice free, the dynamic surface conditions would act to keep a relatively deep MLD. Alternatively, areas with shallow mixed layer depths along the Greenland coast corresponded to inferred areas of lower ice deformation. It was suggested that either atmospheric and/or oceanic heat was imported from southern Baffin Bay. Further, Yackel et al. (2000) observed melt onset dates to occur first along the southeastern edge of

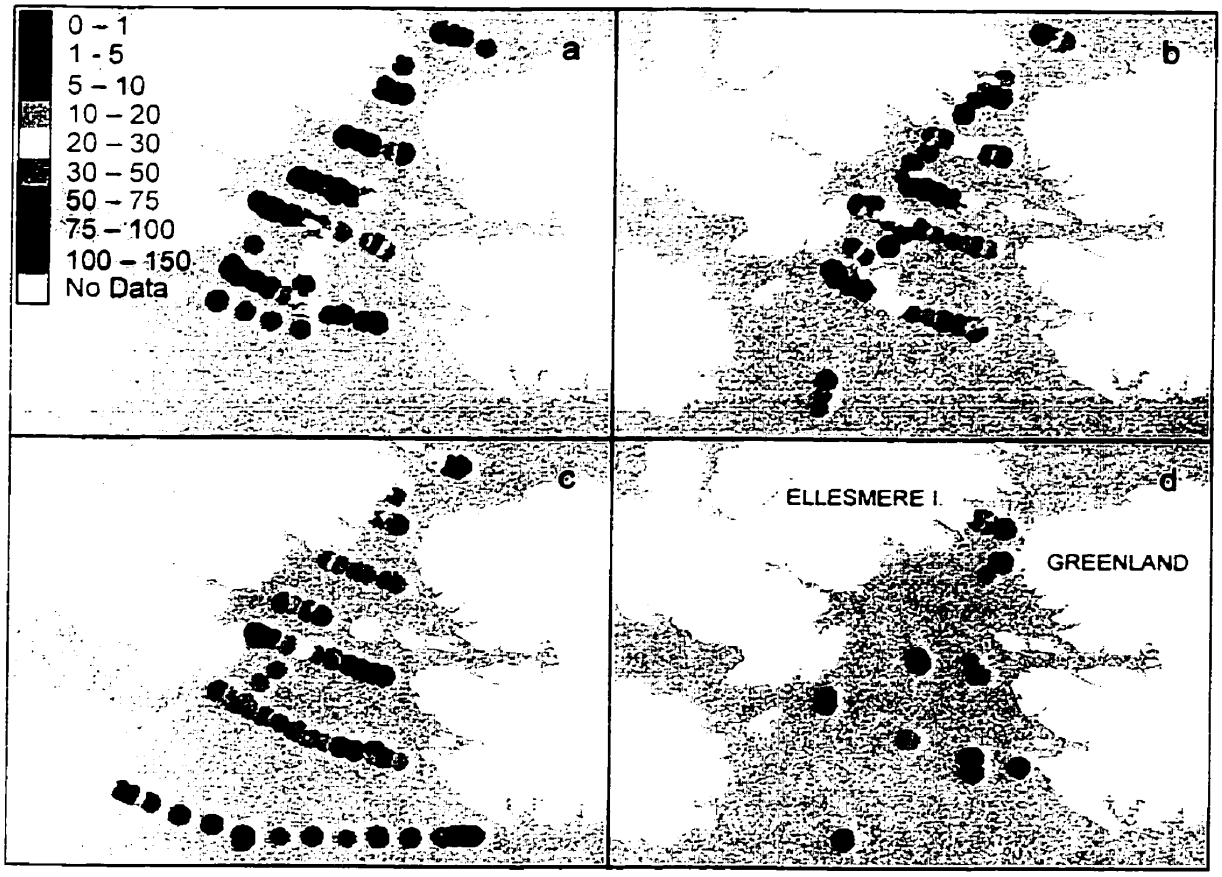


**Figure 5.11.** Mixed layer depths (m) for CTD casts made during Legs 1 (March 26 to May 5 (a)), 2 (May 5 to June 2 (b)), 3 (June 2 to June 29 (c)) and 4 (June 29 to July 27 (d)) of the 1998 International North Water Polynya Study expedition. Interpolated 10 km radii surround each CTD cast location.

the NOW. This inferred that the area warmed prior to areas to the northwest. The relatively calm conditions combined with this heating could have caused thermal stratification of the water column and hence the earlier shallow MLDs observed off the southwest coast of Greenland. Further, the early shallow MLDs observed near Cape Alexander support the possibility of upwelling in the vicinity.

By Legs 3 (June 2 to June 29) and 4 (June 29 to July 27), MLDs were shallow throughout the NOW (Fig. 5.11c and d, repectively), with averages of 12±6 and 9±3 m, respectively. During these periods, sea ice was ablating extensively. Therefore, the low salinity melt water may have acted to stratify the waters, even in areas of high surface deformation as inferred along the Ellesmere Island coast.

In this chapter I have described the results of the spatio-temporal ice cover analysis for the NOW and related it to potential physical mechanisms responsible for the observed patterns. I also discussed the relationship between mixed layer depth observations and the interpreted ice cover results. In the next chapter I provide the conclusions drawn from chapters 4 and 5 and recommendations as to how this data set can be further examined.

# CHAPTER 6: CONCLUSIONS AND RECOMMENDATIONS

The objectives of this thesis have been: (1) To develop a robust ScanSAR sea ice classification scheme; (2) To examine the spatial and temporal patterns of sea ice cover within the North Water (NOW) in relation to the potential physical mechanisms responsible for the NOW polynya's occurrence, and (3) To relate the sea ice spatio-temporal patterns to the potential for biological productivity within the NOW. In this chapter I conclude on the examination of these objectives and recommend future directions for the use of the data set created as part of this thesis.

To meet the first objective of this thesis I developed a hierarchical sea ice classification scheme using over 150 RADARSAT-1 ScanSAR images. The classified ice types were then structured into a Geographic Information System (GIS) framework for subsequent analysis pertaining to my second and third thesis objectives.

To meet my second objective I examined the spatial and temporal patterns of sea ice cover within the North Water (NOW) in relation to the potential physical mechanisms responsible for the resident polynya's occurrence. Ice conditions

demonstrated a clear and consistent spatial structure in the NOW for the winter (WP), spring (SP) and fall (FP) periods of 1998. The consistency of the spatial patterns of sea ice was somewhat surprising but illustrated the strength of sea ice as a proxy indicator of the polynya formation and maintenance processes. An area of high ice deformation (i.e., high rubble ice concentrations) was observed along the Canadian Coast, inferring strong winds and/or currents, which would be consistent with a latent heat polynya mechanism. The composition of thick multiyear and rubble ice within the dynamic region also represented a previously poorly documented contribution to the freshwater flux from the Arctic Basin into Baffin Bay. Opposite to the dynamic area along the eastern Canadian coast, a relatively less dynamic ice environment was inferred along the Greenland coast. As open water was observed along the Greenland coast in early spring and late fall, a sensible heat mechanism was suspected.

Through Smith Sound, tight distributions of thick ice along the Canadian coast and thin ice types and open water along the less dynamic Greenland coast supported Steffen's (1985) explanation for the existence of a sensible heat input at this location. Steffen's rationale suggested that without the existence of an ice edge combined with ice divergence due to winds and/or currents there would be no upwelling of warm Baffin Bay Atlantic water. The location of high open water concentrations observed consistently off the coast of Coburg Island combined with Steffen's (1985) observation of warm water at this location suggests that this mechanism may occur in more than one location within the NOW. An alternative explanation of offshore katabatic winds causing ice divergence off the Greenland

coast in the Smith Sound vicinity was also suggested. Similar to Steffen's (1985) explanation, offshore transport of water could induce upwelling of relatively warm Baffin Bay Atlantic water. However, the latter mechanism would be less dependent on the congestion of ice within Kane Basin.

An exception to the spatial trend described above was observed off the coast of Greenland south of Cape York. Relatively high mean rubble ice (RI) concentrations throughout the winter (WP) and spring (SP) periods and open water during the fall period (FP) were observed along this location. These observations were explained by contributions of the West Greenland surface current and predominate southerly winds.

Additionally, large expanses of open water were observed along the Greenland coast between Whale Sound and Cape York during the SP and FP. It was suggested that a surface influx of atmospheric and/or oceanic heat from south Baffin Bay could explain the open water. This would result in a thinner ice cover causing an earlier spring ablation than surrounding areas. It was also inferred that this sensible heat input was independent of the mechanism occurring through Smith Sound.

Compared to similar observations made by Steffen (1986) for the winter of 1980/81, substantially less open water was observed within Smith Sound during 1998. This was explained in part by the composition of sea ice at the northern entrance to Smith Sound. Kane Basin prior to and after ice bridge formation was noted to consist of very thick multiyear ice of Arctic Basin origin. I speculated that

large multiyear ice floes could contribute to congestion of sea ice at the head of Smith Sound.

Ito and Müller (1977), during the years of 1974 and 1975, observed the Kane Basin ice bridge to be composed of thickly ridged MYI with ice elevations up to 5 m above sea level. Similar observations were made during the International North Water Polynya Study 1998 campaign (personal observation). Multiyear ice is much stronger and more rigid than first-year ice due both to its higher freshwater content and thickness (Weeks and Ackley, 1986). Consequently, MYI may provide extra structural support against the consistently strong northerly winds and southward currents through Smith Sound than would FYI acting alone. That is, smaller and thinner multiyear ice floes would result in a lower probability of sea ice congestion at the head of Smith Sound and a later formation of the Kane Basin ice bridge. Such a scenario is also in accordance with observed trends of decreasing Arctic pack-ice extent (Parkinson *et. al.* 1999) and volume (Rothrock et. al. 1999). A historical analysis of the annual bridge formation further suggested that the ice bridge formation has become less consistent in the 1990's versus the 1980's (Barber et al. 2000). Consequently, observations of ice congestion and bridge formation within Kane Basin may act as a proxy indicator of climate change and/or variability.

Evolution of sea ice in the North Water (NOW) during 1998 provided additional insight into the physical mechanisms that act to form and maintain the polynya. The polynya appeared to be largely controlled by the latent heat mechanism. Prior to the ice bridge formation and during fall freeze-up, there were

some open water areas along the coast of Greenland that could also be explained, at least in part, through sensible heat inputs (i.e., both oceanic and atmospheric). However, no observations were made to prove or disprove the input of sensible heat in the NOW.

During May, nearly two months after the ice bridge formed, the polynya opened rapidly as a result of a positive feedback loop on ice ablation. The feedback was initiated through increased wind speeds and temperatures. The feedback involved increasing lateral and mechanical ablation processes as a result of an increasing open water area. Once the NOW was completely open, the resultant open ocean conditions caused imported sea ice to locally ablate throughout the summer months.

In objective three I began the process of examining the relationship between physical processes (particularly those relating to sea ice) and their biological consequences. In particular I examined the relationship between sea ice spatio-temporal patterns and the observed mixed layer depths (MLDs). The occurrence of a shallow MLD is usually consistent with the occurrence of a primary production bloom in polar waters (e.g., Maynard and Clark 1987). A qualitative comparison made between mixed layer depth (MLD) and sea ice spatio-temporal patterns demonstrated a relationship based on ice deformation. Generally, in areas of lower inferred ice deformation (i.e., off the coast of Greenland), shallow MLDs were observed earlier with the exception of ice-covered waters. It appeared that high surface turbulence from either atmospheric or ocean stress was responsible for slowing the development of shallow MLDs along the

Canadian coasts. With earlier shallow MLDs, a subsequent early primary production bloom could occur due to non-limiting irradiance. Therefore, consistent with Lewis et al. (1996) primary producers would first bloom along the Greenland coast where growth conditions were first favorable. Further, the MLDs observed throughout the North Water in June were indicative that the entire region could support an early primary production bloom relative to surrounding ice-covered areas.

It should be noted that without upwelling the bloom would be short lived due to nutrient depletion. It was suggested in the NOW proposal (1997) that not only an early bloom may occur, but an extended bloom as well. This suggestion was made as a rectification for the rich wildlife found along the adjacent coasts of the NOW. The occurrence of upwelling was not observed with the data used in this thesis and therefore conclusions could not be made. Similarly, no convincing evidence of upwelling was made during the oceanographic portion of the NOW study (Melling et al. 2000). However, the results of this thesis highlight areas of open water that could be explained, at least in part, through the occurrence of upwelling. Consequently, whether an extended bloom occurs in the NOW and its relationship to the physical polynya mechanism have yet to be confirmed. This may be done through a more detailed quantitative analysis of these data, or perhaps a future study of the North Water with a focus on the areas where upwelling may occur (i.e., the southeastern portion of the NOW and off the coasts of Cape Alexander and Coburg Island) may be warranted.

This thesis documented the creation of a high-resolution (both temporal and spatial) GIS database of sea ice type and concentration. The database was created to examine the response of the sea ice to atmospheric and oceanic forcing and to relate sea ice processes to biological production. The results presented in this thesis represent only the first-order approximation of these processes. Biologists, geographers and oceanographers involved in the NOW study are just beginning to make use of the GIS database developed here. Further research will develop ideas of ocean-sea ice-atmosphere processes and further determine the biological and physical interrelationships that exist within the NOW. I recommend the following studies be conducted as a natural evolution of this thesis:

1. A regional surface energy balance study through the use of sea ice cover and modeled atmospheric parameters interpolated to the GIS grids. The model results are being interpolated with weighting on observed ice types and concentrations and surface climate measurements made from ship and on the fast ice during the International North Water Polynya Study 1998 campaign;
2. A sea ice flux study through the combination of surface type, sea ice motion (see Wilson et al. 2000), sea ice deformation and accretion/ablation (obtained from a sea ice thermodynamic model) each interpolated to the GIS grid. The results will be used to estimate

the sea ice budget for the entire 1998 year as well as compare with physical and biological processes occurring within the NOW.

3. A statistical comparison between results obtained through different data sources including ice concentration from the GIS grid, the Special Sensor Microwave Imager (SSM/I) and the Advanced Very High Resolution Radiometer (AVHRR). This will allow us to improve course spatial resolution estimates of sea ice type and concentration and thus provide better historical analysis of the NOW ocean-sea ice-atmosphere processes.

The recommendations above, and the thesis results presented here represent progress in the development of our understanding of ocean-sea ice-atmosphere processes that occur within the North Water Polynya. The combined results from the first series of journal papers will be forthcoming in a special issue of the journal 'Atmosphere-Ocean'. Presented in this special issue is evidence for the fact that the NOW polynya can, and does, respond to climate variability and change. Linking the biological consequences of this change will continue in ongoing analysis of the NOW research network building upon the results in my thesis.

# REFERENCES


Aagaard, K. and E.C. Carmack. 1989. The role of sea ice and other freshwater in the Arctic circulation. *J. Geophys. Res.*, **94**: 14,485-14,498.

Agnew, T. A., 1998. Drainage of multiyear ice from the Lincoln Sea. *Can. Metero. Oceanogr. Soc. Bull.* **26**: 101-103.

Alexander, V. 1994. Primary productivity regimes of the nearshore Beaufort Sea, with reference to the potential role of sea ice biota. IN, *The Coats and Shelf of the Beaufort Sea.* J.C. Reed and J.E. Sater (Eds). Arctic Institute of North America, Arlington, VA, pp. 604-635

Alexander, V. and H.J. Niebauer. 1981. Oceanography of the eastern Bering Sea ice-edge zone in spring. *Limnol. Oceanogr.*, **26**: 1111-1126.

Anderberg, M.R. 1973. *Cluster Analysis for Applications.* Probability and Mathematical Statistics: A Series of Monographs and textbooks, Birnbaum, Z.W. and E. Lukacs (Eds). Academic Press, Inc., New York. 359 pp.

Barber, D.G. and E.F. LeDrew. 1991. SAR sea ice discrimination using texture statistics: A multivariate approach. *Photogramm. Eng. Remote Sens.*, **57**: 385-395.

Barber, D.G., D.D. Johnson and E.F. LeDrew. 1991. Measuring climatic state variables from SAR images of sea ice: The SIMS SAR validation site in Lancaster Sound. *Arctic*, **44**: 108-121.

Barber, D.G., M.E. Shokr, R.A. Fernandes, E.D. Soulis, D.G. Flett and E.F. LeDrew. 1993. A comparison of second-order classifiers for SAR sea ice discrimination. *Photogramm. Eng. Remote Sens.*, **59**: 1397-1408.

Barber, D.G., T.N. Papakyriakou, E.F. LeDrew and M.E. Shokr. 1995. An examination of the relation between the spring period evolution of the scattering coefficient ($\sigma°$) and radiative fluxes over land fast sea-ice. *Int. J. Remote* Sensing, **16**: 3343-3363.

Barber, D.G. and S.V. Nghiem. 1999. The role of snow on the thermal dependence of microwave backscatter over sea ice. *J. Geophys. Res.*, **104**: 25,789-25,803.

Barber, D.G., J. Hanesiak and J. Piwowar. Sea ice – atmosphere processes within the North Water polynya (NOW): Part 1 – Seasonal and annual averages between 1979 and 1996. *A-O*, In Review 2000.

Barry, R.G., M.C. Serreze, J.A. Maslanik, and R.H. Preller. 1993. The Arctic Sea Ice-Climate System: Observations and Modelling. *Rev. Geophys.*, **31**: 397-422.

Bauer, J. and S. Martin. 1983. A model of grease ice growth in small leads. *J. Geophys. Res.*, **88**: 2917-2925.

Bel'chanskiy, G.I., D.C. Douglas and N.N. Kozlenko. 1996. Assessment of sea-ice conditions using two-channel active and passive microwave systems. *Polar Geog.* **20**: 294-305.

Bishop, Y.M.M., S.E. Fienberg and P.W. Holland. 1975. *Discrete Multivariate Analysis: Theory and Practice*. MIT Press, Cambridge.

Boertman, D. and A. Mosbech. 1998. Distribution of the little Auk (Alle alle) breeding colonies in Thule district, northwest Greenland. *Polar Bio.*, **19**: 206-210.

Bourke, R.H. and R.G. Paquette. 1991. Formation of Baffin Bay bottom and deep waters. IN *Deep Convection and Deep Water Formation in the Oceans*, P.C. Chu and J.C. Gascard (Eds), Elsevier, Amsterdam, pp. 135-155.

Bromwich, D.H., Y. Du and K. M. Hines. 1996. Wintertime surface winds over the Greenland Ice Sheet. *Mon. Wea. Rev.*, **124**: 1941-1947.

Brown, R.G.B. and D.N. Nettleship. 1981. The biological significance of polynyas to Arctic colonial seabirds. IN, *Polynyas in the Canadian Arctic*, Stirling, I. and H. Cleator. (Eds) Canadian Wildlife Service, Ottawa (Occasional Paper No. 45.), pp. 59-65.

Carmack, E.C. 1990. Large-scale physical oceanography of polar oceans. IN, *Polar Oceanography Part A: Physical Science*, W.O. Smith (Ed), Academic Press, New York, pp. 171-211.

Comiso, J.C., C.R. McClain, C.W. Sullivan, J.P. Ryan and C.L. Leonard. 1993. Coastal Zone Color Scanner pigment concentrations in the southern ocean and relationships to geophysical surface features, *J. Geophys. Res.*, **98:** 2419-2451.

Darby, M.S., A.J. Willmott and L.A. Mysak. 1994. A nonlinear steady-state model of the North Water polynya, Baffin Bay. *J. Phys. Oceanogr.*, **24**: 1011-1020.

De Bastiani, P. 1990. *Canadian Arctic Marine Ice Atlas – Winter 1987/88 with Perspectives from 1986/87 and 1988/89*. Canarctic Shipping Company Limited, Ottawa, ON, 116 pp.

Dunbar, M.J. 1969. The geophysical position of the North Water. *Arctic*, **22**: 438-441.

Dunbar, M.J. 1981. Physical causes and biological significance of polynyas and other open water in sea ice. IN, *Polynyas in the Canadian Arctic*, Stirling, I. and H. Cleator. (Eds) Canadian Wildlife Service, Ottawa (Occasional Paper No. 45.), pp. 29-43.

Dunbar, M. and M.J. Dunbar. 1972. The history of the North Water. *Proc. R.S.E. (B)*, **72**: 231-241.

Finley, K.J. and W.E. Renaud. 1980. Marine mammals inhabiting the Baffin Bay North Water in winter. *Arctic*, **33**: 724-738

Gosselin, M. and L. Legendre. 1990. Light and nutrient limitation of sea-ice microalgae (Hudson Bay, Canadian Arctic). *J. Phycol.*, **26**: 220-232.

Hall, R.J. and D.A. Rothrock. 1987. Photogammetric observations of the lateral melt of sea ice floes. *J. Geophys. Res.*, **92**: 7045-7048.

Haralick, R.M., K. Shanmugan and I. Dinstein. 1973. Textural features for image classification. *IEEE Trans. Sys. Man Cybernet.*, 3, no. 6, 610-621.

Haverkamp, D. and C. Tsatsoulis. 1999. Information fusion for estimation of summer MIZ ice concentration from SAR imagery. *IEEE Trans. Geosci. Remote Sens.*, **37**: 1278-1291.

Hirche, H.-J., M.E.M. Baumann, G. Kattner and R. Gradinger. 1991. Plankton distribution and the impact of copepod grazing on primary production in Fram Strait, Greenland Sea. *J. Mar. Syst.*, **2**: 477-494.

Holmes, Q.A., D.R. Nuesch and R.A. Shuchman. 1984. Textural analysis and real-time classification of sea-ice types using digital SAR data. *IEEE Trans. Geosci. Remote Sens.*, **22**: 113-120.

Holst, M. and I. Sirling. 1999. A note on sightings of bowhead whales in The North Water Polynya, Northern Baffin Bay, May-June, 1998. *J. Cetacean Res. Manage.* 1:153-156.

IAPP. 1989. International Arctic Polynya Program. Arctic Ocean Sciences Board. Institute of Marine Sciences, University of Fairbanks, Alaska. 99775-1080. 28 pp.

Ito, H. 1985. Decay of the sea ice in the North Water area: observation of ice cover in Landsat imagery. *J. Geophys. Res.*, **90**: 8102-8110.

Ito, H. and F. Müller. 1977. Horizontal movement of fast ice in the North Water area. *J. Glaciol.*, **19:** 547-554.

Ito, H. and F. Müller. 1982. Ice Movement through Smith Sound in northern Baffin Bay, Canada, observed in satellite imagery. *J. Glaciol.*, **28:** 129-143.

Kwok, R., E. Rignot, B. Holt, and R. Onstott. 1992. Identification of sea ice types in spaceborne synthetic aperture radar data. *J.Geophys. Res.*, **97**: 2391-2402.

Lewis, E.L., D. Ponton, L. Legendre and B. LeBlanc. 1996. Springtime sensible heat, nutrients and phytoplankton in the Northwater Polynya, Canadian Arctic. *Cont. Shelf Res.*, **16:** 1775-1792.

Livingstone, C.E., R.G. Onstott, L.D. Arsenault, A.L. Gray and K.P. Singh. 1987. Microwave ice signatures near the onset of melt. *IEEE Trans. Geosci. Remote Sens.*, **25:** 174-187.

MANICE. 1994. *Manual Standard Procedures for Observing and Reporting Ice Conditions 8th edition.* Ice Services Branch, Atmospheric Environment Service, Ottawa, ON.

Manly, B.F.J. 1986. *Multivariate Statistical Methods.* Chapman and Hall, London.

Marceau, D.J., P.J. Howarth, J.-M. M. Dubois and D.J. Gratton. 1990. Evaluation of the grey-level co-occurrence matrix method for land-cover classification using SPOT imagery. *IEEE Trans. Geosci. Remote Sens.*, **28:** 513-519.

Martin, S., R. Drucker and M. Fort. 1995. A laboratory study of frost flower growth on the surface of young sea ice. *J. Geophys. Res.*, **100**: 7027-7036.

Massom, R.A. 1988. The biological significance of open water within the sea ice covers of the polar regions. *Endeavour, New Series*, **12**: 21-27.

Maykut, G.A. 1978. Energy exchange over young sea ice in the central Arctic. *J. Geophys. Res.*, **83**: 3646-3658.

Maykut, G.A. 1982. Large-scale heat exchange and ice production in the central Arctic. *J. Geophys. Res.*, **87**: 7971-7984.

Maykut, G.A. and T.C. Grenfell. 1975. The spectral distribution of light beneath first-year sea ice in the Arctic Ocean. *Limnol. Oceanogr.*, **20**: 554-563.

Maynard, N.G. and D.K. Clark. 1987. Satellite color observations of spring blooming in Bering Sea shelf waters during the ice edge retreat in 1980, *J. Geophys. Res.*, **92**: 7127-7139.

McBean, G. 1992. The Earth's climate system. *WMO Bull.*, **41**: 393-401.

McLaren, A.S. 1988. Analysis of under-ice topography in the Arctic Basin as recorded by the USS *Nautilus* during August 1958. *Arctic*, **41**: 117-126.

Melling, H., Y. Gratton and G. Ingram. Oceanic circulation within the North Water polynya in Baffin Bay. *A-O*, In Review 2000.

Minnett, P.J. Meteorological conditions in the North Water Polynya: spring and summer, 1998. *A-O*, In Review 2000.

Muench, R.D. 1971. The physical oceanography of the northern Baffin Bay region. IN *The Baffin Bay-North Water Project Report 1.* Arctic Institute of North America, Calgary, 150 pp.

Muench, R.D. and H.E. Sadler. 1973. Physical oceanographic observations in Baffin Bay and Davis Strait. *Arctic*, **26**: 73-76.

Mundy, C.J. and D.G. Barber. On the relationship between the temporal evolution of sea ice spatial patterns and the physical mechanisms creating and maintaining the North Water polynya. *A-O*, In Review March 2000.

Mysak, L.A. and F. Huang. 1992. A latent- and sensible-heat polynya model for the North Water, northern Baffin Bay. *J. Phys. Oceanogr.*, **22**: 596-608.

Nettleship, D.N. and P.G.H. Evans. 1985. Distribution and status of the Atlantic Alcida. IN, *The Atlantic Alcidae*, D.N. Nettleship and T.R. Birkhead (Eds), Academic Press, London, Pp. 53-154.

Nghiem, S.V., S. Martin, D.K. Perovich, R. Kwok, R. Drucker and A.J. Gow. 1997. A laboratory study on the effect of frost flowers on C band radar backscatter from sea ice. *J. Geophys. Res.*, **102**: 3357-3370.

Niebauer, H.J. and W.O. Smith. 1989. A numerical model of mesoscale physical-biological interactions in the Fram Strait marginal ice zone. *J. Geophys. Res.*, **94**: 16,151-16,175.

Nutt, D.C. 1969. The North Water of Baffin Bay. *Polar Notes*, **9**: 1-25.

Nystuen, J.A. and F.W. Garcia, Jr. 1992. Sea ice classification using SAR backscatter statistics. *IEEE Trans. Geosci. Remote Sens.*, **30**: 502-509.

NOW (International North Water Polynya Study) Proposal. 1997. University of Laval, GIROQ, ftp://kestrel.fsg.ulaval.ca/home/giroq/now/. 70 pp.

Parkinson, C.L., D.J. Cavalieri, P. Gloersen, H.J. Zwally and J.C. Comiso. 1999. Arctic sea ice extents, areas, and trends, 1978-1996. *J. Geophys. Res.*, **104**: 20,837-20,856.

Pease, C.H. 1987. The size of wind-driven coastal polynyas. *J. Geophys. Res.*, **92**: 7049-7059.

Ramsay, B., L. Weir, K. Wilson and D. Bradley. 1997. Utilization of RADARSAT data in the Canadian Ice Service. *Proceedings of the International Symposium GER'97- Geomatics in the Era of RADARSAT*, Ottawa, Canada, May 25-30.

Rothrock, D.A., Y. Yu and G.A. Maykut. 1999. Thinning of the Arctic sea-ice cover. *Geophys. Res. Lett.*, **26**: 3469-3472.

Salmonsen, F. 1981. Birds. IN, *The fauna of Greenland*, F. Salmonsen (Ed.), Glyldenal, Copenhagen, pp. 161-360.

*SAR Ice Interpretation Guide Volume II*. 1994. Atmospheric Environment Service Ice Branch, Environment Canada. 136 pp.

Schledermann, P. 1980. Polynyas and prehistoric settlement patterns. *Arctic*, **22**: 292-302.

Schneider, N. and P. Müller. 1990. The meridional and seasonal structures of the mixed-layer depth and its diurnal amplitude observed during the Hawaii-to-Tahiti Shuttle experiment. *J. Phys. Oceanogr.*, **20**: 1395-1404.

Shokr, M.E. 1991. Evaluation of second-order texture parameters for sea ice classification from radar images. *J. Geophys. Res.*, **96**: 10625-10640.

Shokr, M.E., L.J. Wilson and D.L. Surdu-Miller. 1995. Effect of radar parameters on sea ice tonal and textural signatures using multi-frequency polarimetric SAR data. *Photogramm. Eng. Remote Sens.*, **61**: 1463-1473.

Shokr, M.E., R. Jessup and B. Ramsay. 1999. An interactive algorithm for deriviation of sea ice classifications and concentrations from SAR images. *Can. J. Remote Sens.*, **25**: 70-79.

Smith, D.M., E.C. Barrett and J.C. Scott. 1995. Sea-ice classification from ERS-1 SAR data based on grey level and texture information. *Polar Rec.*, **31**: 135-146.

Smith, M. and B. Rigby. 1981. Distribution of polynyas in the Canadian Arctic. IN, *Polynyas in the Canadian Arctic*, Stirling, I. and H. Cleator. (Eds) Canadian Wildlife Service, Ottawa (Occasional Paper No. 45.), pp. 7-28.

Smith, S.D., R.D. Muench and C. Pease. 1990. Polynyas and leads: An overview of physical processes and environment. *J. Geophys. Res.*, **95**: 9461-9479.

Smith, W.O. 1995. Primary productivity and new production in the Northeast Water (Greenland) Polynya during summer 1992. *J. Geophys. Res.*, **100**: 4357-4370.

Smith, W.O. and D.M. Nelson. 1986. Phytoplankton growth and new production in the Weddell Sea marginal ice zone during austral spring and autumn. *Limnol. Oceanogr.*, **35**: 809-921.

Soh, L.-K. and C. Tsatsoulis. 1999. Texture analysis of SAR sea ice imagery using gray level co-occurrence matrices. *IEEE Trans. Geosci. Remote Sens.*, **37**: 780-795.

Steffen, K. 1985. Warm water cells in the North Water, northern Baffin Bay during winter. *J. Geophys. Res.*, **90**: 9129-9136.

Steffen, K. 1986. Ice conditions of an Arctic polynya: North Water in winter. *J. Glaciol.*, **32**: 383-390.

Steffen, K. and A. Ohmura 1985. Heat exchange and surface conditions in North Water, northern Baffin Bay. *Ann. Glaciol.*, **6**: 178-181.

Stirling, I. 1980. The biological importance of polynyas in the Canadian Arctic. *Arctic*, **33**: 303-315.

Stirling, I. 1997. The importance of polynyas, ice edges, and leads to marine mammals and birds. *J. Mar. Sys.*, **10**: 9-21.

Stirling, I. and H. Cleator. 1981. Polynyas in the Canadian Arctic. Canadian Wildlife Service, Ottawa (Occasional Paper No. 45), 73 pp.

Sullivan, C.W., C.R. McClain, J.C. Comiso and W.O. Smith, Jr. 1988. Phytoplankton standing crops within an Antarctic ice edge assessed by satellite remote sensing. *J. Geophys. Res.*, **93**: 12,487-12,498.

Thorndike, A.S., D.A. Rothrock, G.A. Maykut and R. Colony. 1975. The thickness distribution of sea ice. *J. Geophys. Res.*, **80**: 4501-4513.

Ulaby, F.T., R.K. Moore and A.K. Fung. 1982. *Microwave Remote Sensing Active and Passive*, Volume II Radar Remote Sensing and Surface Scattering and Emission Theory. Addison-Wesley Publishing Company, Inc., Reading, Massachusetts, pp. 457-1064.

Weeks, W.F. and S.F. Ackley. 1986. The growth, structure and properties of sea ice. IN *The Geophysics of Sea Ice*, N. Untersteiner (Ed). NATO ASI Series B: Physics vol. 146, Plenum Press, New York. pp. 9-164.

Welch, H.E. and M.A. Bergmann. 1989. Seasonal development of ice algae and its prediction from environmental factors near Resolute, N.W.T., Canada. *Can. J. Fish. Aquat. Sci.*, **46**: 1793-1804.

Welch, H.E., M.A. Bergmann, T.D. Siferd, K.A. Martin, M.F. Curtis, R.E. Crawford, R.J. Conver and H. Hop. 1992. Energy flow through the marine ecosystem of the Lancaster Sound Region, Arctic Canada. *Arctic*, **45**: 343-357.

Wilson, K.J., D.G. Barber and D. King. Validation of RADARSAT-1 derived ice dynamics in the 1998 North Water polynya (NOW) season. *A-O*, In Review 2000.

Wohl, G.M. 1995. Operational sea ice classification from synthetic aperture radar imagery. *Photogramm. Eng. Remote Sens.*, **61**: 1455-1462.

World Meteorological Organization. 1970. *WMO Sea ice nomenclature*. WMO Rep. 259, T.P. 145, Geneva, 147 pp. + 8 suppl.

Yackel, J.J., D.G. Barber and T.N. Papakyriakou. On the Estimation of Spring Melt in the North Water (NOW) using RADARSAT-1. *A-O*, In Review 2000.